

AFFDL-TR-78-33

APPLICATION OF SUPERSONIC FAVORABLE AERODYNAMIC INTERFERENCE TO FIGHTER TYPE AIRCRAFT

*BOEING AEROSPACE COMPANY
BOEING MILITARY AIRPLANE DEVELOPMENT
SEATTLE, WASHINGTON 98124*

APRIL 1978

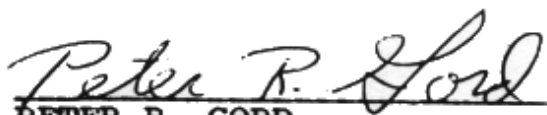
TECHNICAL REPORT AFFDL-TR-78-33
Final Report for Period May 1977 — January 1978

Distribution limited to U. S. Government Agencies only; test and evaluation; statement applied February 1978. Other requests for this document must be referred to A.F. Flight Dynamics Laboratory (AFFDL/FXG), Wright-Patterson Air Force Base, Ohio 45433.

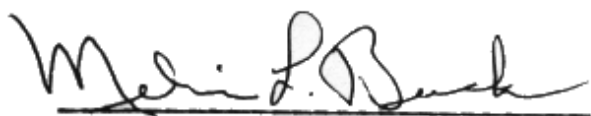
AIR FORCE FLIGHT DYNAMICS LABORATORY (AFFDL/FXG)
AIR FORCE WRIGHT AERONAUTICAL LABORATORIES
AIR FORCE SYSTEM COMMAND
WRIGHT-PATTERSON AIR FORCE BASE, OHIO 45433

NOTICE

When Government drawings, specifications, or other data are used for any purpose other than in connection with a definitely related Government procurement operation, the United States Government thereby incurs no responsibility nor any obligation whatsoever; and the fact that the government may have formulated, furnished, or in any way supplied the said drawings, specifications, or other data, is not to be regarded by implication or otherwise as in any manner licensing the holder or any other person or corporation, or conveying any rights or permission to manufacture, use, or sell any patented invention that may in any way be related thereto.



PETER R. GORD
Project Engineer



MELVIN L. BUCK
Branch Chief
High Speed Aero Performance Branch



COL ROBERT D. MCKELVEY
Chief
Aeromechanics Division

Unclassified

SECURITY CLASSIFICATION OF THIS PAGE (When Data Entered)

REPORT DOCUMENTATION PAGE		READ INSTRUCTIONS BEFORE COMPLETING FORM
1. REPORT NUMBER AFFDL-TR-78-33	2. GOVT ACCESSION NO.	3. RECIPIENT'S CATALOG NUMBER
4. TITLE (and Subtitle) APPLICATION OF SUPERSONIC FAVORABLE AERODYNAMIC INTERFERENCE TO FIGHTER TYPE AIRCRAFT		5. TYPE OF REPORT & PERIOD COVERED Final Technical Report May 1977 - January 1978
		6. PERFORMING ORG. REPORT NUMBER D180-24059-1
7. AUTHOR(s) Robert M. Kulfan, Hideo Yoshihara, Bruce J. Lord, and Gottfried O. FriebeI		8. CONTRACT OR GRANT NUMBER(s) F33615-77-C-3056
9. PERFORMING ORGANIZATION NAME AND ADDRESS Boeing Aerospace Company Boeing Military Airplane Development Seattle, Washington 98124		10. PROGRAM ELEMENT, PROJECT, TASK AREA & WORK UNIT NUMBERS Project 2404 Task 240407 Work Unit 24040706
11. CONTROLLING OFFICE NAME AND ADDRESS Air Force Flight Dynamics Laboratory/FXG Air Force Systems Command Wright-Patterson Air Force Base, Ohio 45433		12. REPORT DATE April 1978
		13. NUMBER OF PAGES 126
14. MONITORING AGENCY NAME & ADDRESS (if different from Controlling Office)		15. SECURITY CLASS. (of this report) Unclassified
		15a. DECLASSIFICATION/DOWNGRADING SCHEDULE
16. DISTRIBUTION STATEMENT (of this Report) Distribution limited to U.S. Government Agencies only; test and evaluation; statement applied February 1978. Other requests for this document must be referred to A. F. Flight Dynamics Laboratory (AFFDL/FXG) Wright Patterson AFB, Ohio 45433		
17. DISTRIBUTION STATEMENT (of the abstract entered in Block 20, if different from Report)		
18. SUPPLEMENTARY NOTES		
19. KEY WORDS (Continue on reverse side if necessary and identify by block number) Aerodynamic Interference, Supersonic Aircraft, Parasol Wings, Wave Riders, Supersonic Biplanes, Flat Top Wing Bodies, Wave Cancellation, Interference Lift		
20. ABSTRACT (Continue on reverse side if necessary and identify by block number) A conceptual design study was made to identify various ways that favorable interference can increase the aerodynamic efficiency of supersonic fighter aircraft. Identification of candidate favorable interference concepts was initiated by a literature search of technical references which describe features and ap- plications of various aerodynamic concepts. The literature search revealed		

Unclassified

SECURITY CLASSIFICATION OF THIS PAGE(When Data Entered)

a number of potentially applicable aerodynamic interference concepts including ring-wings, parasol-wing arrangements, supersonic biplanes, and wave-rider concepts such as caret wings and Nonweiler wings.

The parasol wing concept was selected as most promising. Aerodynamic studies were made to formulate a number of parasol wing design guidelines.

A reference zero-interference aircraft configuration and a favorable interference configuration incorporating a double parasol wing concept were developed. The results indicate that the favorable interference concept lift/drag ratio exceeded the lift/drag ratio of the reference configuration by approximately 25 to 35%.

Test theory comparisons were made to identify the validity of the aerodynamic design and analysis methods used in the study. Existing experimental results were used when necessary to support the analytical studies.

A first cut in mission performance optimization at Mach 3.0 shows the parasol wing configuration to have a 5% improvement in range over the reference baseline. The results illustrate that a higher gross weight than the 26,000 lb limit for the parasol wing configuration would provide a more optimal aircraft.

Unclassified

SECURITY CLASSIFICATION OF THIS PAGE(When Data Entered)

FOREWORD

This is the final technical report on the application of supersonic favorable interference concepts to fighter type aircraft. This report, which has been assigned Boeing Document number D180-24059-1, for internal use, covers work performed by the Boeing Aerospace Company, Boeing Military Airplane Development, Seattle, Washington 98124. This work was under the technical direction of P. R. Gord, Air Force Flight Dynamics Laboratory/FXG, Air Force Systems Command, Wright-Patterson Air Force Base, Ohio.

Dr. H. Yoshihara was the program manager and R. M. Kulfan was the technical integrator and principal investigator. The other study members included G. O. Friebe (configuration design), B. J. Lord (aerodynamics), P. E. Osterbeck (performance) and D. J. Fraser (weights).

The work was performed under contract F33615-77-C-3056, Project 2404 "Aeromechanics", Task 240407 "Aeroperformance and Aeroheating Technology." The study period included June 1977 - January 1978.

TABLE OF CONTENTS

<u>SECTION</u>	<u>PAGE</u>
I. SUMMARY	1
II. INTRODUCTION	3
III. APPROACH	6
IV. REFERENCE CONFIGURATION AERODYNAMIC PERFORMANCE STUDIES	10
1. Preliminary Drag Estimates	10
2. Configuration Optimization	13
3. Preliminary Performance Evaluation	16
V. AERODYNAMIC INTERFERENCE CONCEPTS SELECTIONS AND EVALUATIONS	17
1. Initial Selection	17
2. Supersonic Biplanes	20
3. "Wave Rider" Configurations	20
4. Flat Top Wing/Body Configuration	26
5. Parasol Wing Investigations	27
6. Final Favorable Interference Concept Selection	39
VI. PARASOL WING AERODYNAMIC DESIGN GUIDANCE STUDIES	42
1. Parasol Planform Cutout Area	42
2. Multiple Shock Reflections	46
3. Wing/Body Incidence Effects	47
4. Parasol Lateral Curvature	47
5. Nacelle Parasol Versus Body Parasol Studies	51
6. Final Parasol Concept Selection	58
7. Double Parasol Wing Planform Development	62
VII. CONFIGURATION DESCRIPTIONS	64
1. Reference "Zero-Interference" Configuration, Model 3056-1	66
2. Favorable Supersonic Interference Configuration, Model 3056-2	71
3. Configuration Weight Comparisons	78
VIII. CONFIGURATION AERODYNAMIC AND PERFORMANCE COMPARISONS	85
1. Aerodynamic Analysis Approach	85
2. Parasol Wing A/P Optimization Studies	87
3. Aerodynamic Comparisons	90
4. Performance	98
IX. CONCLUSIONS	103
APPENDIX AERODYNAMIC METHODS SUBSTANTIATION	106
1. Aerodynamic Design and Analysis Methods	106
2. Conventional Aircraft Configurations Test Versus Theory Comparisons	111
3. Parasol Wing-Body Test Versus Theory Comparisons	111
REFERENCES	121

LIST OF ILLUSTRATIONS

<u>FIGURE</u>		<u>PAGE</u>
1	USAF Supersonic Favorable Interference Study	7
2	USAF Wind Tunnel Model Definition of the Reference Configuration	11
3	Computer Representation of the Initial Baseline Airplane	12
4	Baseline Configuration Zero Lift Wave Drag	14
5	Baseline Configuration Cruise Lift/Drag Ratio	14
6	Optimum Camber and Twist Definition	15
7	Favorable Interference Concepts	18
8	Caret and Nonweiler Wing Aerodynamics	22
9	Nonweiler Wing Geometry	23
10	Nonweiler Wing (L/D) _{MAX} , M = 3.0 Buildup	23
11	Drag Buildup at $C_L = 0.15$, M = 3.0	24
12	Anhedral Effect on Lift and Drag on a Flat Top Wing/Body	28
13	Wing/Body Lift Interference	29
14	Dihedral Effect on Body Wave Drag	32
15	Reflection Surface Effect on Body Wave Drag	33
16	Maximum Body Wave Drag Cancellation	34
17	Optimum Shroud Geometry	36
18	Interference Lift	37
19	Parasol Wing Interference Lift Dihedral Factor	38
20	Parasol Wing Configuration Features	40
21	Parasol Canard Configuration Features	41
22	Basic Body Induced Pressures (1.5 Diameters Above Body)	44
23	Effects of Wing Planform Length and Body Separation Distance	45
24	Planforms for Parasol Curvature Study	48
25	Parasol Wing Lateral Curvature Study Results	50
26	Effect of Parasol Curvature on Nacelle Wave Drag	52
27	Effect of Parasol Curvature on Body Wave Drag	54
28	Effects of Body Slenderness and Inlet Diameter on Optimum Wing/Body Separation	55
29	Effect of Nacelle Area Growth on Interference Lift	56
30	Body Parasol Wing Planform Geometry	59
31	Nacelle Parasol Wing Planform Geometry	60
32	Mach = 3.0 Nacelle Pressure Area on Final Parasol Wing Planform	63
33	Baseline Mission	65
34	Study Reference Airplane, Model 3056-1	67
35	Fuel Tanks and Weapons Installation, Model 3056-1	68
36	Reference Zero Interference Airplane General Arrangement, Model 3056-1	69

37	Favorable Interference Airplane, Model 3056-2	73
38	Fuel Tanks and Weapons Installation, Model 3056-2	74
39	Double Parasol Wing Configuration General Arrangement, Model 3056-2	75
40	Weight Comparisons	82
41	Computer Representation of Model 3056-1	86
42	Computer Representation of Model 3056-2	88
43	Double-Parasol-Wing Nacelle Optimization	89
44	Double-Parasol-Wing Camber Optimization	91
45	Reference Configuration, Model 3056-1, Drag Analysis	92
46	Double Parasol Wing Configuration Model 3056-2, Drag Analysis	93
47	Double Parasol Wing Configuration Model 3056-2, $M = 3.0$, Cruise Drag Analysis	94
48	Lift Curve Slope Comparison	95
49	Maximum Lift/Drag Ratio Comparison	96
50	Double Parasol Wing Aerodynamic L/D Improvement	97
51	Performance Evaluation	99
52	Super Cruiser Type Configuration Test-Theory Comparison	112
53	NASA Parasol Wing/Body Wind Tunnel Model	114
54	Middleton - ADASSA Analytic Model of the NASA Parawing Wind Tunnel Model	115
55	Comparison of Parasol Wing Theoretical Predictions	116
56	Lift/Drag Ratio and Interference Lift Test Versus Theory Comparisons	118
57	Comparison of Predicted Shock Locations	119

LIST OF TABLES

<u>TABLE</u>		<u>PAGE</u>
1	Relative Aerodynamic Efficiency Comparisons	19
2	Nacelle Versus Body Parasol Configuration Comparisons	61
3	Design Data	79
4	Group Weight Statement (Lb)	81
5	Weight and Balance Summary	84
6	Drag Estimation Procedures	107
7	Aerodynamic Design Methods	108

LIST OF ABBREVIATIONS AND SYMBOLS

accel	acceleration
ADASSA	aerodynamic design and analysis system for supersonic aircraft
AIC	aerodynamic influence coefficients
AR	aspect ratio
a/p	airplane
B.L.	butt line
c	chord
C_D	drag coefficient
C_{D_L}	drag-due-to-lift coefficient
C_{D_F}	friction drag coefficient
$C_{D_{WAVE}}$	zero lift wave drag coefficient
$C_{D_{SYM}}$	symmetric drag coefficient
$C_{D_{TRIM}}$	trim drag coefficient
C_{D_W}	wave drag coefficient
c.g.	center of gravity
C_L	lift coefficient
C_M	pitching moment coefficient
C_p	pressure coefficient
D	diameter, drag
deg	degree
D_p	pressure drag
EA.	each
EST	estimated

EW	empty weight
Exp.	expendable
FLEXSTAB	flexible airplane analysis computer system
F.S.	fuselage station
ft	feet
g	acceleration due to gravity
GW	gross weight
h	altitude, diverter height
in., IN.	inches
Ke	envelope drag due to lift factor
Kn	knots
L	length
lb, LB	pounds
l _B	body length
L/D	lift/drag ratio
L.E.	leading edge
M	Mach number
M.A.C.	mean aerodynamic chord
MAX.	maximum
MI., mi.	miles
MIN	minutes
nmi	nautical miles
OEW, O.E.W.	operational empty weight
OPT	optimum

OW	operating weight
P/L	payload
q	dynamic pressure
r	radius
REF.	reference
REFL.	reflection
s	distance of nacelle from wing surface
S	area
SFC	specific fuel consumption
Sh	parasol height
S.L.	sea level
STA.	station
S _w	wing area, parasol width
t	thickness
TOGW	takeoff gross weight
TSLs	sea level static thrust
T/W	thrust to weight ratio
vol	volume
W.L.	water line
W/S	wing loading
X	distance from body nose
X/C	length to chord ratio
X _{REFL}	length of body for which pressures are reflected off the wing surface
2D	two-dimensional
2y/b	nondimensional span distance

SYMBOLS

α	angle of attack
β	$\sqrt{M^2-1}$
Δ	incremental
δ	boundary layer thickness
Γ	dihedral
Λ	leading edge sweep angle
π	3.14159
θ	diverter half angle
ξ	angle relating the interference lift to the direct lift of a Nonweiler wing

SUBSCRIPTS

B	body
eq	equivalent
INTER	interference
ISOL	isolated
max	maximum
P	pressure
REF	reference

SECTION I

SUMMARY

A conceptual design study was made to identify various ways that favorable interference can increase the aerodynamic efficiency of supersonic fighter aircraft.

Identification of candidate favorable interference concepts was initiated by a literature search of technical references which describe features and applications of various aerodynamic concepts. The literature search revealed a number of potentially applicable aerodynamic interference concepts including ring-wings, parasol-wing arrangements, supersonic biplanes, and wave-rider concepts such as caret wings and Nonweiler wings.

The parasol wing concept was selected as most promising. Aerodynamic studies were made to formulate a number of parasol wing design guidelines.

A reference zero-interference aircraft configuration and a favorable interference configuration incorporating a double parasol wing concept were developed. The results indicate that the favorable interference concept lift/drag ratio exceeded the lift/drag ratio of the reference configuration by approximately 25 to 35%.

Test theory comparisons were made to identify the validity of the aerodynamic design and analysis methods used in the study. Existing experimental results were used when necessary to support the analytical studies.

A first cut in mission performance optimization at Mach 3.0 shows the parasol wing configuration to have a 5% improvement in range over the reference baseline. The results illustrate that a higher gross weight than the 26,000 lb limit for the parasol wing configuration would provide a more optimal aircraft.

SECTION II

INTRODUCTION

Aircraft capable of extended range while cruising at supersonic Mach numbers offers promise of a substantial improvement in military effectiveness, particularly for interdiction, strike, reconnaissance and interceptor missions. The incorporation of favorable interference is an effective means to increase supersonic aerodynamic efficiency. Considerable development of favorable interference technology took place in association with maneuverable orbital entry vehicle and hypersonic vehicle studies. The application of these favorable aerodynamic interference concepts to supersonic combat aircraft has not been explored in depth.

The objectives of this study included:

- Identify various ways that favorable interference can increase the aerodynamic efficiency of supersonic fighter type aircraft.
- Conduct a literature survey of technical references, which describe methods and applications of supersonic favorable aerodynamic interference.

In order to achieve these objectives, the study was structured into the following tasks

- 1) Literature survey and Bibliography compilation
- 2) Development of a reference baseline configuration from the geometrical description and baseline mission configuration supplied by the government.
- 3) Selection and evaluation of specific aerodynamic interference concepts suitable for the configuration design constraints and mission objectives.
- 4) Development of a final optimized favorable interference configuration that incorporates the best interference concepts. Evaluate the aerodynamic and weight characteristics of the optimized configuration and compare with the baseline configuration.

The study approach is presented in Section III. Sections IV, V and VI describe the development of the reference configuration, development of the favorable interference configuration, and evaluations of various interference concepts. The geometrical descriptions, aerodynamic and performance characteristics of the final study configurations are contained in Sections VII and VIII. Appendix A describes the aerodynamic design and analysis methods that have been used. This section also contains test versus theory comparisons made to validate the

use of these analytical tools to the study configurations.
Section IX presents the main conclusions of the study.

SECTION III

APPROACH

The approach used to achieve the study objectives is summarized in Figure 1.

The initial task was to develop a preliminary reference configuration. This reference configuration, which incorporates conventional aerodynamic concepts, was developed from a wind tunnel model definition and mission objectives supplied by the Air Force Flight Dynamics Laboratory.

Initial aerodynamic evaluations together with an existing data base of previous Boeing fighter and supercruise vehicle studies were used to estimate the reference aircraft preliminary size characteristics. Performance estimates were then made to determine mission radius capability. Additional studies were made to determine the mission radius capability sensitivity to design Mach number, lift/drag ratio, and to aircraft empty weight.

The fuselage of this preliminary reference configuration was "area ruled" and a minimum drag due to lift wing camber and twist definition was developed to define the aerodynamic potential of this configuration. Additionally, lower boundary estimates were made of the volume wave drag, vortex drag and lift wave drag.

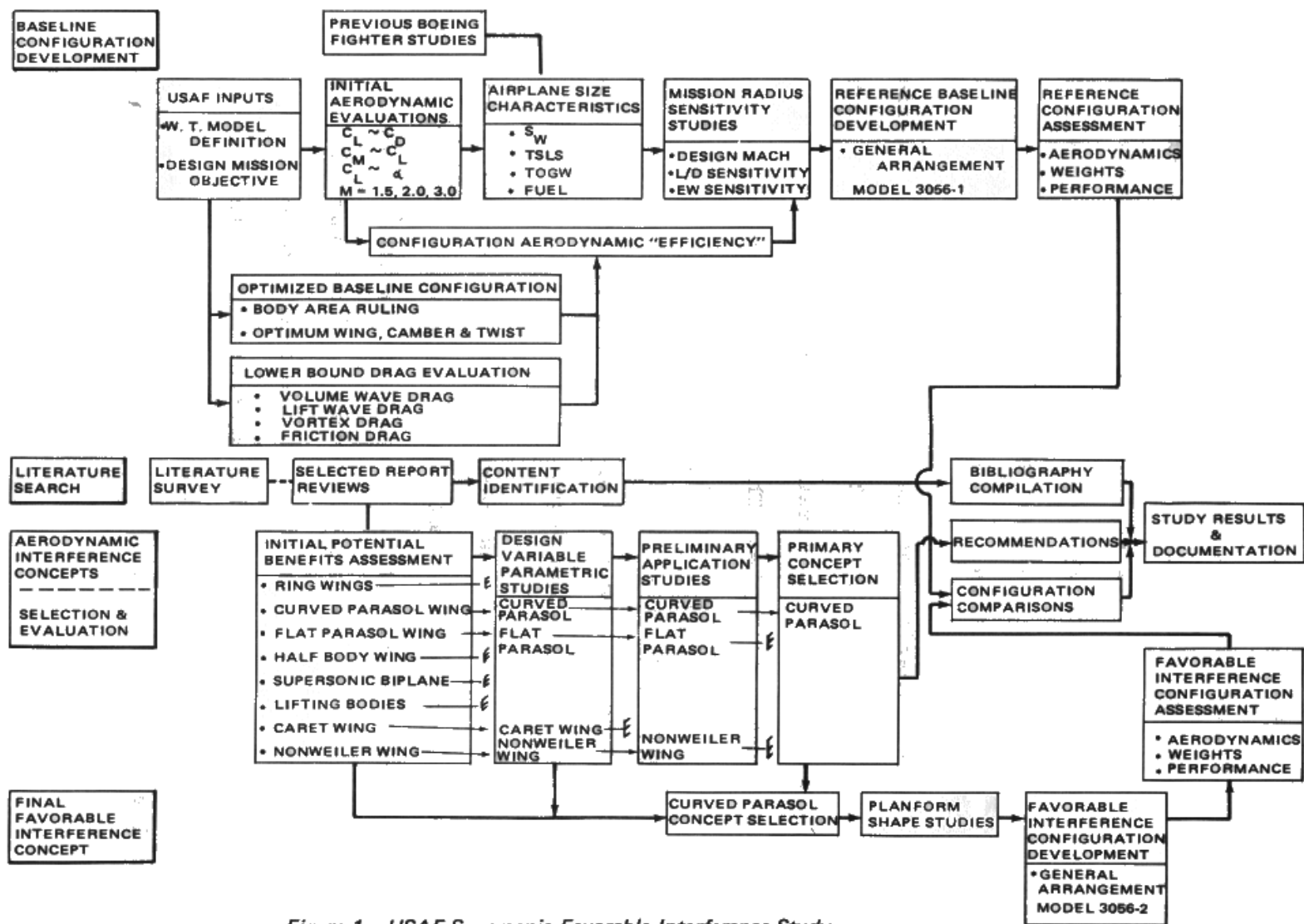


Figure 1 USAF Supersonic Favorable Interference Study

The detailed general arrangement definition of the finalized baseline configuration was developed from the preliminary reference configuration by incorporating design changes to produce a balanced aircraft configuration with necessary space and volume allotments for systems, fuel and payload requirements. Aerodynamic, and weight analyses were then made of this "zero interference" configuration.

The identification of candidate favorable interference concepts was initiated by a literature survey of technical references which describe features and applications of the various aerodynamic concepts. The literature search revealed a number of potentially applicable aerodynamic interference concepts. These concepts included ring wings, parasol-wing arrangements, supersonic biplanes, and "wave rider" concepts such as caret wings and Nonweiler wings.

Qualitative assessments were made to determine which of these concepts were most suitable for application to meet the mission and design objectives. Aerodynamic parametric evaluation studies were made to obtain a fundamental understanding of the desirable aerodynamic features of the selected concepts and to provide preliminary aerodynamic assessments. These results identified the curved wing concept as a most promising concept. Additional aerodynamic studies were then performed to support the

final definition of the favorable interference configuration design development.

The detailed general arrangement drawing of the favorable interference airplane incorporating the parasol wing concept was developed. This provided the geometrical definition necessary for final aerodynamic and weight evaluations. Comparisons were made of the geometrical, aerodynamic, performance, and weight characteristics of the baseline "zero interference" configuration and the favorable interference configuration.

Specifically conducted test versus theory comparisons were made to check and validate the aerodynamic design and analysis methods for application to the study configurations.

SECTION IV

REFERENCE CONFIGURATION AERODYNAMIC & PERFORMANCE STUDIES

This section contains the results of the aerodynamic evaluations of the preliminary reference "zero-interference" configuration. The effects of aerodynamically optimizing this configuration by area-ruling the fuselage and incorporating a minimum cruise-drag camber and twist design are also shown. Preliminary performance results along with "lower bound" drag estimates are also included.

1. Preliminary Drag Estimates

Supersonic aerodynamic evaluations were made of the initial reference zero-interference configuration as defined by the USAF wind tunnel model shown in Figure 2. Figure 3 shows the computer "modeling" that has been used to represent this configuration. The fuselage/engine arrangement has been represented as an equivalent area fuselage. The cross-sectional area of this fuselage matches the fuselage/engine cross-sectional area with the inlet stream tube area removed.

The drag calculations included:

- Friction drag
- Isolated component wave drag

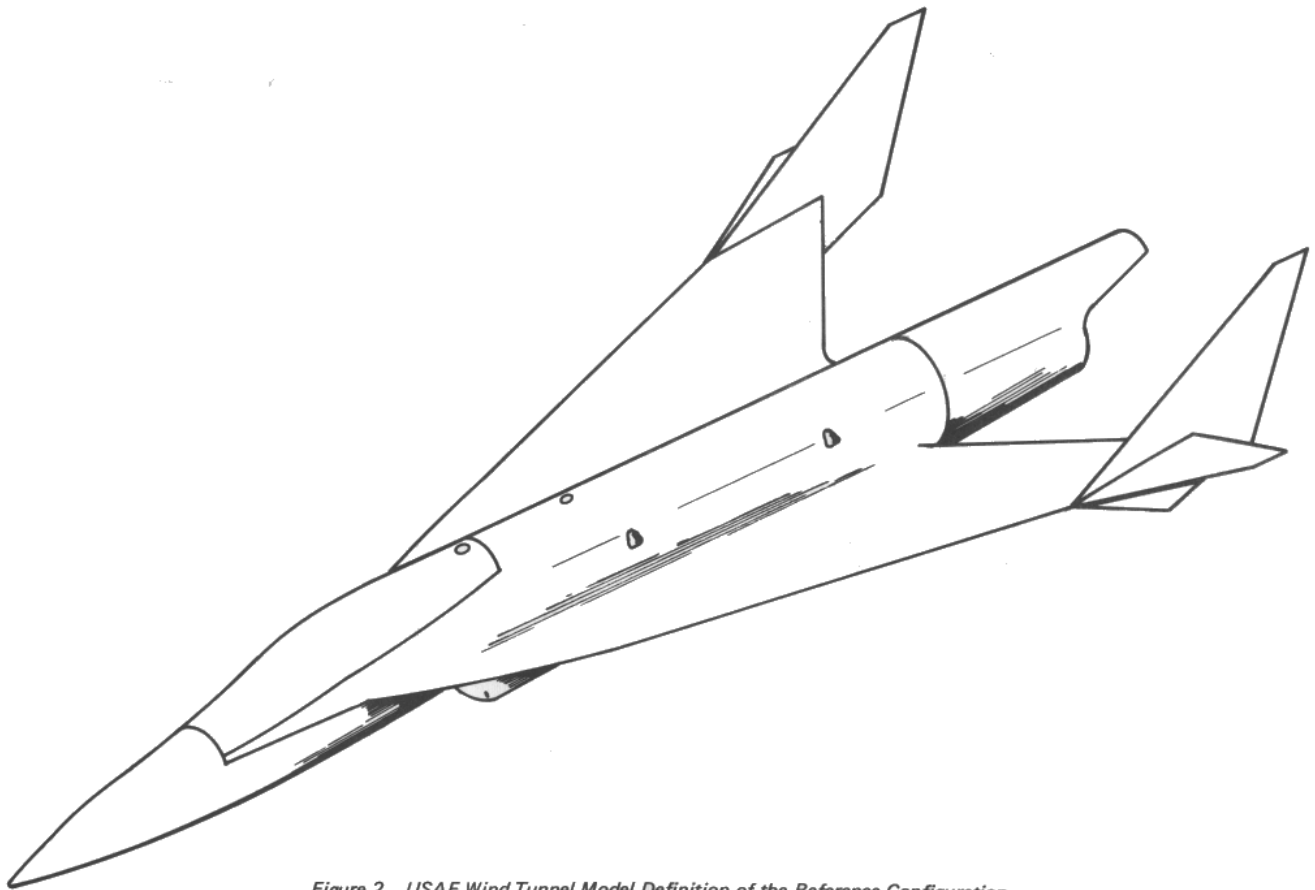


Figure 2 USAF Wind Tunnel Model Definition of the Reference Configuration

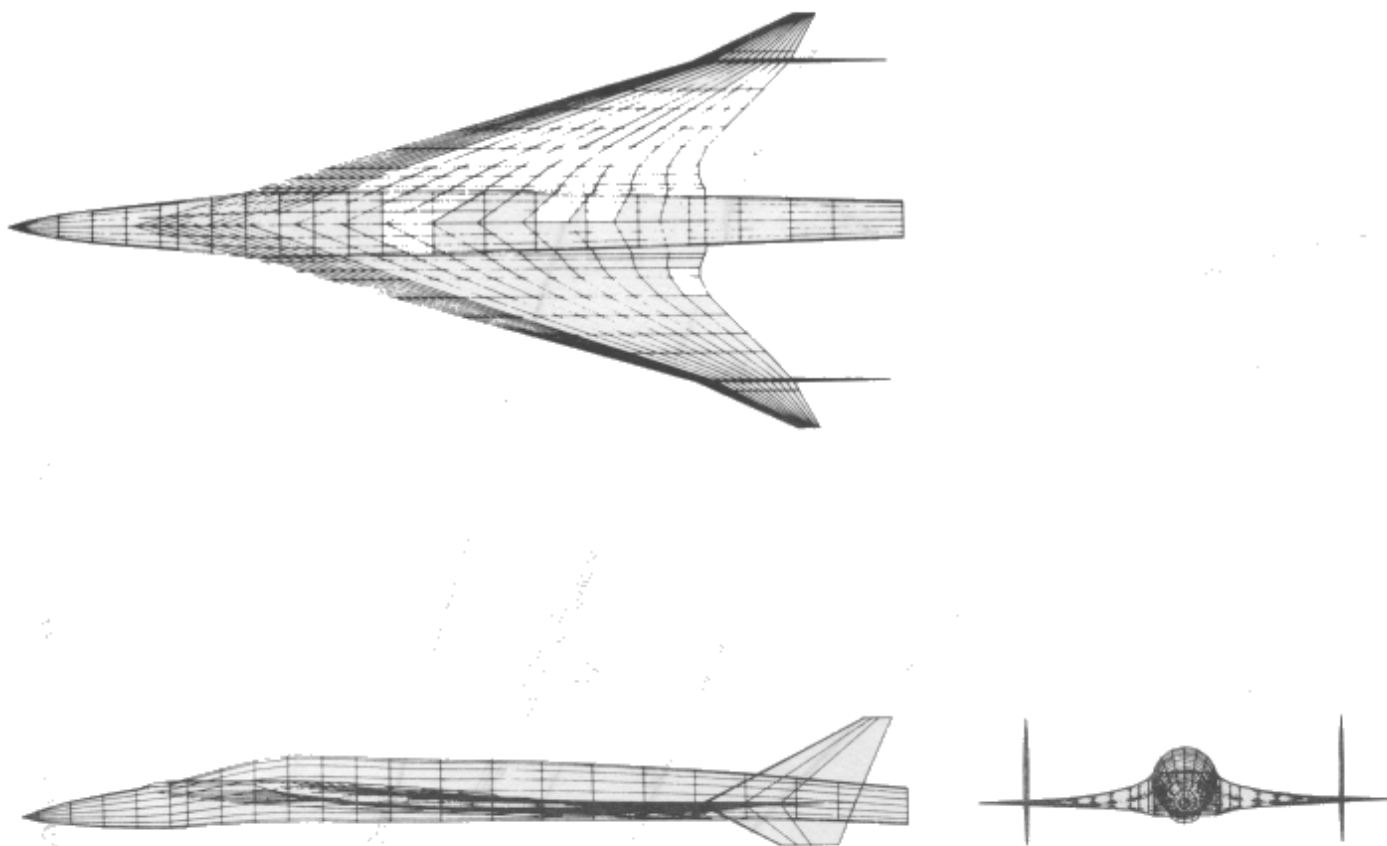


Figure 3 Computer Representation of the Initial Baseline Airplane

- Integrated configuration wave drag
- Flat wing drag due to lift
- Twisted wing drag due to lift
- Twisted wing plus body drag due to lift

The wave drag results in Figure 4 show that the reference "no interference" configuration actually has favorable interference for Mach numbers less than 2.2. At higher Mach numbers, the wave drag interference is unfavorable.

The drag due to lift calculations indicated that the wing twist reduced the drag due to lift relative to the flat wing with zero leading edge suction. The body, however, increased the drag due to lift. The lift/drag ratio comparisons of Figure 5 indicate that the reference "no interference" configuration actually experiences a slight net favorable interference over the entire supersonic cruise Mach number range.

2. Configuration Optimization

The initial reference "no interference" configuration was then "optimized" using conventional aerodynamic optimization techniques and design "tools". The fuselage was "area ruled" for a design Mach number of 3.0. In addition, an optimum wing camber shape shown in Figure 6, was determined. The Mach 3.0 cruise

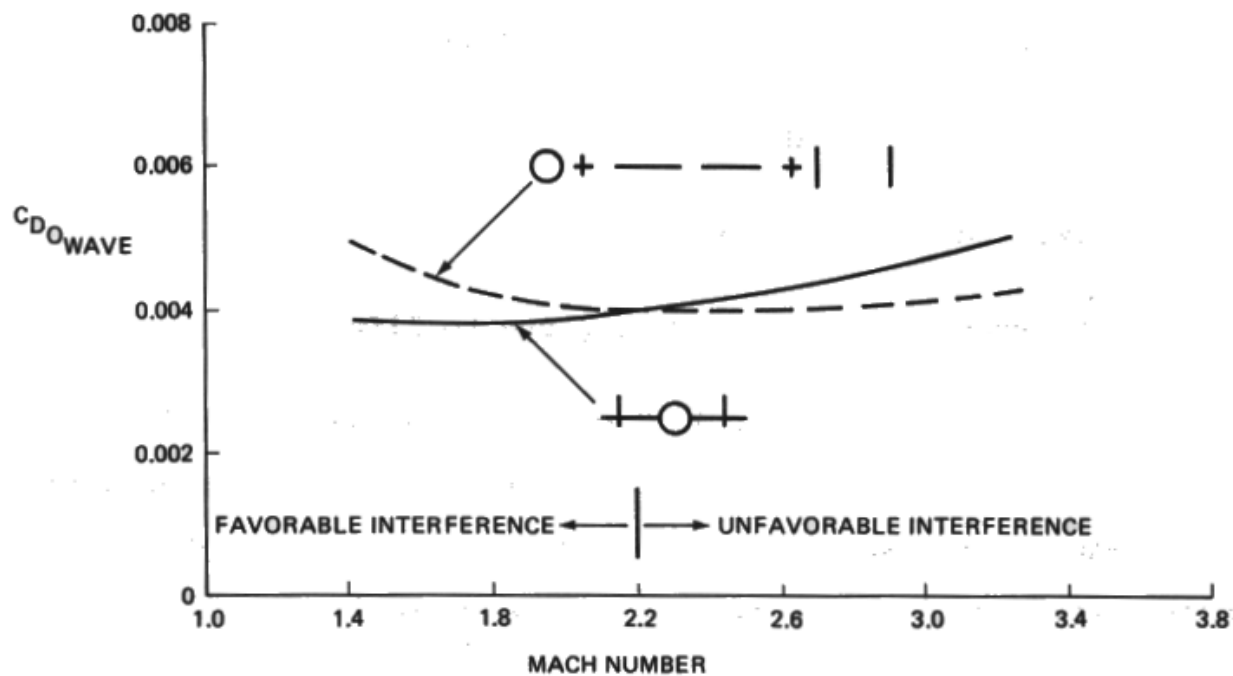


Figure 4 Baseline Configuration Zero Lift Wave Drag

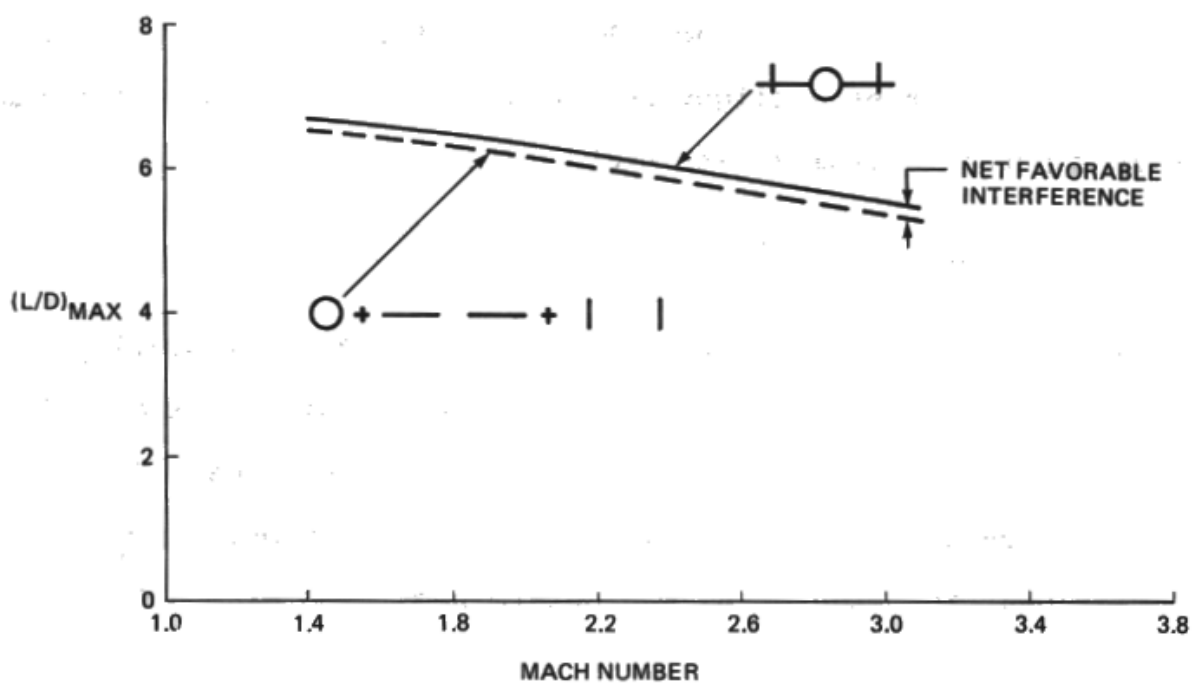


Figure 5 Baseline Configuration Cruise Lift/Drag Ratio

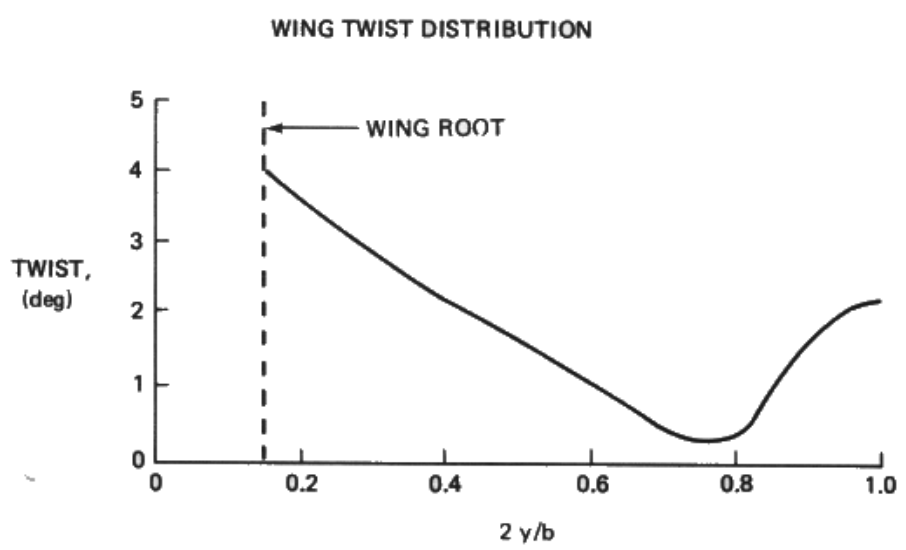
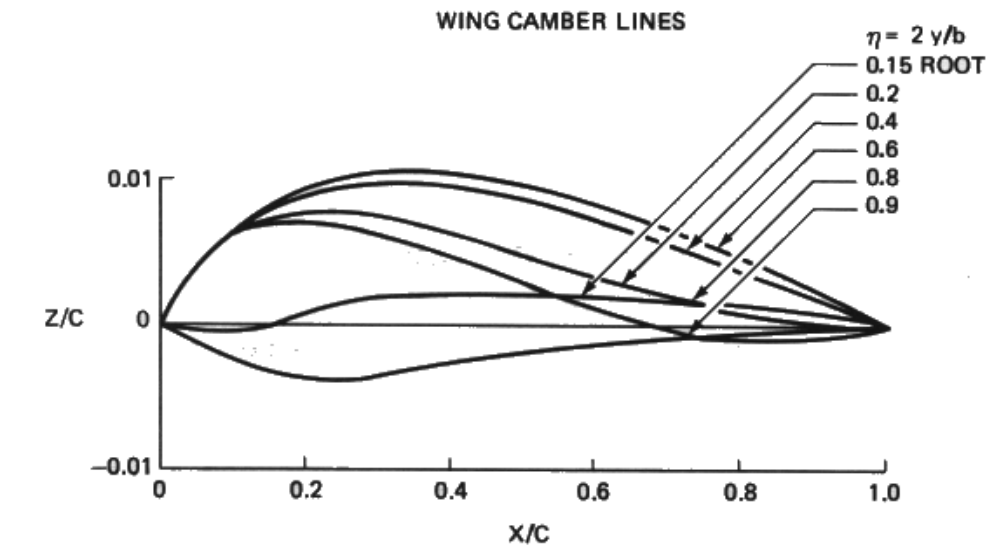


Figure 6 Optimum Camber and Twist Definition

lift/drag ratio for this configuration is 6.4. This is approximately a 16% increase over the lift/drag ratio of the reference no interference configuration ($L/D = 5.5$).

3. Preliminary Performance Evaluation

Preliminary performance calculations were made to determine the appropriate wing area and engine size for the reference configuration. A design gross weight of 26,000 lb was selected to restrict the size of the aircraft. The mission payload of 2 - 2,000 lb stores is treated as an overload condition resulting in a mission gross weight of 30,000 lb.

The required wing area is 440 ft² and the engine thrust is 21,570 lb. (sea level static). Design Mach numbers of 2.0 and 3.0 were examined. The operating weights for the reference airplane were estimated from Boeing parametric statistical weight data.

SECTION V

AERODYNAMIC INTERFERENCE CONCEPTS SELECTIONS AND EVALUATIONS

The identification of candidate favorable aerodynamic interference concepts for consideration in this study was initiated by a literature survey of technical references which describe features and applications of various interference concepts. The section describes the process by which the particular favorable aerodynamic concept was selected for integration into the final study aircraft.

1. Initial Selection

The literature search revealed a number of potentially applicable interference concepts shown in Figure 7. Qualitative assessments such as shown in Table 1 were made to determine which of these concepts were most suitable for application to meet the mission and design objectives.

The caret wing, Nonweiler wing, supersonic biplane and parasol wing concepts were then identified as the potentially most promising concepts. The study effort was then directed at obtaining a fundamental understanding of the desirable aerodynamic features of the selected concepts and to better define the potential aerodynamic efficiency of configurations

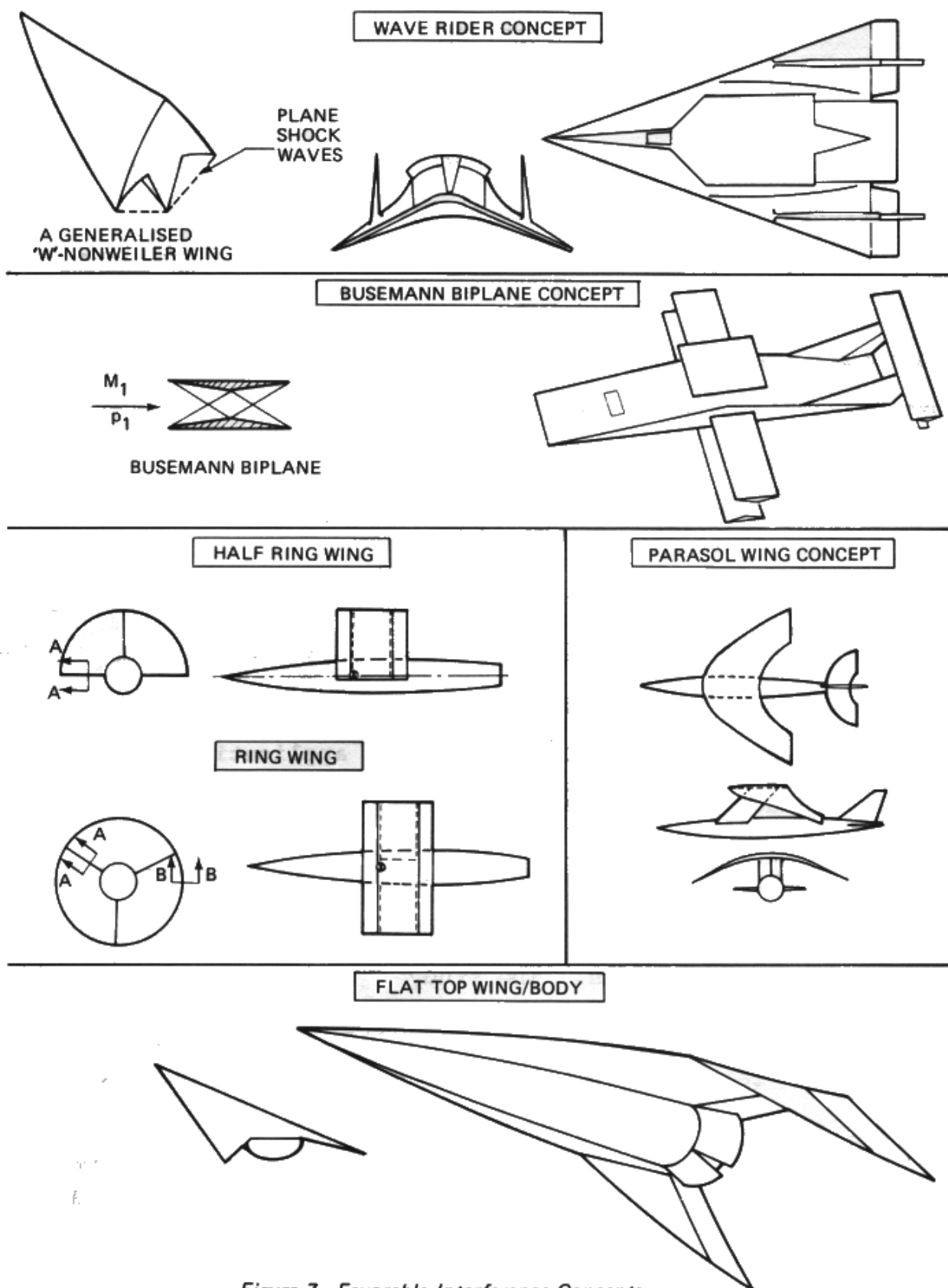


Figure 7 Favorable Interference Concepts

Table 1 Relative Aerodynamic Efficiency Comparisons (Mach 2.0 → 3.0)

AERODYNAMIC CONCEPT	AERODYNAMICALLY EFFICIENT COMPONENTS				FAVORABLE INTERFERENCE				COMPATIBILITY WITH OTHER A/P COMPONENTS			POINTS	
	LOW DRAG DUE TO LIFT	LOW VOL. WAVE DRAG	MAX. USABLE COMPONENTS	LOW WETTED AREA	INTERFERENCE DRAG				INTERFERENCE LIFT	FUSELAGE	ENGINES		TAILS
					VOL-VOL	VOL-LIFT	LIFT-VOL	LIFT-LIFT					
RING WING	○	●	○	○	●	○	○	—	—	●	○	●	1
CURVED PARASOL	●	●	●	●	●	—	●	—	●	●	●	●	15
FLAT PARASOL	●	●	●	●	●	—	●	—	●	●	●	●	15
MERGED WING/BODY	●	●	●	●	○	—	○	—	●	○	○	●	3
SUPERSONIC BIPLANE	●	●	○	○	●	—	●	—	—	●	●	●	7
LIFTING BODIES	○	●	●	●	—	—	—	—	—	●	○	●	5
CARET WING	●	●	●	●	●	●	○	●	●	●	●	●	11
NONWEILER WING	●	●	●	○	●	●	—	●	●	●	●	●	11

CODE		SCORE
—	NEGLIGIBLE	0
○	POOR	-1

CODE		SCORE
●	GOOD	+1
●	VERY GOOD	+2

IDENTIFICATION OF FAVORABLE INTERFERENCE ITEMS		
ITEM	DEFINITION	EXAMPLE
VOL-VOL	INTERACTION BETWEEN THE THICKNESS PRESSURE FIELDS OF ADJACENT COMPONENTS	NACELLE PRESSURE IMPINGING ON THE WING THICKNESS
VOL-LIFT	INFLUENCE OF A COMPONENT'S THICKNESS PRESSURE FIELD ACTING ON AN ADJACENT LIFTING SURFACE	FUSELAGE VOLUME PRESSURE FIELD ACTING ON THE WING CAMBER SURFACE
LIFT-VOL	INFLUENCE ON A COMPONENT'S THICKNESS RESULTING FROM AN ADJACENT LIFTING SURFACE'S PRESSURE FIELD	THE WING CAMBER PRESSURE FIELD ACTING ON THE FUSELAGE
LIFT-LIFT	INTERFERENCE BETWEEN LIFTING PRESSURE FIELDS OF VARIOUS CONFIGURATION COMPONENTS	AN INTERFERENCE WING'S PRESSURES INTERACTING WITH THE MAIN WING'S PRESSURES, i.e., A NONWEILER WING
INTERFERENCE LIFT	LIFT RESULTING FROM THE PRESSURE FIELD OF AN ADJACENT COMPONENT IMPINGING ON A WING SURFACE	BODY PRESSURES REFLECTING OFF THE LOWER SURFACE OF A PARASOL SURFACE

incorporating the concepts. Results of these investigations are summarized in the sections that follow.

2. Supersonic Biplanes

The Busemann supersonic biplane offers the potential of significant reduction in wing thickness wave drag (1, 2, 3, 4, 5). The drag reductions can be obtained by mutual thickness interference and also by interference between wing lift and wing thickness. The Busemann biplane type of interference is commonly called "wave cancellation" since the shock waves produced by one surface are cancelled by an expansion pressure field produced on the adjacent surface.

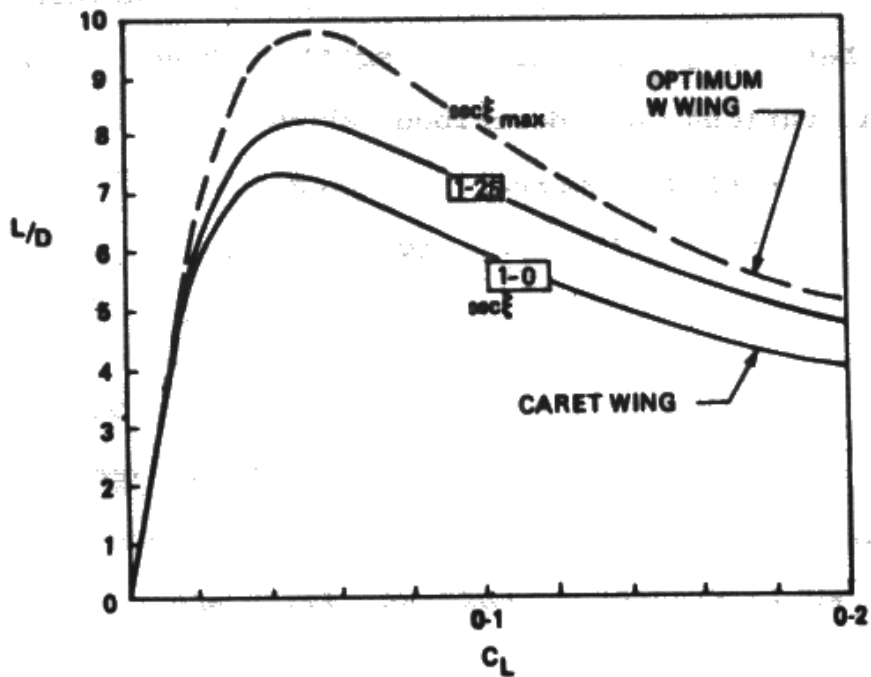
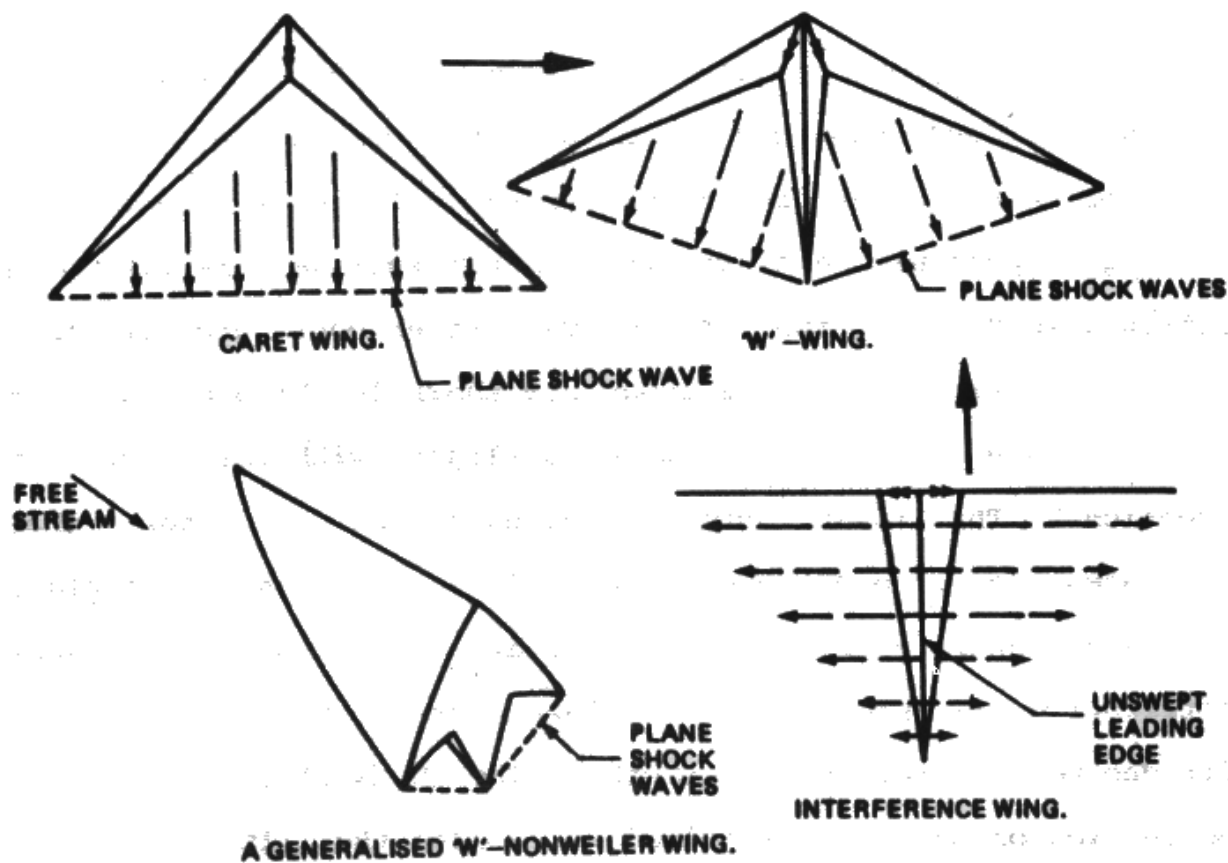
To achieve the drag reduction, adjacent reflection surfaces are necessary. The reflection surface increases the friction drag. Additionally, the wing planform is required to have a supersonic leading edge, which tends to increase the drag due to lift at supersonic speeds. The drag due to lift can be reduced somewhat by optimization of the camber and twist distribution. However, the net aerodynamic benefits of a supersonic biplane are considered typically small and were not investigated further in the study.

3. "Wave Rider" Configurations

Previous hypersonic studies (6, 7, 8, 9, 10, 11) have indicated that "wave rider" concepts such as the caret wing and the Nonweiler wing offer higher aerodynamic efficiency potential at very high supersonic Mach numbers than conventional slender wing configurations. The two types of wave rider configurations that have been considered in this study are shown in Figure 8. The upper surface of the caret wing is aligned with the freestream direction. The lower surface increases as a wedge that terminates in an open base. The leading edge lies in the plane shock wave generated by the thickness growth. A uniform pressure distribution is produced on the lower surface thereby producing lift due to the thickness growth. The Nonweiler wing is a combination of Caret wings joined to enhance the lift production.

At high Mach numbers both lift by upper surface suction pressures and base drag tend to be small. Hence, the "wave rider" configurations as described above having lift only produced by lower surface compression pressures and also having large base areas offer relatively high lift/drag ratios as shown in Figure 8.

At lower Mach numbers both suction lift and base drag are important. Consequently aerodynamic evaluations were made of these wave rider concepts at the design Mach number = 3.0. The results are shown in Figures 9 through 11. Exact shock wave



THE PERFORMANCE OF 'W'-WINGS AT $M = 4$
WITH $C_{Df} = 0.0028$.

Figure 8 Caret and Nonweiler Wing Aerodynamics

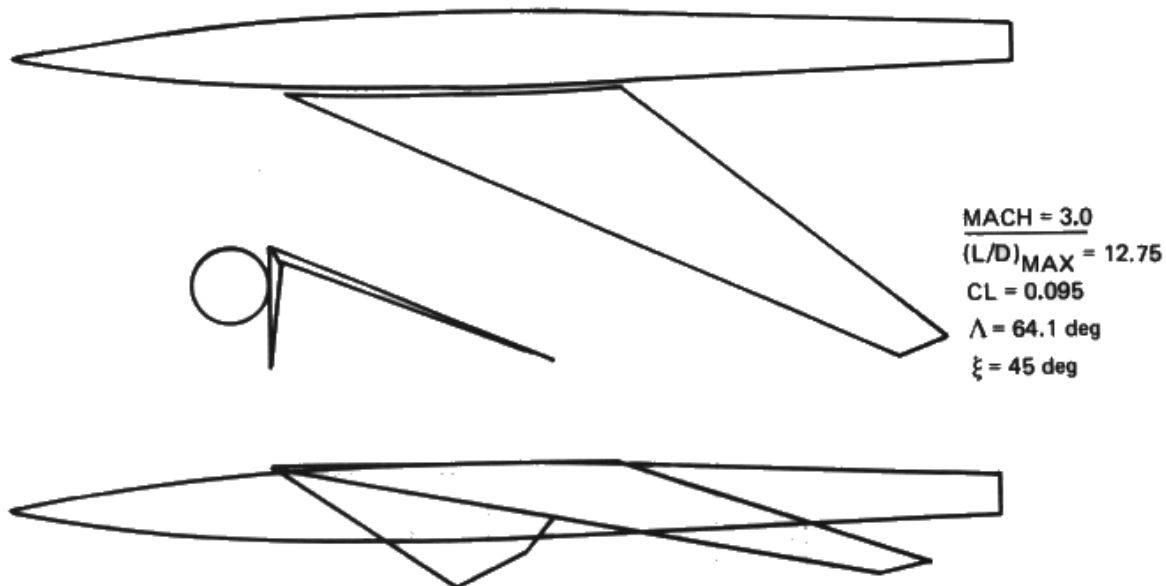


Figure 9 Nonweiler Wing Configuration Geometry

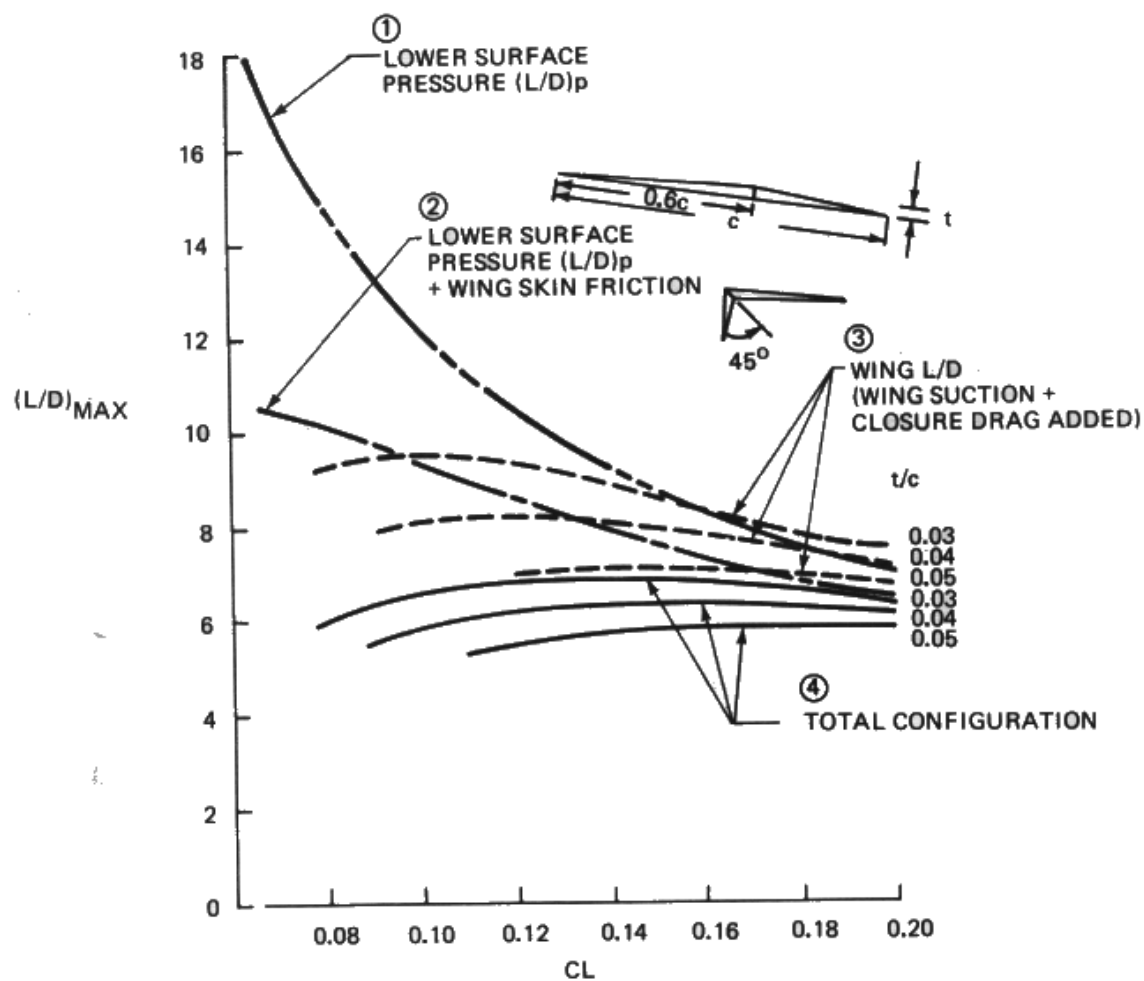


Figure 10 Nonweiler wing $(L/D)_{MAX}$ $M=3.0$ Buildup

CONFIGURATION	$C_L (L/D)_{MAX}$	$(L/D)_{MAX}$
INITIAL REFERENCE	0.120	5.49
OPTIMIZED INITIAL REFERENCE	0.132	6.40
NONWEILER	0.150	6.35

NOTE: CANOPY AND STORE
DRAG NOT INCLUDED

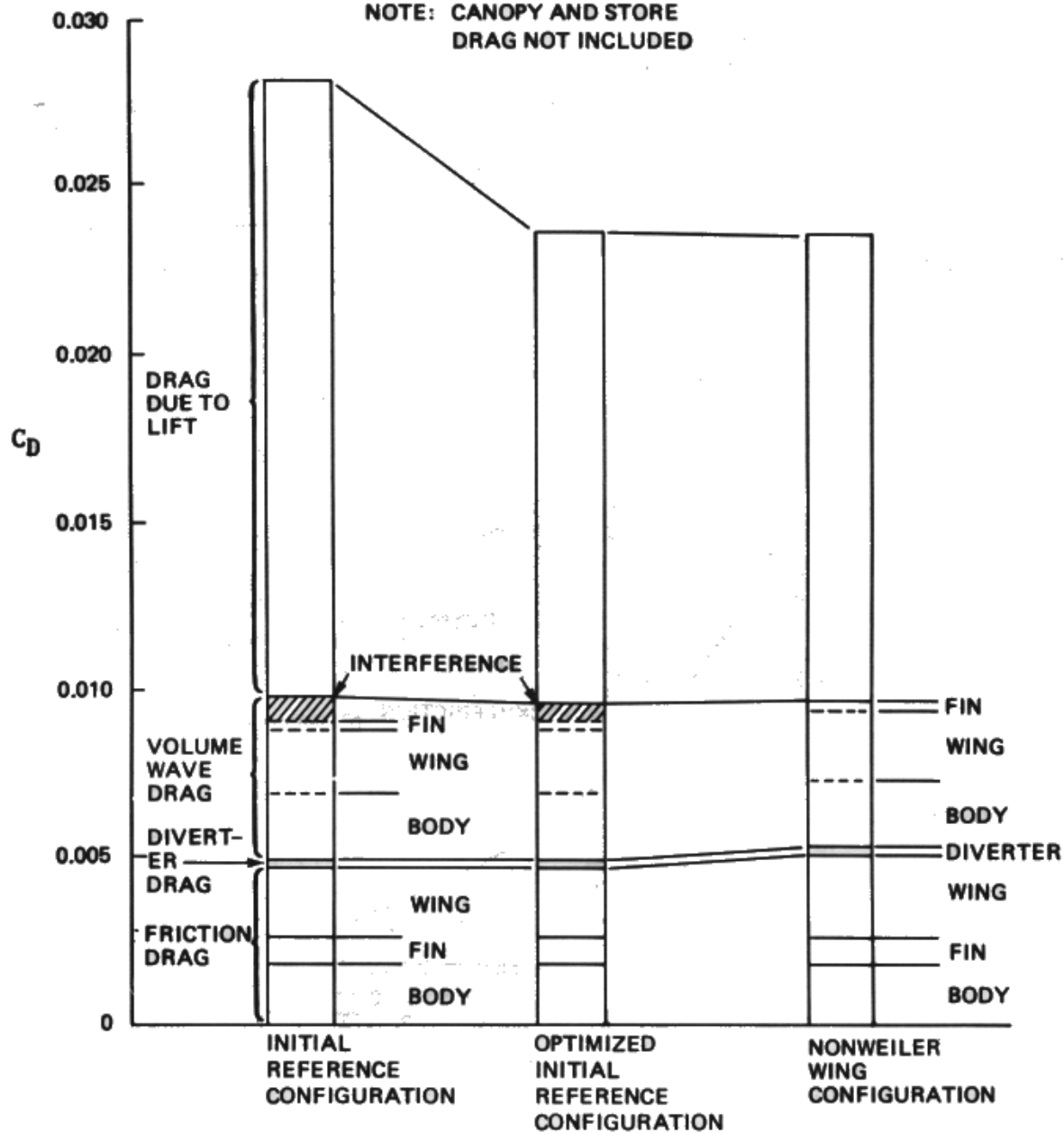


Figure 11 Drag Buildup at $C_L = 0.15$, $M = 3.0$

equations were used to determine the wing leading edge sweep and to estimate the maximum inviscid lift/drag ratios $(L/D)_{P_{MAX}}$ of the caret and Nonweiler "W" wing. The results indicated that the "W" wing concept had a greater $(L/D)_{MAX}$ potential.

Estimates were then made to determine the $M = 3.0$ lift/drag ratio of a configuration incorporating the Nonweiler "W" wing concept. The body and wing planform used for this study are shown in Figure 9.

In order to identify the impact on lift/drag ratio of integrating the Nonweiler wing concept into an airplane configuration, the following analyses were made:

- 1) Isolated Nonweiler wing with the upper surface aligned with the free stream and with zero base drag. The lift and drag are the forces associated with the lower surface compression pressures.
- 2) The skin friction drag on the upper and lower surfaces was then included.
- 3) The wing upper surface was then modified to close the airfoils at the trailing edge. Double wedge airfoil sections were selected. The wing thickness/chord ratio, and the chordwise location of the maximum thickness were varied. These changes introduced upper

surface suction lift and drag of the "closed" Nonweiler wing.

- 4) The friction and wave drag of the fuselage and fins were added to obtain the total configuration L/D values.

Results of these studies, such as shown in Figure 10, indicate that integrating the Nonweiler wing into an airplane configuration reduced the $(L/D)_{MAX}$ potential from 18 for the basic isolated wing without closing, to approximately 6.4 for the complete airplane. The suction lift produced by closing the wing airfoils more than compensated for the upper surface pressure drag and resulted in an increase in aerodynamic efficiency, (L/D) at the higher lift coefficients. The location of the wing maximum thickness was not found to be important. Increased wing thickness and the drag of the body and fins have a significant effect on L/D .

Drag build up's from Section IV for the preliminary reference configuration and optimized initial configuration are compared with the Nonweiler configuration in Figure 11. The L/D of the Nonweiler configuration is about equal to that of the optimized reference airplane.

4. Flat Top Wing/Body Configuration

An alternate form of a "wave rider" concept is the flat top wing body arrangement. This configuration produces interference lift associated with the body area growth under the wing. The body produces a conical shock. The wing leading edge coincides with the shock wave produced by the body. This configuration has been studied by previous investigations (7, 12, 13, 14, 15, 16, 17, 18) as a possible configuration concept for high supersonic Mach numbers.

The lift produced by the flat top wing/body combination can be increased by wing anhedral as shown in Figure 12.

The body wave drag for equal base areas is, however, also increased by the wing anhedral. Additionally, as shown in Figure 13, the configuration experiences unfavorable interference drag between the wing and body at lifting conditions so that the improvement in lift-drag ratio over a symmetric wing body arrangement is relatively small.

5. Parasol Wing Investigations

Previous investigations (16, 19 to 32) have shown that the parasol wing/body arrangement can combine wave-cancellation and interference lift effects into an aerodynamically efficient design. The body in a parasol wing arrangement is positioned below the wing so that at supersonic speeds the bow shock and

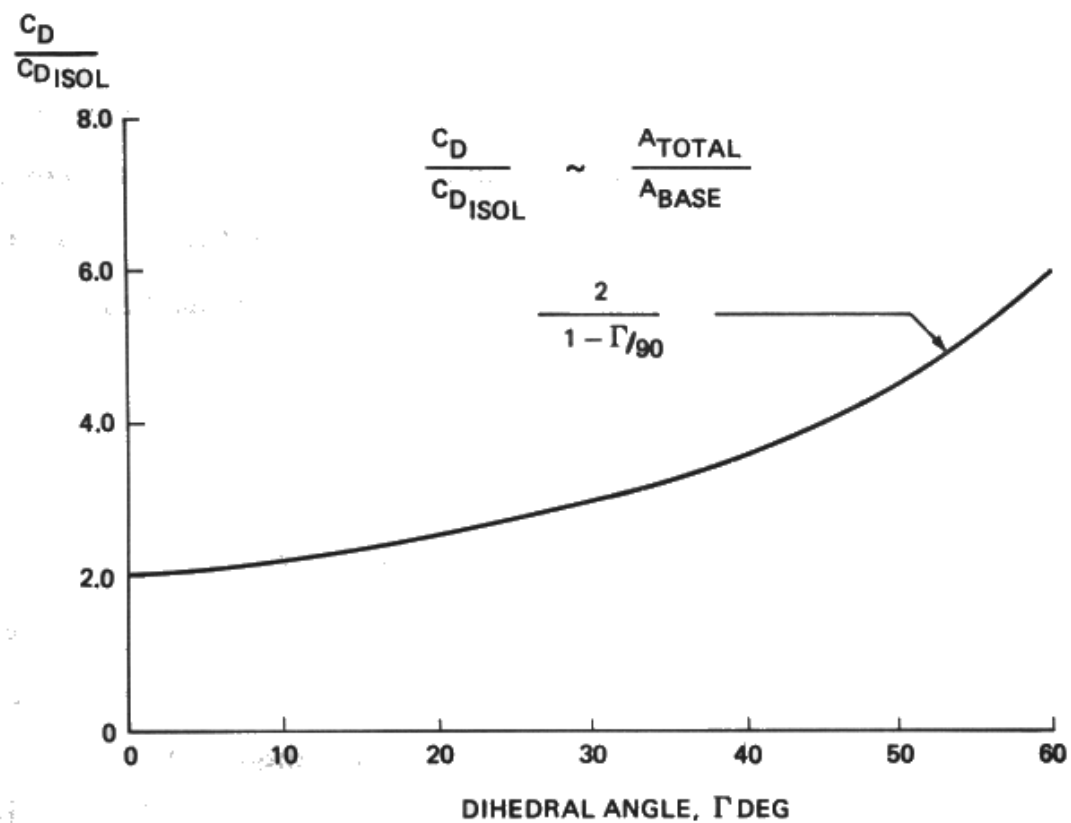
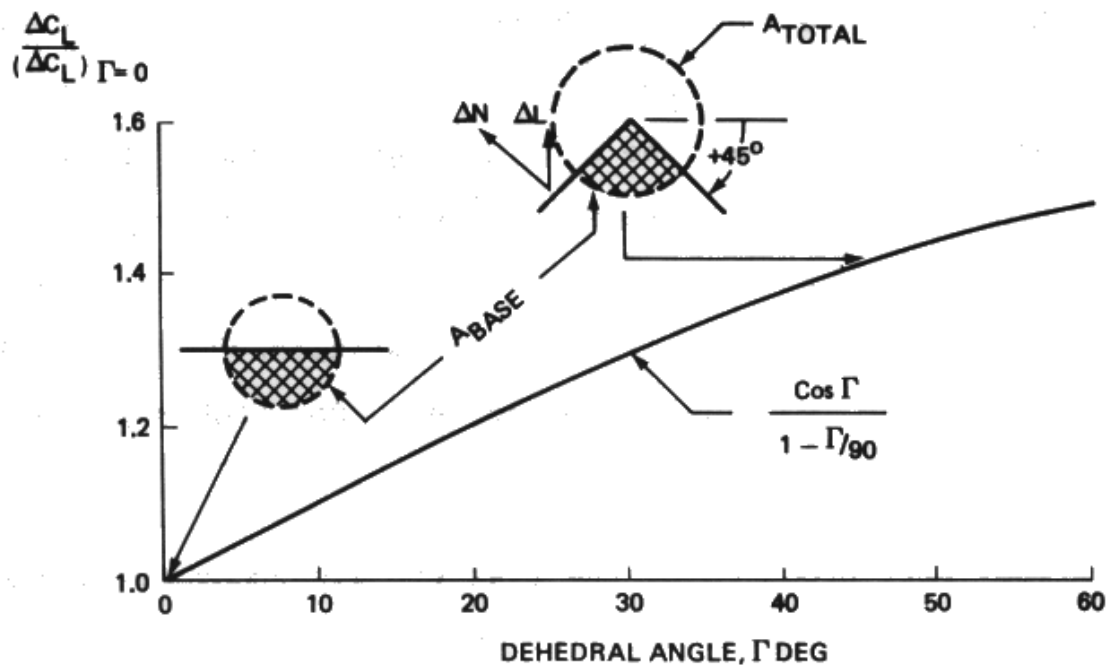


Figure 12 Anhedral Effect on Lift and Drag on a Flat Top Wing Body



BODY COMPRESSIONS
CREATE LIFT AT ZERO
ANGLE OF ATTACK



AT ANGLE OF ATTACK,
LIFTING WING PRESSURES
ACT UNFAVORABLY ON
BODY



FOR SAME FRONTAL AREA,
SYMMETRIC ARRANGEMENT
HAS LESS WAVE DRAG AT ZERO LIFT

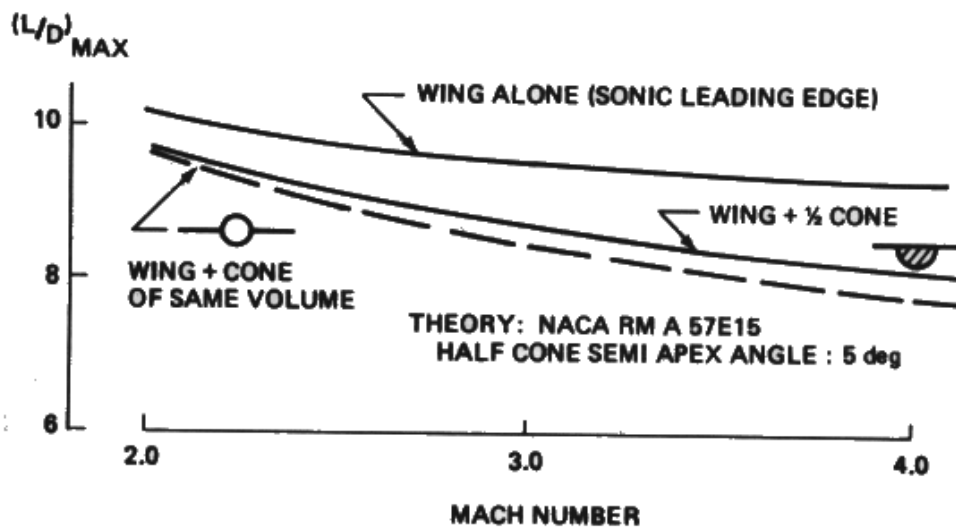


Figure 13 Wing/Body Lift Interference

forebody pressure field impact on the wing lower surface. The body wave cancellation effect is produced by the body pressures glancing off the wing surface and back onto the aft end of the body producing a thrusting force. The body pressures reflecting off the wing also produce an interference lift force.

Parametric studies were made to investigate body wave drag cancellation and lift interference generation for a body located below a wing. The objective of these investigations was to provide design guidance for defining study configurations employing the parasol wing concept. The results are summarized in this section.

The body geometry used in the wave drag cancellation studies was a minimum wave drag body having the same length, base area, maximum area, and forebody area distribution as the analysis body for the reference "no interference" configuration. The study variables included:

- wing/body spacing distance
- rectangular shroud and half shroud geometries
- forebody fineness ratio and aft body closure

The analyses were made for Mach = 3.0. However, the results can be applied to other Mach numbers by scaling the spacing distances by the ratio $\beta_{M=3.0}/\beta$; $\beta^2 = (M^2 - 1)$.

The study focused on identifying the importance of body spacing, wing dihedral and parasol curvature effects for enhancing the body wave drag cancellation.

The effect of wing dihedral and body spacing on body wave drag is shown in Figure 14. The effects of flat wing reflection, 45% dihedral wing, half shroud wing and full shroud wing on body wave drag are shown in Figure 15. The results of these two studies are summarized in Figure 16. The optimum half shroud arrangement reduced the body wave drag by nearly 50%.

The analysis body which represents an optimized version of the initial baseline configuration has a finite base area equal to the body + engine aft area minus the inlet streamtube area. Greater percentage drag reductions could be achieved with a closed body.

Additional wave drag analyses were made of the simple rectangular half-shrouded wing arrangement. Shroud geometries having different ratios of shroud width, S_w , to shroud height, S_h , were investigated. For each arrangement the shroud height was varied to determine the minimum drag arrangement. The

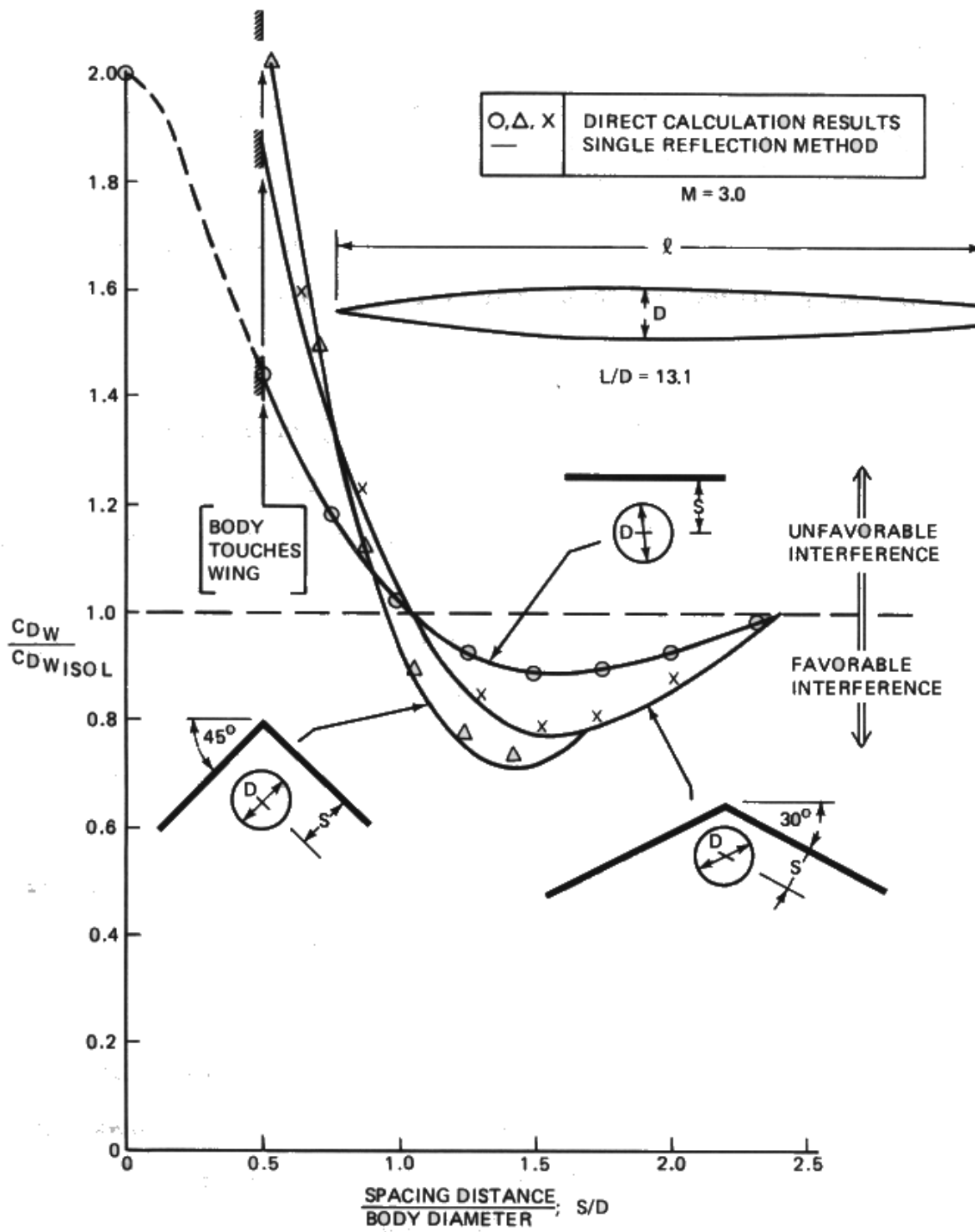


Figure 14 Dihedral Effect on Body Wave Drag

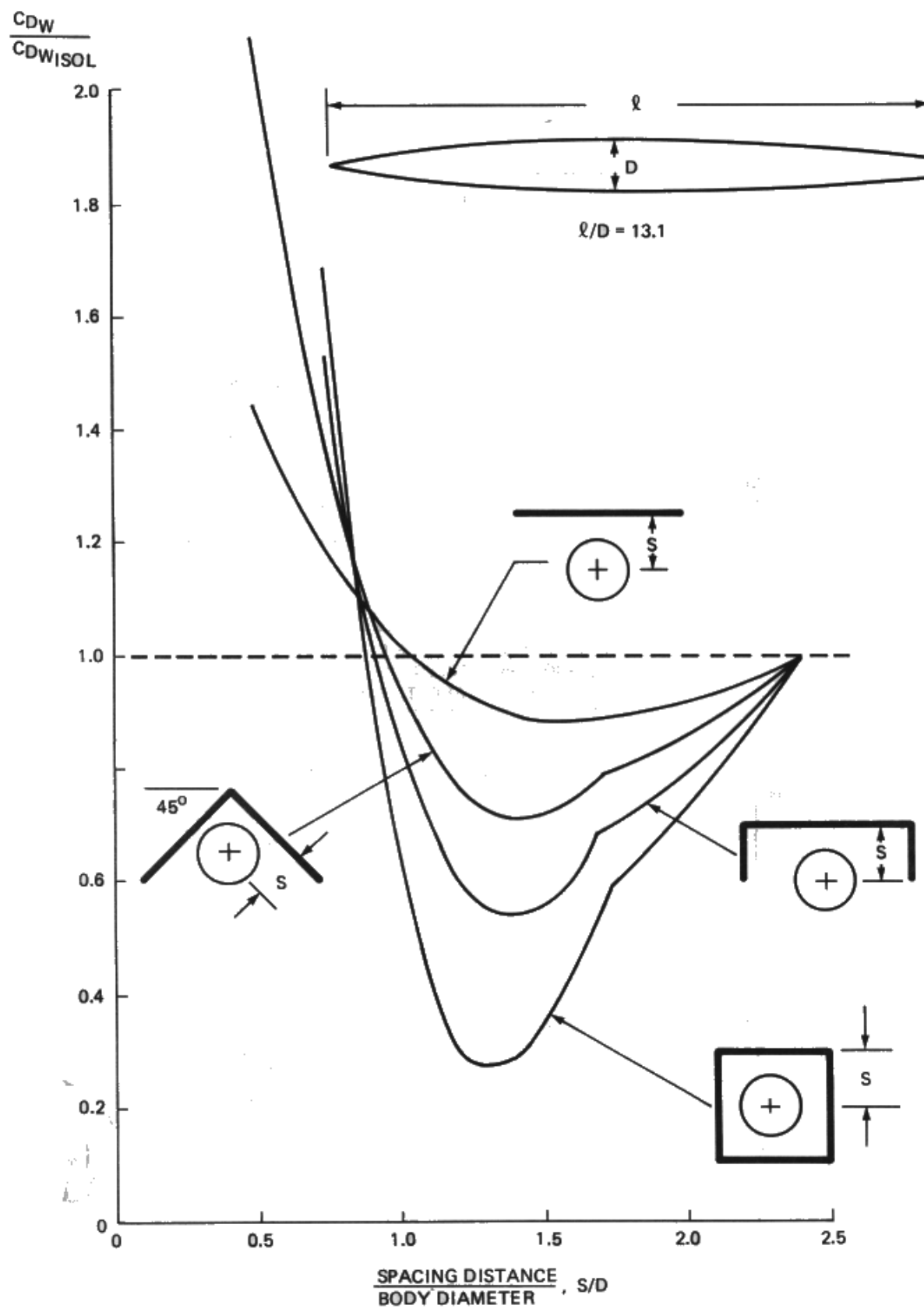
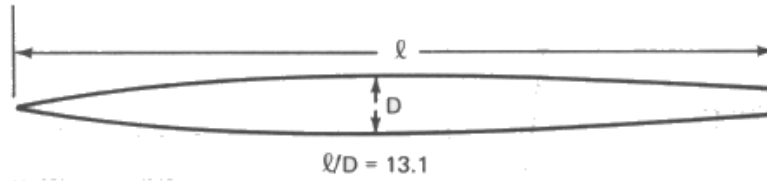
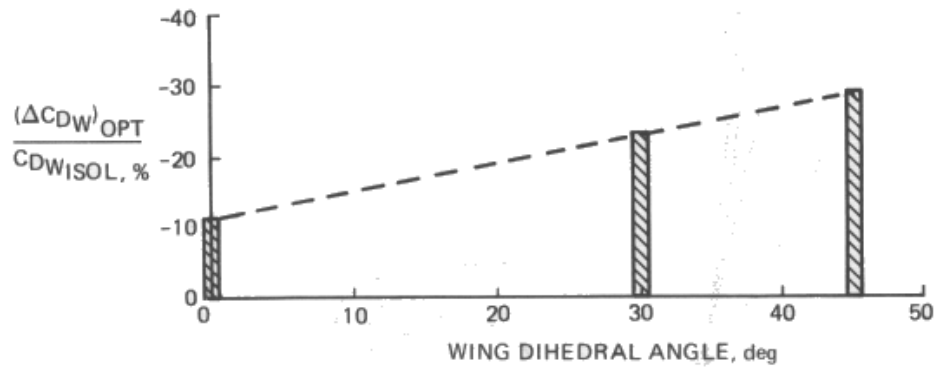


Figure 15 Reflection Surface Effect on Body Wave Drag

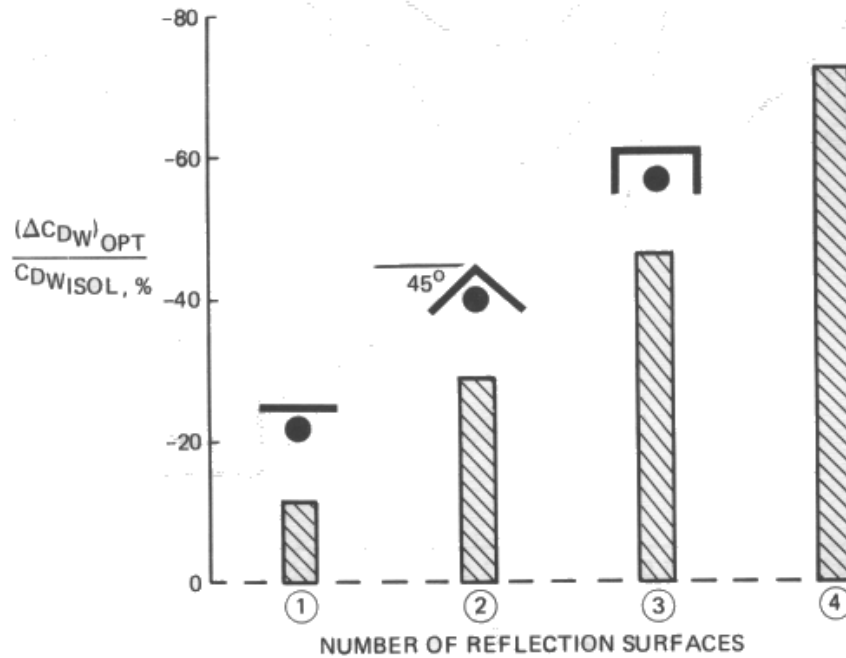


MAXIMUM BODY WAVE DRAG REDUCTION—
WING ANHEDRAL EFFECT



- MACH = 3.0
- OPTIMUM BODY/
WING SPACING

MAXIMUM BODY WAVE DRAG
REDUCTION—EFFECT OF
NUMBER OF REFLECTION SURFACES



- MACH = 3.0
- OPTIMUM BODY/
WING SPACING

Figure 16 Maximum Body Wave Drag Cancellation

optimum shroud geometries for the rectangular shroud and the equivalent elliptic shroud are shown in Figure 17. These results indicate that for a design Mach number of 3.0, a low drag elliptic shroud should have a semi-span of 1.8 to 1.9 body diameters and be located 1.2 to 1.5 diameters above the body centerline.

The body pressures acting on the reflection surfaces of the flat wing, dihedral wing, or half shrouded wing produce an interference lift associated with the pressures reflecting off the wing surface. The amount of interference lift depends on the portion of body pressures captured by the wing surface. As shown by the slender body theory estimates in Figure 18, capturing the forebody pressures can result in an interference lift coefficient of 0.025. This is approximately 25% of the cruise lift coefficient. Hence, a significant reduction in drag due to lift could be potentially achieved with this interference lift.

Slender body theory has been used to estimate the effects of wing anhedral on the interference lift. The results shown in Figure 19 indicate that the effect of anhedral angle on interference lift is exactly the same as predicted for the flat top wing/body arrangement (Figure 12).

These results show that the parasol wing and flat top wing/body concepts are equally efficient in producing

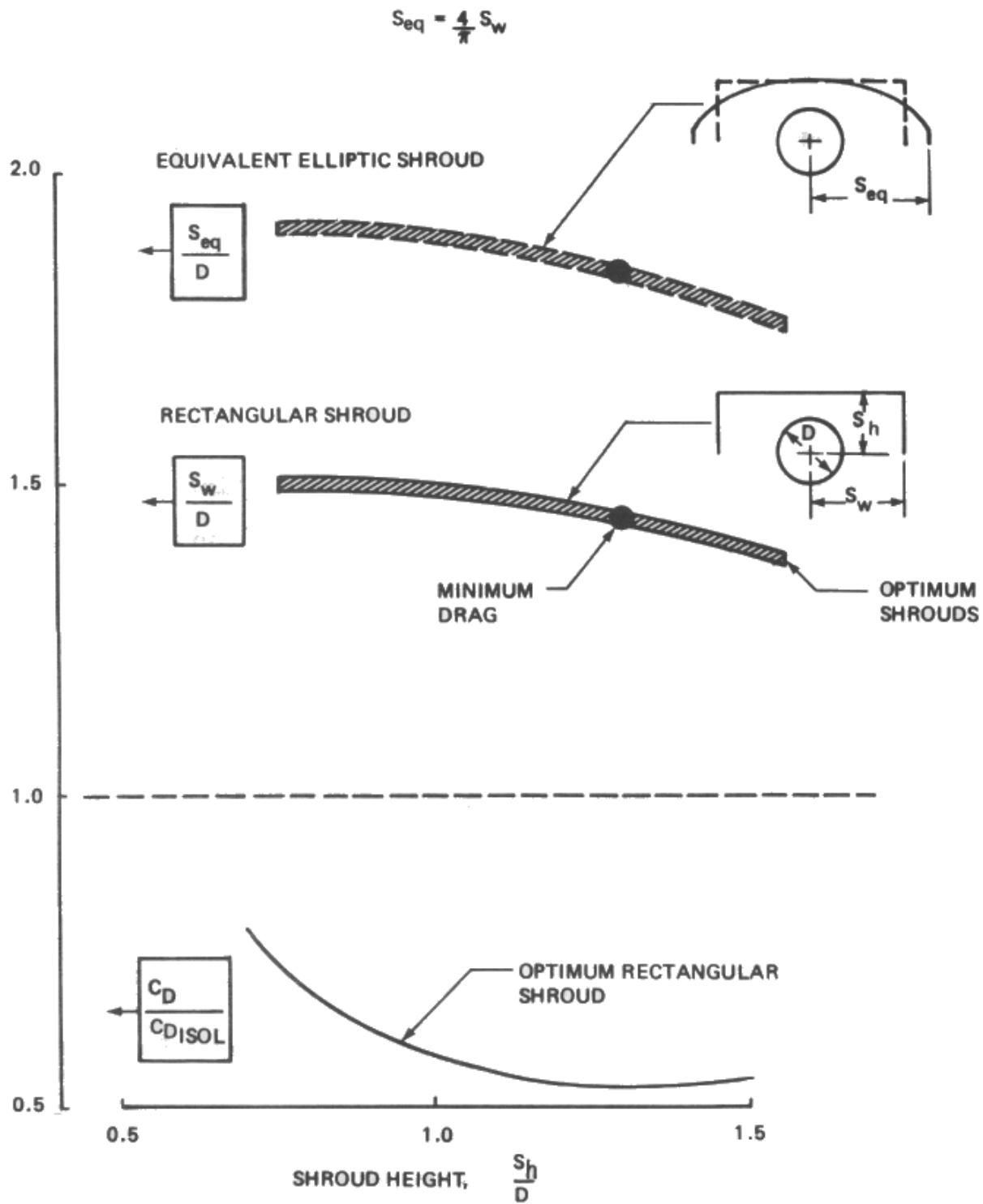


Figure 17 Optimum Shroud Geometry

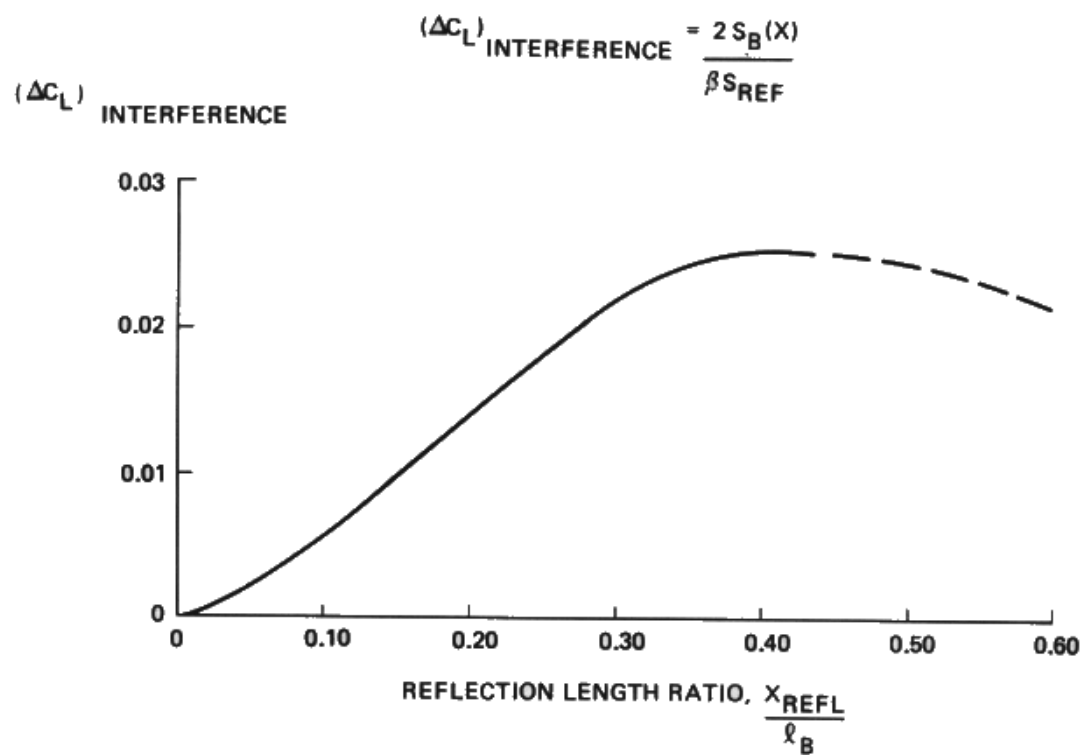
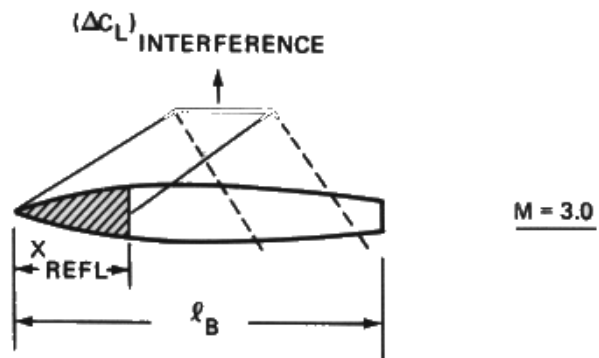


Figure 18 Interference Lift

$$\Delta C_L = \frac{2 k_F \Delta_{BASE}}{\beta S_{REP}}$$

$$k_F = \frac{\Delta C_L}{\Delta C_{L_F = 0^\circ}}$$

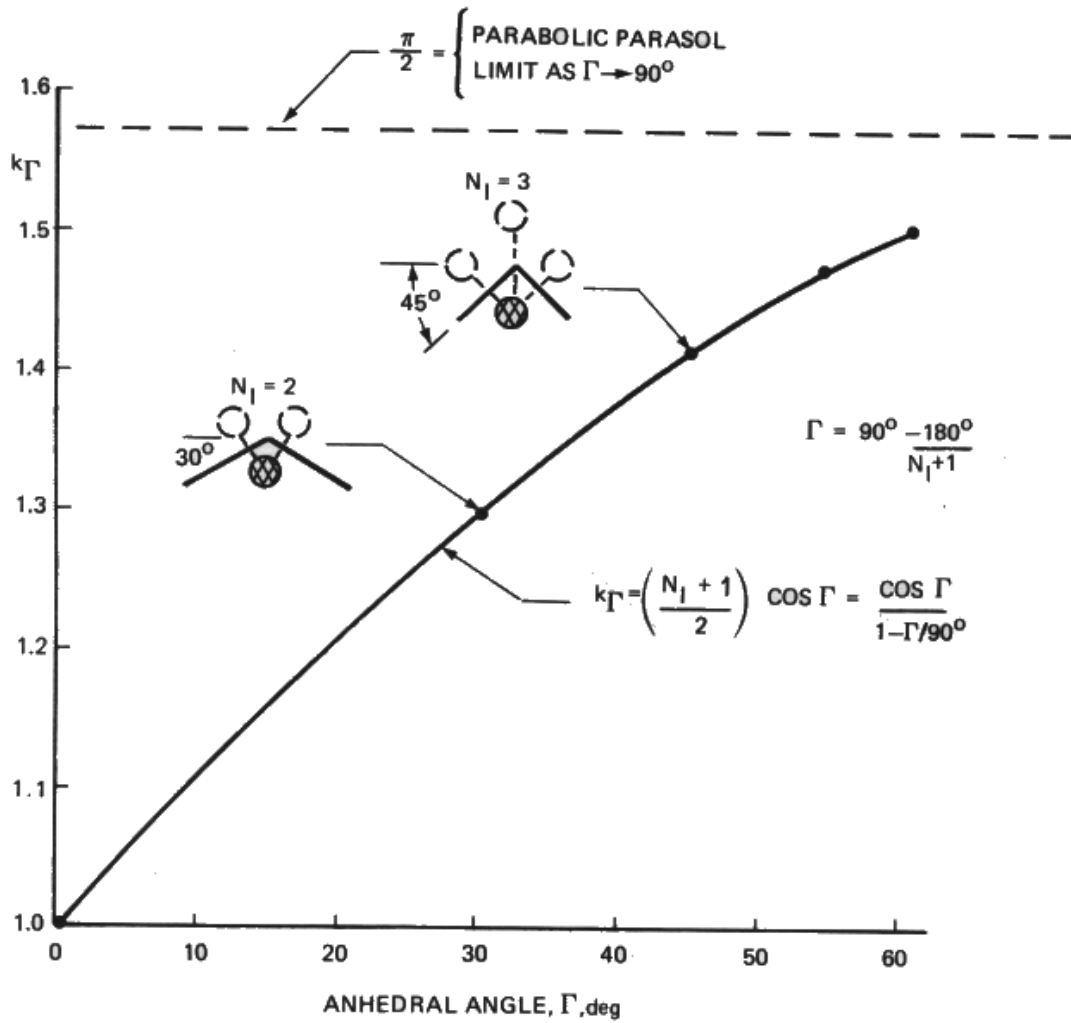
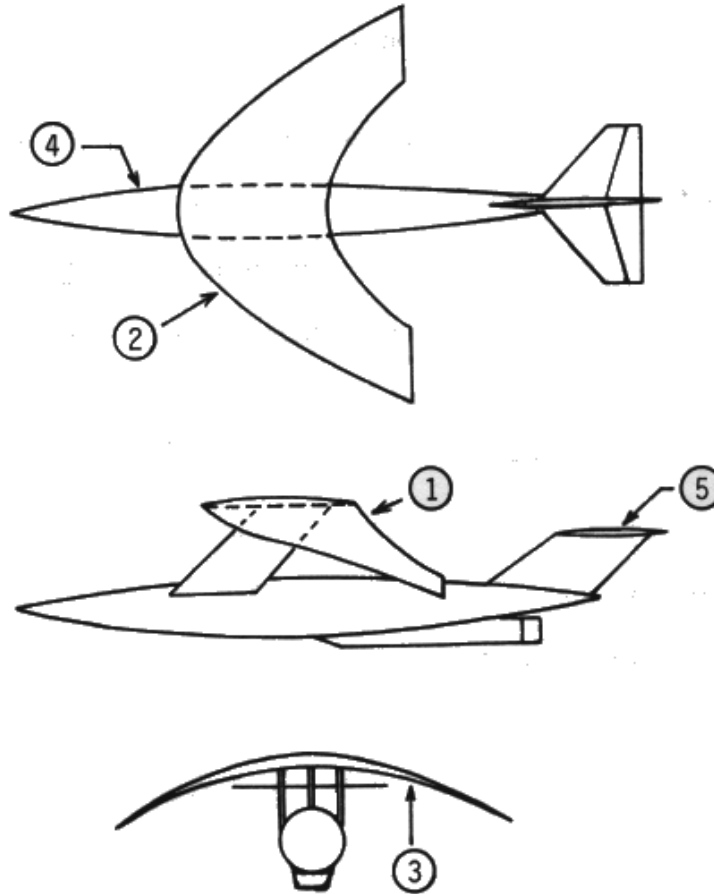


Figure 19 Parasol Wing Interference Lift Dihedral Factor

interference lift. The parasol wing by virtue of the wave cancellation effects has lower body wave drag as well as more favorable wing/body interference drag.

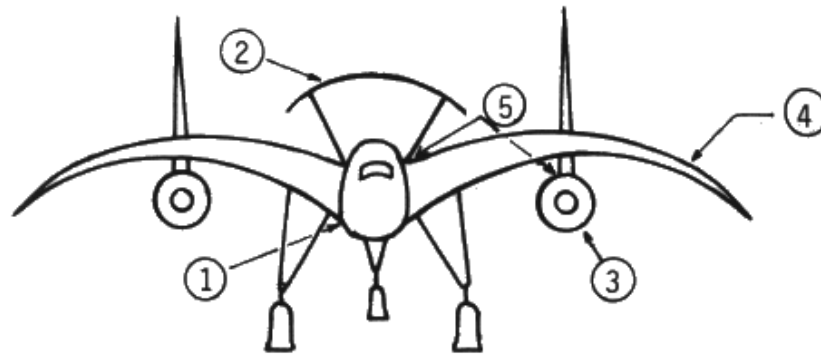
6. Final Favorable Interference Concept Selection

The aforementioned studies have indicated that the parasol wing concept offered the greatest aerodynamic potential for achieving the design mission objectives. Studies were then made to integrate the parasol concept into an aircraft configuration. Two configuration arrangements that were considered are shown schematically in Figures 20 and 21. Additional aerodynamic studies were conducted to provide design guidance for developing the final parasol wing arrangement. The results of these studies are discussed in Section VI.



DESIGN FEATURES		AERODYNAMIC OBJECTIVES
①	CAMBERED PARASOL WING	CAPTURE FOREBODY INTERFERENCE FOCUS REFLECTED PRESSURES OF AFT BODY FOR MORE CANCELLATION EFFECT OPTIMIZE BODY/WING VOLUME/LIFT INTERFERENCE
②	PARABOLIC PLANFORM SHAPE	MINIMIZE WING CAPTURE AREA
③	PARABOLIC CURVATURE	MAXIMIZE BODY INTERFERENCE LIFT
④	AREA RULED CAMBERED BODY	OPTIMIZE BODY WAVE CANCELLATION EFFECTS
⑤	HIGH TAIL	AVOID BODY REFLECTION PRESSURES

Figure 20 Parasol Wing Configuration Features



DESIGN FEATURES		AERODYNAMIC OBJECTIVES
①	AREA RULED BLENDED WING BODY	<ul style="list-style-type: none"> • LOW FRONTAL AREA • REDUCE WETTED AREA • FAVORABLE BODY/WING VOLUME INTERFERENCE
②	VARIABLE INCIDENCE PARABOLIC PARASOL CANARD	<ul style="list-style-type: none"> • CAPTURE FOREBODY/CANOPY INTERFERENCE LIFT • MAXIMIZE CAPTURED LIFTING PRESSURES • FOCUS REFLECTED PRESSURES ON AFT BODY FOR WAVE CANCELLATION EFFECT • MINIMIZE TRIM DRAG
③	WING STRUT AFT MOUNTED NACELLES	<ul style="list-style-type: none"> • CAPTURE NACELLE INTERFERENCE LIFT • NACELLE WAVE DRAG CANCELLATION BY REFLECTION • NACELLE ON WING THICKNESS FAVORABLE INTERFERENCE • WING LIFTING PRESSURE/NACELLE BOATTAIL FAVORABLE INTERFERENCE
④	CAMBERED WING WITH PARABOLIC CURVATURE	<ul style="list-style-type: none"> • MINIMIZE DRAG DUE TO LIFT • MAXIMIZE NACELLE INTERFERENCE LIFT • OPTIMIZE NACELLE/WING VOLUME/LIFT INTERFERENCE
⑤	LOCALIZED AREA RULING AND CONTOURING	<ul style="list-style-type: none"> • MINIMIZE STRUT WAVE DRAG

Figure 21 Parasol Canard Configuration Features

SECTION VI

PARASOL WING AERODYNAMIC DESIGN GUIDANCE STUDIES

Theoretical aerodynamic studies were made to investigate the following parasol wing/body design characteristics:

- Parasol wing planform area cutout
- Parasol height
- Body/parasol relative incidence effects
- Parasol lateral curvature (anhedral/dihedral) effects
- Nacelle parasol characteristics (open nose body)
- Body versus nacelle parasol selection
- Double parasol planform development

The theoretical studies were supplemented where possible with results of several previously conducted Boeing wind tunnel test programs (29, 30, 31) and available experimental results of other sources (23, 26, 27, 28).

1. Parasol Planform Cut Out Area

Surface pressure distributions, bow shock locations and body interference pressures acting on a planar surface above the body were calculated using ADASSA⁽⁸⁾.

The theoretical pressure distribution calculated on a planar wing 1.5 body diameters above the basic body is shown in Figure

22. This pressure distribution reveals a negative pressure region, which diminishes the lift produced by the positive pressures. If this region is eliminated by a wing cut out along a line where the pressure coefficient is zero, appreciably higher interference lifts can be obtained than the maximum values predicted by slender body theory.

Theoretical predictions of interference lift for planforms tailored to capture only the positive pressures are shown in Figure 23. Interference lift is seen to increase dramatically over the slender body theory maximum value. The results do not indicate a significant effect of the wing/body separation distance. This is because the theory does not account for multiple shock reflections that can actually further increase the interference lift. This is discussed further in the section below.

Note that the wing capture area grows rapidly as the streamwise length increases or as the parasol height increases. The net effect is that the interference lift coefficient based on the total wing capture area decreases with increasing parasol height or streamwise length.

The above results suggest the following design guidelines:

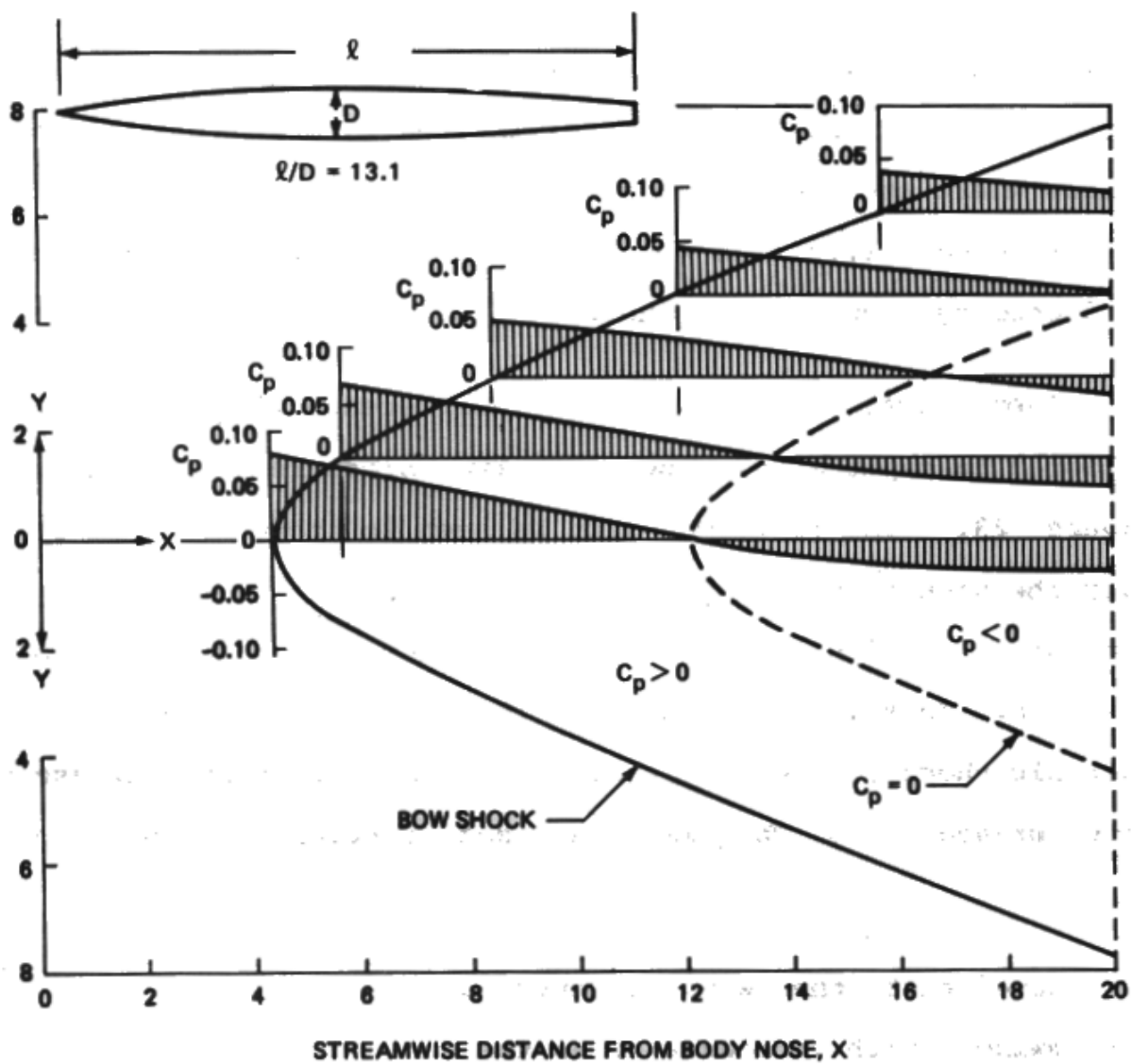


Figure 22 Basic Body Induced Pressures (1.5 Diameters Above Body)

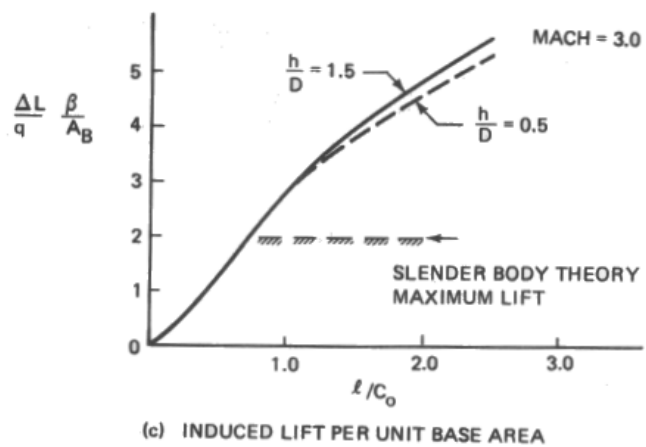
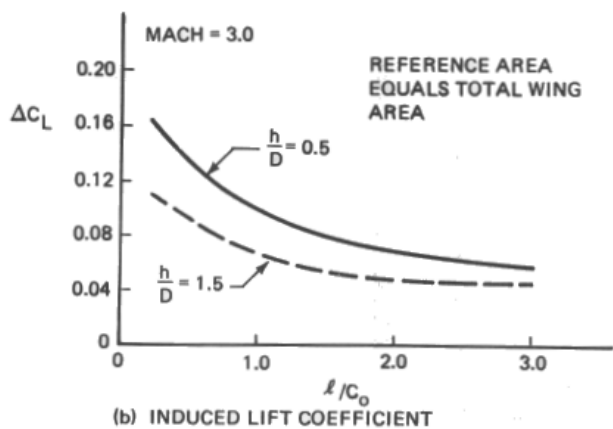
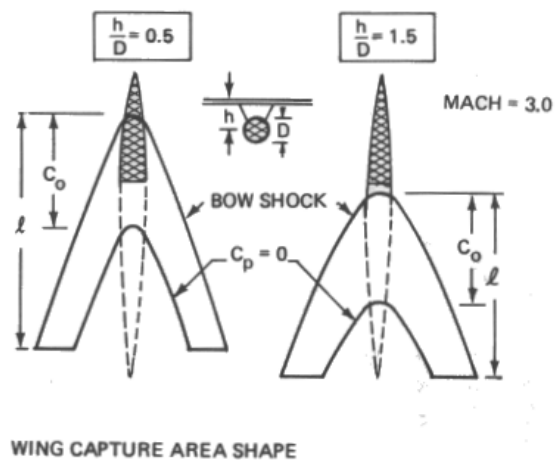
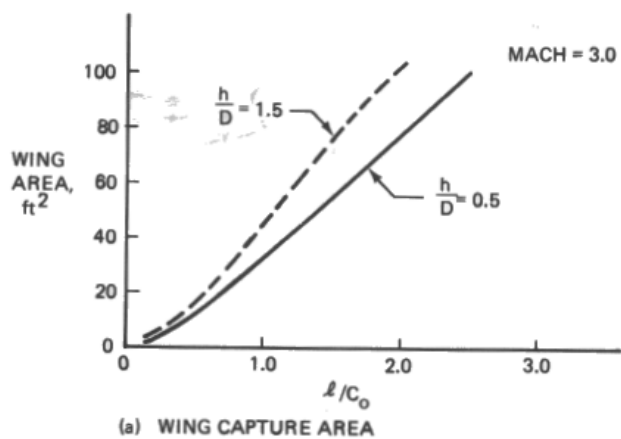


Figure 23 Effects of Wing Planform Length and Body Separation Distance

DESIGN GUIDELINE 1. To minimize the capture area and maximize the interference lift, design the wing planform so that the leading edge matches the body bow shock in the plane of the wing, and the trailing edge cuts off any negative interference pressures on the wing.

DESIGN GUIDELINE 2. "ADASSA" which predicts body bow shocks using Witham's theory can be used for determining the wing shape.

2. Multiple Shock Reflections

Experimental interference lift data (29, 31) obtained with a number of different body geometries indicate large increases in interference lift as the separation distances are decreased. This is the result of multiple shock reflections between the body and the wing. This shock reflection increased the lift on the wing but had an insignificant effect on the bodies.

DESIGN GUIDELINE 3. The interference lift can be increased by reducing the "gap" to permit multiple reflections between the body and wing. Linear theory can predict the effect of small "gaps" on drag but not the effect on interference lift.

3. Wing/Body Incidence Effects

Experimental studies reported in References 24 and 30 investigated the effect of the incidence angle between the wing and body. The results indicate a significant effect on the interference lift. Rotating the body nose down increases the interference lift. Conversely, increasing the body attitude decreases the interference lift.

DESIGN GUIDELINE 4. The interference lift can be increased by mounting the body nose down relative to the wing. The effect on drag is small.

4. Parasol Lateral Curvature

The results obtained using slender body theory in Section V indicate that parasol wing anhedral can be used to amplify the interference lift. A study was made to determine if FLEXSTAB could predict this effect.

The wing planforms evaluated for this study were derived from the NASA parasol wing planform that was used for the test versus theory comparisons in Appendix A. The study planforms are shown in Figure 24. The minimum distance between the body and each planform was held constant.

WIND TUNNEL MODEL

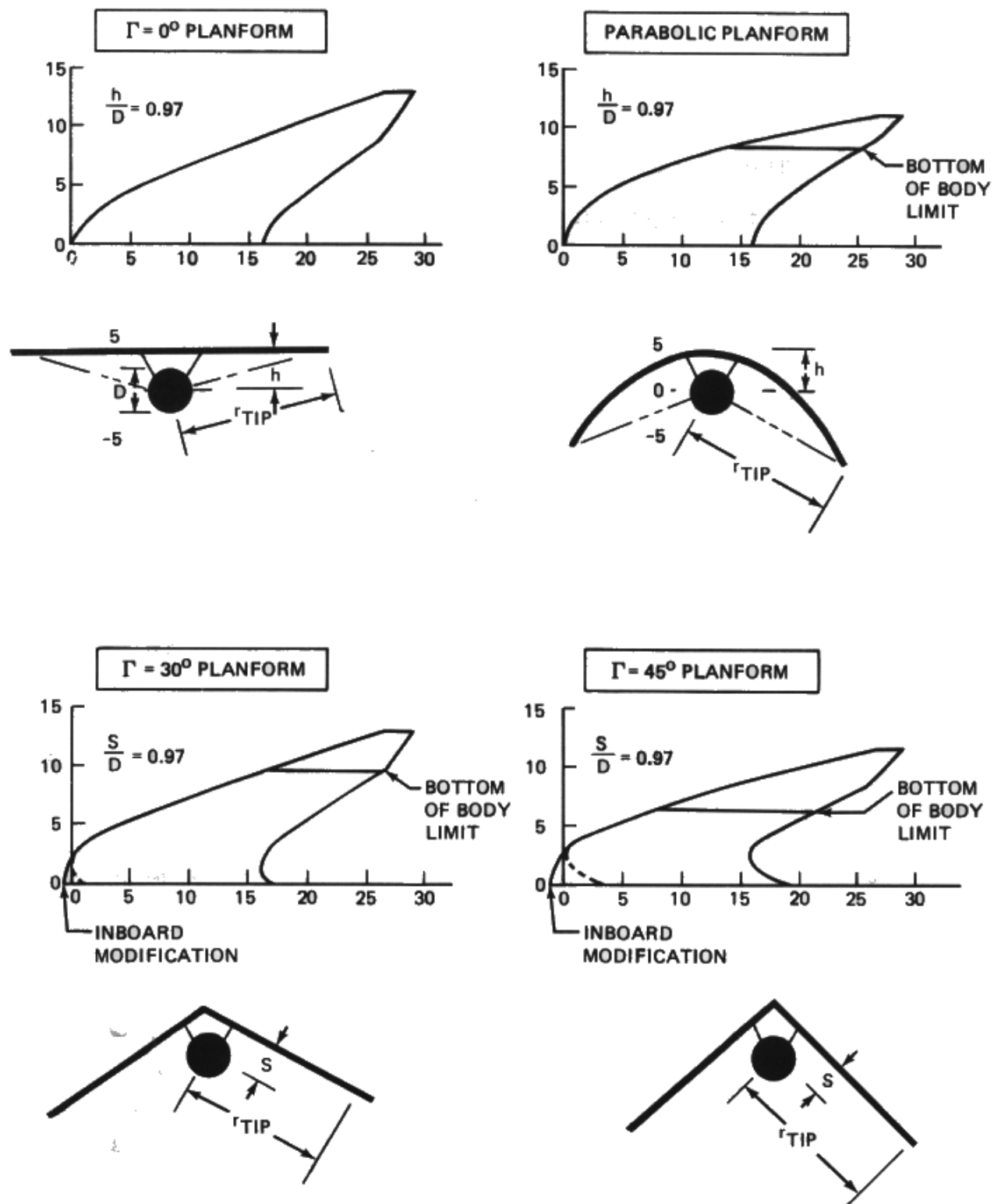


Figure 24 Planforms for Parasol Curvature Study

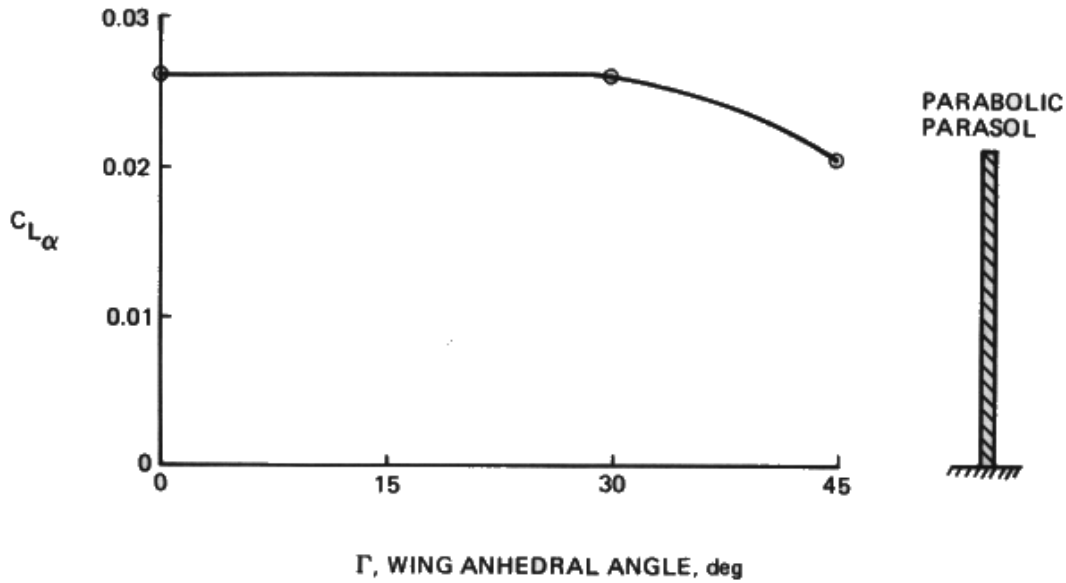
The study planforms were developed from the flat parasol wing by maintaining the same relations between the wing leading edge and also the wing trailing edge and the radial distance from the body in planes perpendicular to the body axis. The results of the analyses are shown in Figure 25. The FLEXSTAB results show an increase in interference lift similar to the slender body theory trends. The parabolic parasol has approximately 50% more interference lift than the flat parasol. The wing struts included in the analyses had a detrimental effect on interference lift.

The lift curve slope, $C_{L\alpha}$ decreases for anhedral angles above 30°. It should be noted that the wing span for the flat parasol and 30° anhedral parasol are nearly equal. The span for the parabolic parasol and 45° anhedral parasol are nearly equal to each other and are less than the spans of the other planforms. These results tend to indicate that the effect of wing anhedral on lift curve slope can be reduced by keeping the wing span constant.

DESIGN GUIDELINE 5. Interference lift can be increased by wing anhedral. FLEXSTAB can be used to predict wing anhedral effects on interference lift.

EFFECT OF WING ANHEDRAL ON LIFT CURVE SLOPE

MACH = 3.0



EFFECT OF WING ANHEDRAL ON INTERFERENCE LIFT

MACH = 3.0

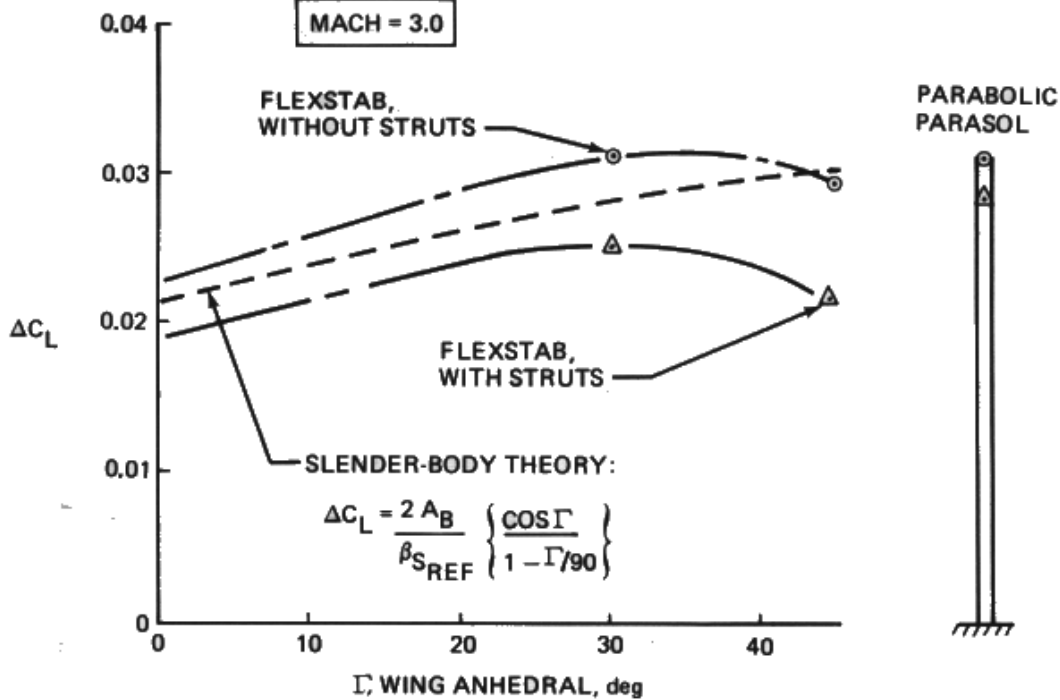


Figure 25 Parasol Wing Lateral Curvature Study Results

DESIGN GUIDELINE 6. Parabolic lateral curvature results in approximately a 50% increase in interference lift.

DESIGN GUIDELINE 7. Maintain a large projected wing span in order to reduce the adverse effects of wing planform lateral curvature (anhedral, dihedral) on lift curve slope.

5. Nacelle Parasol Versus Body Parasol Studies

Theoretical investigations were made to compare the aerodynamic characteristics of a parasol designed to capture interference lift from a nacelle (open nose body) with a parasol designed to capture interference lift from a fuselage (closed nose body).

The basic nacelle geometry used for this investigation was designed to contain the advanced engine for the study airplanes with the minimum area growth. The fuselage definition was derived from the fuselage definition of the reference zero interference airplane.

The calculated wave drag for the nacelle in the presence of a parasol is shown in Figure 26. These results indicate that the nacelle centerline should be located approximately .7 to .8 of the maximum diameter below the wing to derive maximum wave

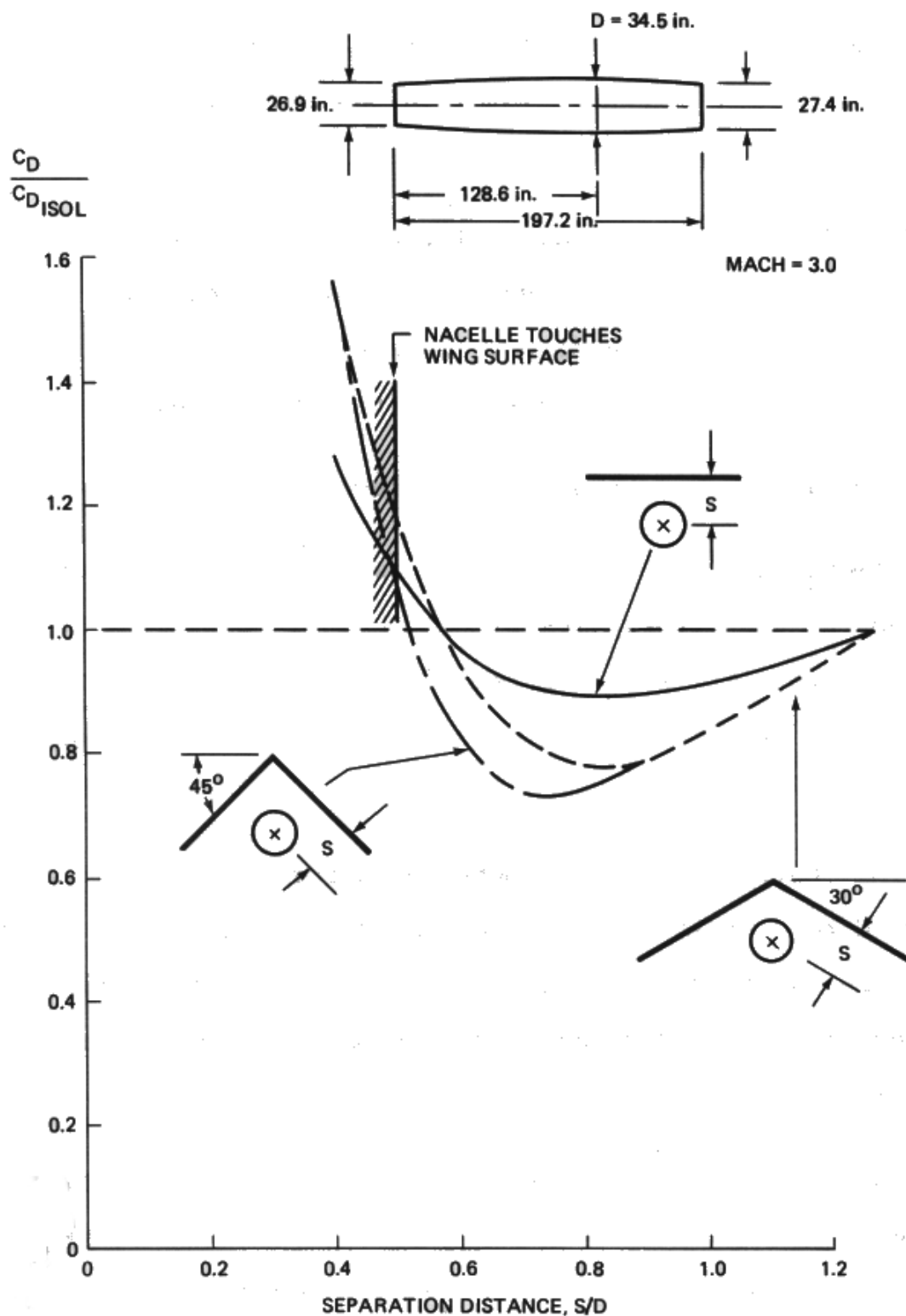


Figure 26 Effect of Parasol Curvature on Nacelle Wave Drag

cancellation effects. It also appears that the wave drag of the nacelles can be reduced by 10% to 40% depending on the parasol lateral curvature.

The results of a similar study for the fuselage are shown in Figure 27. The fuselage must be located approximately 1.5 to 1.6 diameters below the wing to achieve optimum wave cancellation. This is much greater than that required for the nacelle parasol. The fuselage wave drag reduction by wave cancellation is only 5% to 15% depending on the parasol lateral curvature.

The results in Figure 28 show the theoretical effect of body fineness ratio and inlet area in reducing the parasol/body separation distance necessary to achieve maximum wave drag cancellation.

The calculated interference lifts for the fuselage and for the nacelle with various fore cowl angles are shown in Figure 29. The fuselage generates more interference lift than for the basic nacelle shape which as previously mentioned has the minimum area growth necessary to contain the engine. The nacelle induced interference lift grows rapidly as the nacelle forecowl angle is increased. The nacelle interference lift equals that generated by the fuselage when the forecowl angle is increased to 4 degrees.

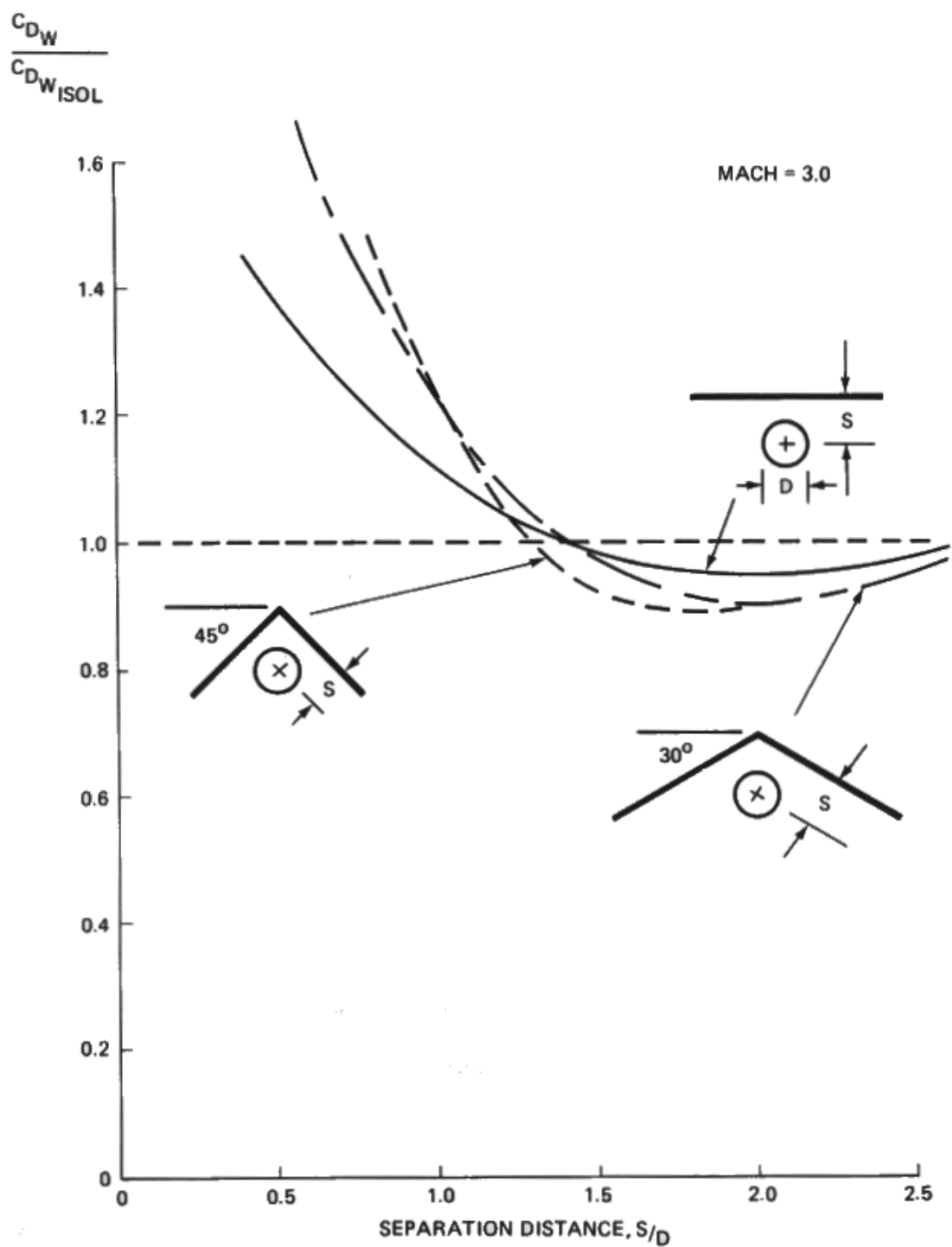


Figure 27 Effect of Parasol Lateral Curvature on Body Wave Drag

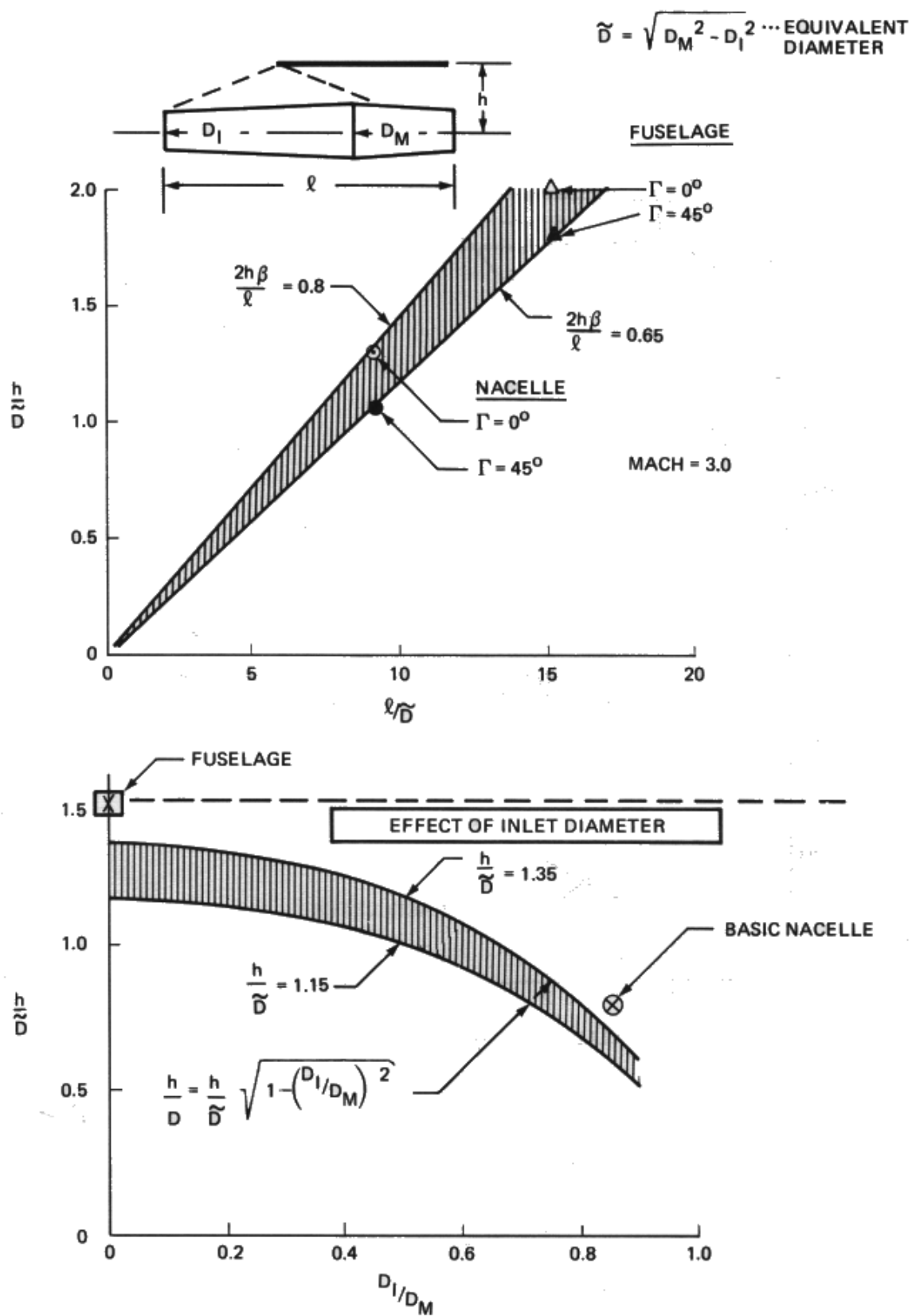
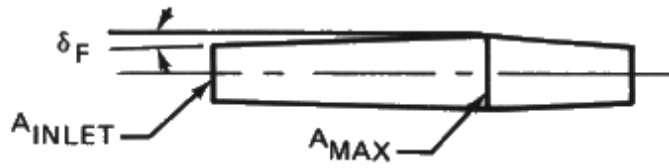


Figure 28 Effects of Body Slenderness and Inlet Diameter on Optimum Wing/Body Separation



MACH = 3.0

$$\Delta C_L = \frac{2}{\beta} \frac{A_{MAX} - A_{INLET}}{S_{REF}}$$

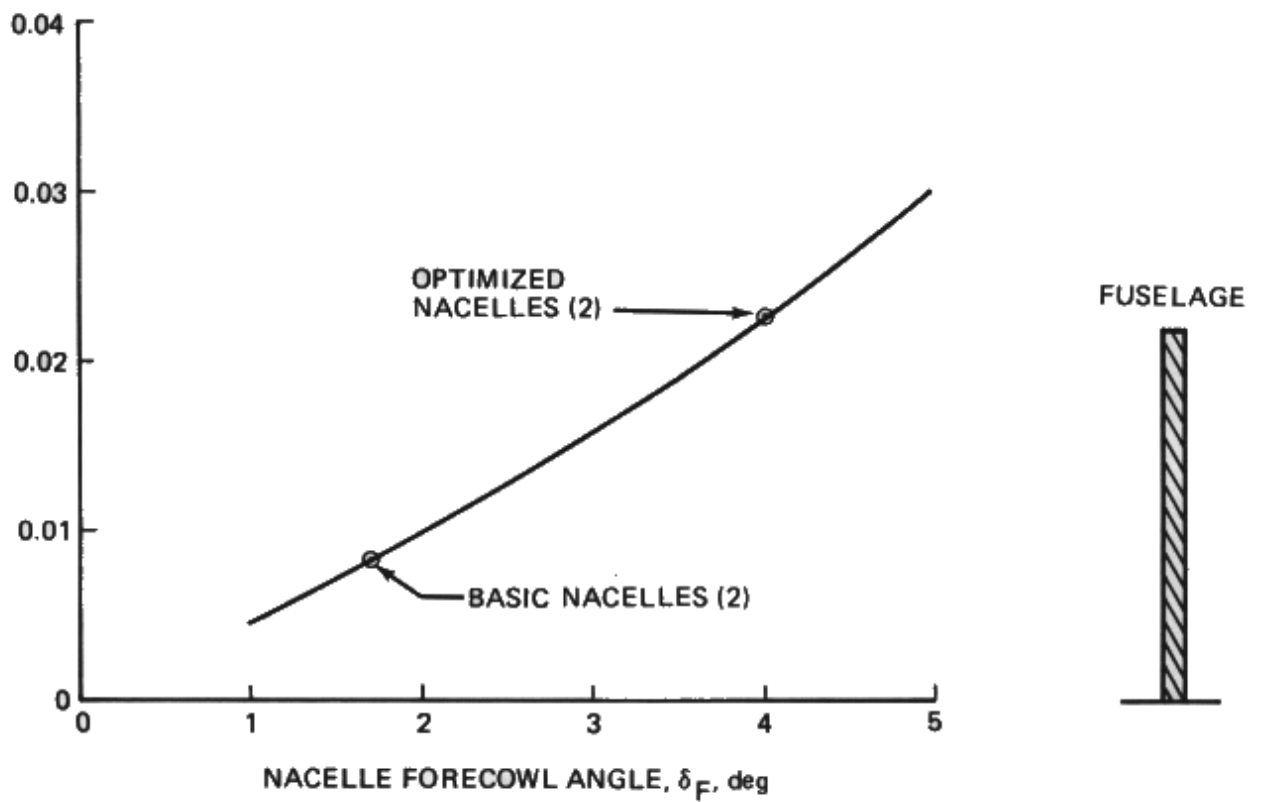


Figure 29 Effect of Nacelle Area Growth on Interference Lift

The experimental data from Reference 32 indicate that the net interference lift on a wing/nacelle parasol arrangement can be increased above the slender body theory level if the separation distance is small enough to result in multiple shock reflections. The optimum nacelle/wing separation distance is close enough to allow multiple reflections. Conversely, the optimum separation distance for the body parasol wing arrangement greatly exceeds that for multiple reflections. Hence the fuselage parasol cannot derive additional interference lift due to multiple reflections.

DESIGN GUIDELINE 8. Lower body fineness ratios reduce the optimum body/wing separation distance.

DESIGN GUIDELINE 9. The optimum separation distances for a nacelle parasol is small enough to achieve multiple shock reflections and thereby increase interference lift (design guideline 3). This also results in shorter struts to support the nacelle.

DESIGN GUIDELINE 10 The optimum separation distance for a typical fuselage is so large that desirable multiple shock wave reflection between the wing/body will not occur.

DESIGN GUIDELINE 11 Nacelle forecowl angle offers the capability to increase interference lift. The forecowl angle should be selected to optimize the trade between increased interference lift and increased nacelle wave drag.

6. Final Parasol Concept Selection

Wing parasol geometries have been calculated for the basic nacelle and for the fuselage using the aforementioned design guidelines number 1, 2, 3, 5 and 6. The results are shown in Figures 30 and 31. The body parasol is quite far from the body and would therefore require a pair of rather large struts. The nacelles can be supported by a single short strut thus saving both weight and drag. The wing span for the body parasol is much larger than the span for the nacelle parasol. However, a configuration design incorporating a nacelle parasol on each side of the fuselage would have approximately the same span as the fuselage parasol.

The relative aerodynamic characteristics of the nacelle parasol and fuselage parasol are summarized in Table 2. The nacelle parasol is seen to offer a number of potential benefits. Consequently the double parasol configuration shown conceptually in Figure 20 was selected for the final favorable interference

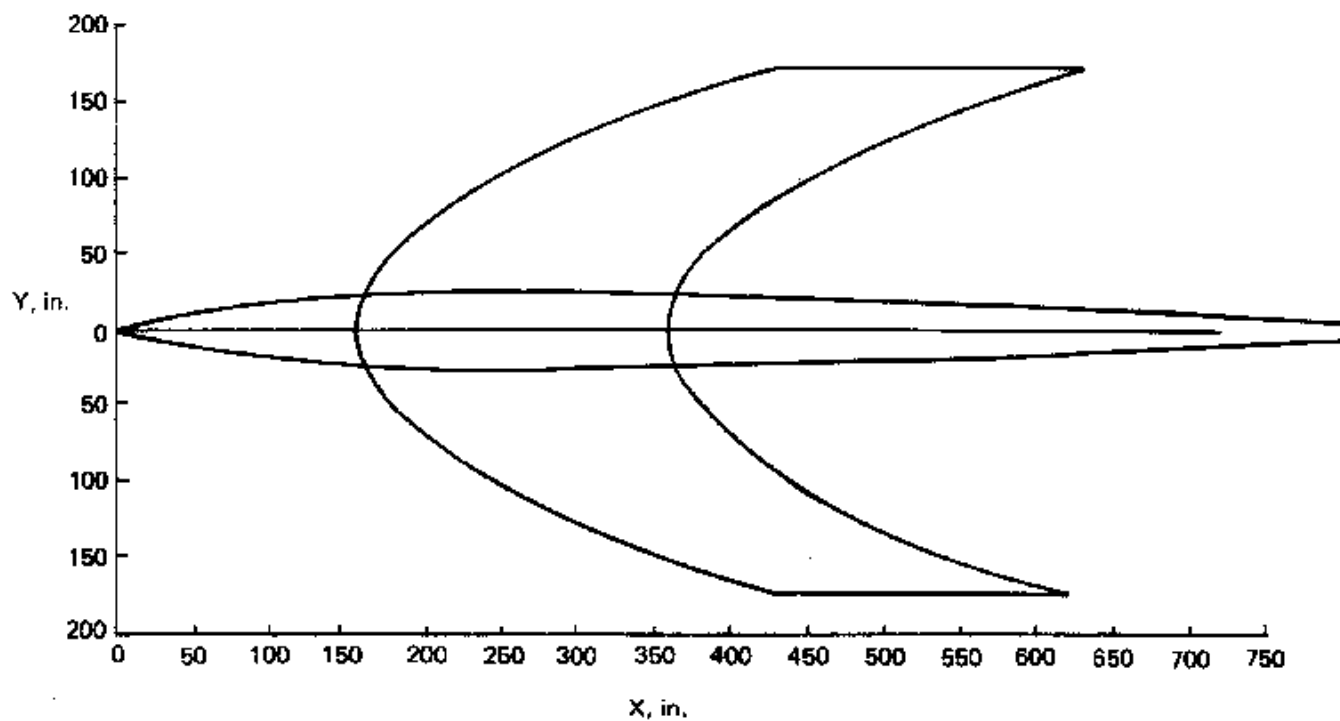
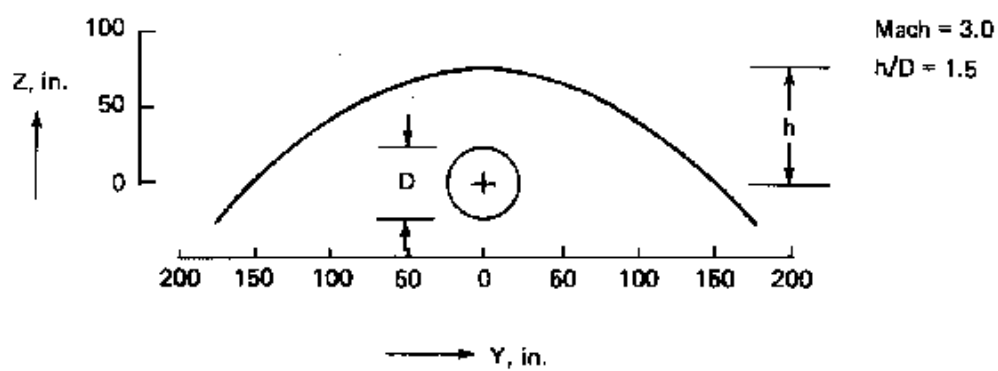
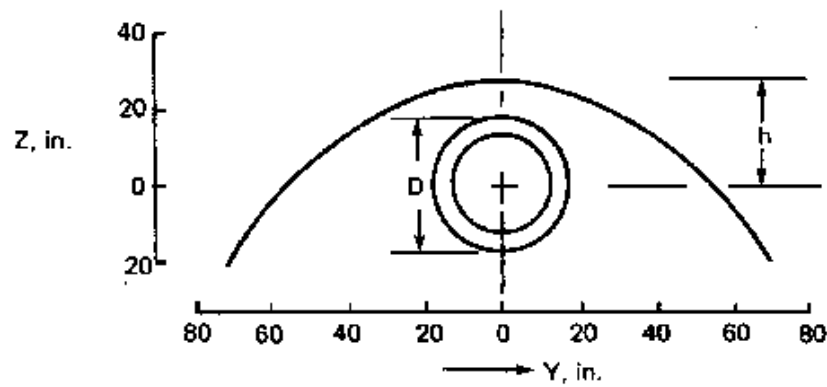


Figure 30: Body Parasol-Wing Planform Geometry



MACH = 3.0
 $h/D = 0.8$

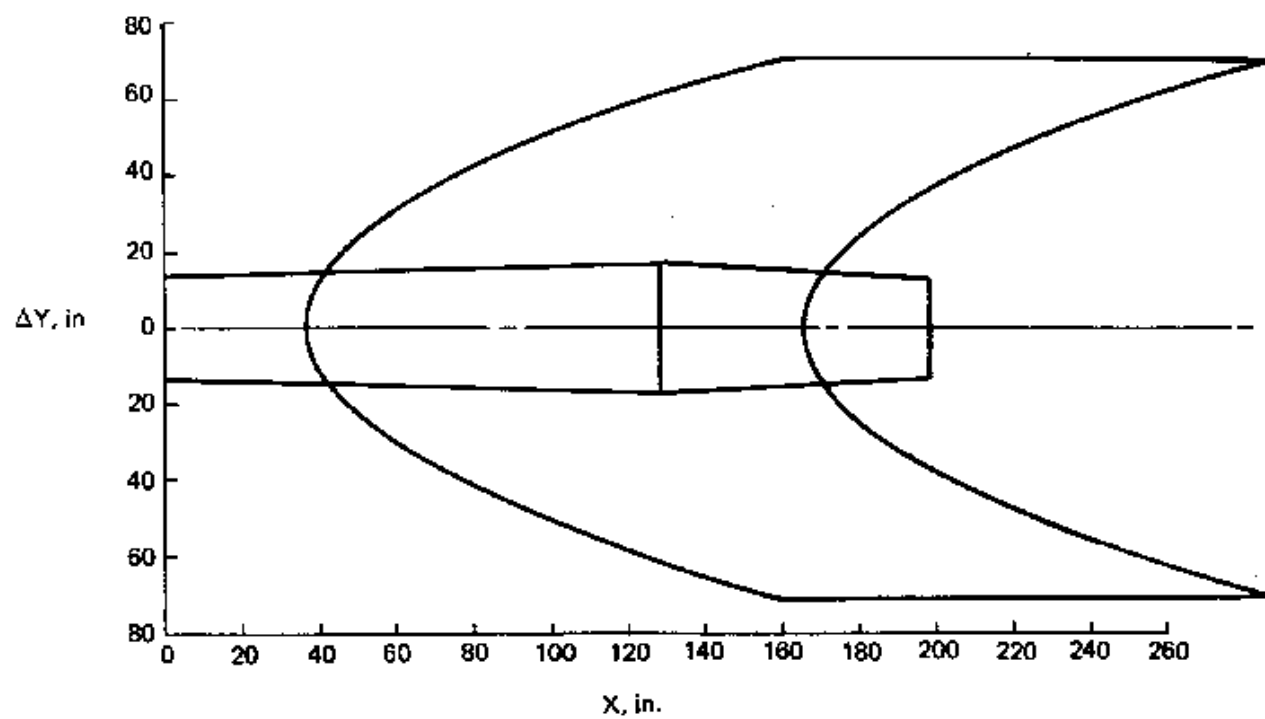


Figure 31 Nacelle Parasol Wing Planform Geometry

Table 2 Nacelle vs. Fuselage Parasol Configuration Comparisons

Item	Fuselage parasol "FP"	Nacelle double- parasol "DP"	Advantage	
			"FP"	"DP"
<div>Wave drag cancellation</div> <ul style="list-style-type: none"> • % C_{D_W} Reduction • Optimum spacing Y/D 	5%→10%	10%→40%		X
	1.8→2.0	0.6→0.8		X
<div>Interference lift</div> <ul style="list-style-type: none"> • ΔC_L --- Basic lift • Curvature amplification • Incidence amplification • Multiple shock reflection 	0.022	0.009→0.025	X	X
	• Possible for both concepts		X	X
	• Possible for both concepts		X	X
	• Too far from wing	• Possible		X
<div>Wing planform</div> <ul style="list-style-type: none"> • Wing span • Root chord limitations 	• About equal for both concepts		X	X
	• Leading edge limited by balance and vision	• Leading edge can be extended		X
	• Trailing edge limited by $-C_p$	• Trailing edge further aft		X
	• Short root chord	• Larger root chord		X
<div>Strut geometry</div> <ul style="list-style-type: none"> • Number/size • Drag • Weight 	• Two large struts	• One small strut per nacelle		X
	• Greater for "FP"	• Less for "DP"		X
	• Greater for "FP"	• Less for "DP"		X

concept. The wing planform geometry for this double parasol concept is derived in the section below.

7. Double Parasol Wing Planform Development

The double parasol wing planform was derived using the above design guidelines. The nacelles are located .8 diameters below the wing chord plane. The wing inboard of the nacelle has parabolic dihedral to enhance the lift interference. The wing has a flat section outboard of the nacelle to increase the wing span. Near the tip, the wing has parabolic anhedral to increase the interference lift. The nacelles are tilted down relative to the wing to better align the inlets with the freestream and to increase the interference lift. The wing leading edge inboard of the nacelle increases the wing root chord and blends into the leading edge determined from the bow shock location calculations. The final parasol wing planform is shown in Figure 32 with the $M = 3$ design interference lift areas. This is the wing planform incorporated into the final favorable interference concept described in Section VII. Optimization of the nacelle forecowl angle is discussed in Section VIII.

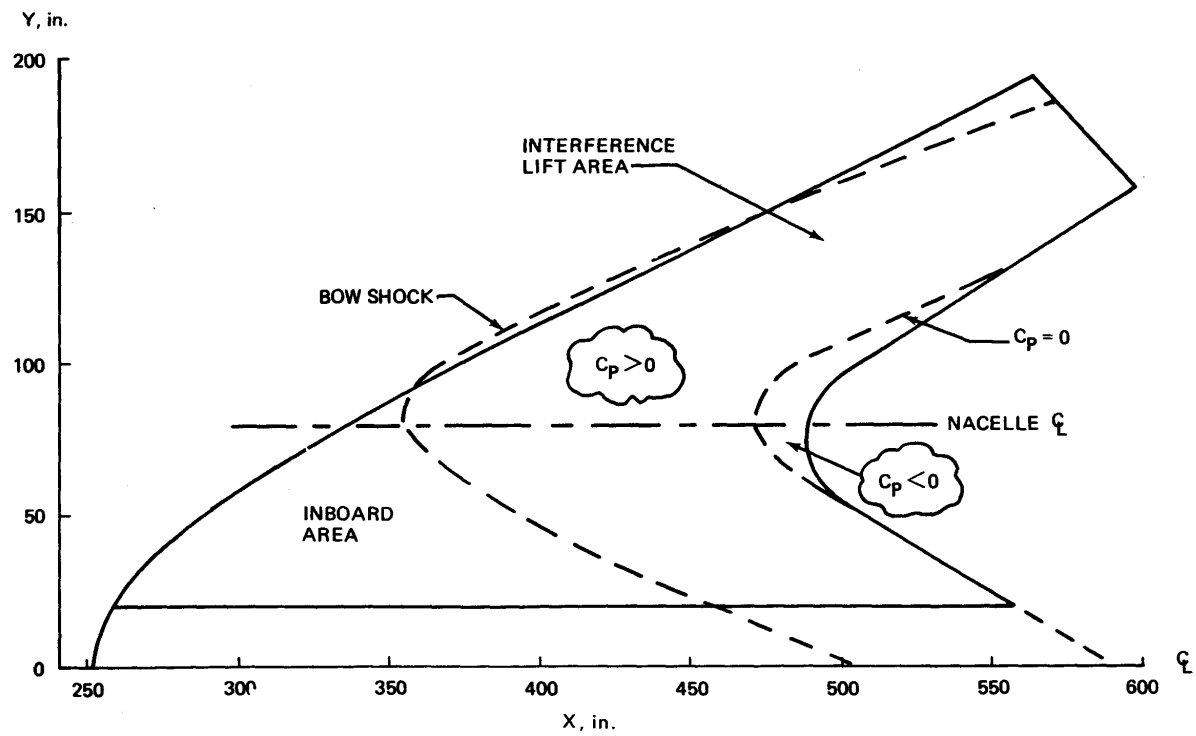


Figure 32 Mach = 3.0 Nacelle Pressure Area on Final Wing Planform

SECTION VII

CONFIGURATION DESCRIPTIONS

This section contains descriptions and general arrangement drawings of the two final configurations that have been developed to assess the effects of favorable supersonic aerodynamic interference on a Lightweight supercruise aircraft. The aerodynamic development studies of the reference "zero interference" airplane and of the favorable interference airplane were discussed in Sections IV and VI, respectively.

The design mission objectives include:

- Cruise Mach numbers = 1.5 to 3.0
- Mission radius - 500 n.mi.
- Disposable payload = 4,000 lbs

A design gross weight of 26,000 lb and a restricted overload gross weight of 30,000 lb were selected for both configurations to restrict the size of the aircraft. The cruise Mach number of 3.0 was selected to ease the design integration tasks of incorporating the favorable aerodynamic interference concepts which become more difficult at lower supersonic Mach numbers. The mission radius objectives would provide a large effective area of operation. The baseline mission is shown in Figure 33.

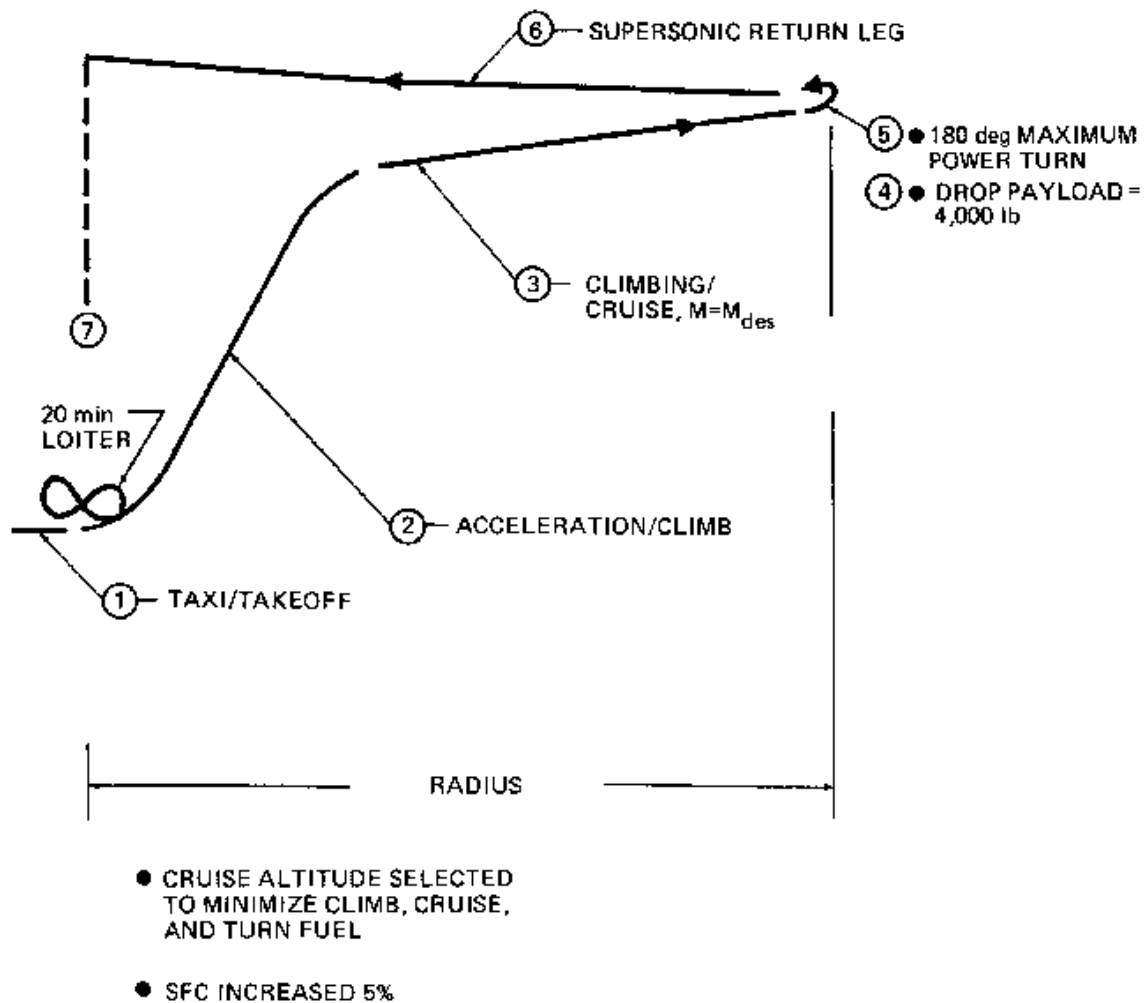


Figure 33 Baseline Mission

1. Reference "Zero Interference" Configuration, Model 3056-1

The reference configuration has been developed from the Mach 2 wind tunnel model definition provided to the contractor by the USAF Flight Dynamics Laboratory, (Wright-Patterson AFB). A schematic of this wind tunnel model definition was shown previously in Figure 2. The geometrical features of the reference zero interference airplane are shown in Figure 34. The fuel tanks locations and weapons installations are shown in Figure 35. The general arrangement of this configuration is shown in Figure 36.

The wing area of this configuration is 440 ft². The sea level static thrust with full after-burning is 21,570 lb of thrust. The fuel volume requirements were estimated for the overload gross weight condition. NASA SCAT 15 wind tunnel data with flexibility corrections have been used to establish the aft limit at 45% mean aerodynamic chord for the airplane balance exercise. The design payload includes two 2,000 lb missiles with SRAM length and volume. The missiles are fully submerged and may be released in a modified SRAM-type fashion, ejected upwards.

The engine is mounted below the fuselage and has a two-dimensional air-intake of 185 lbs/sec airflow. The two-dimensional inlet provided an anticipated higher maneuver angle of attack capability but with increased side slip sensitivity

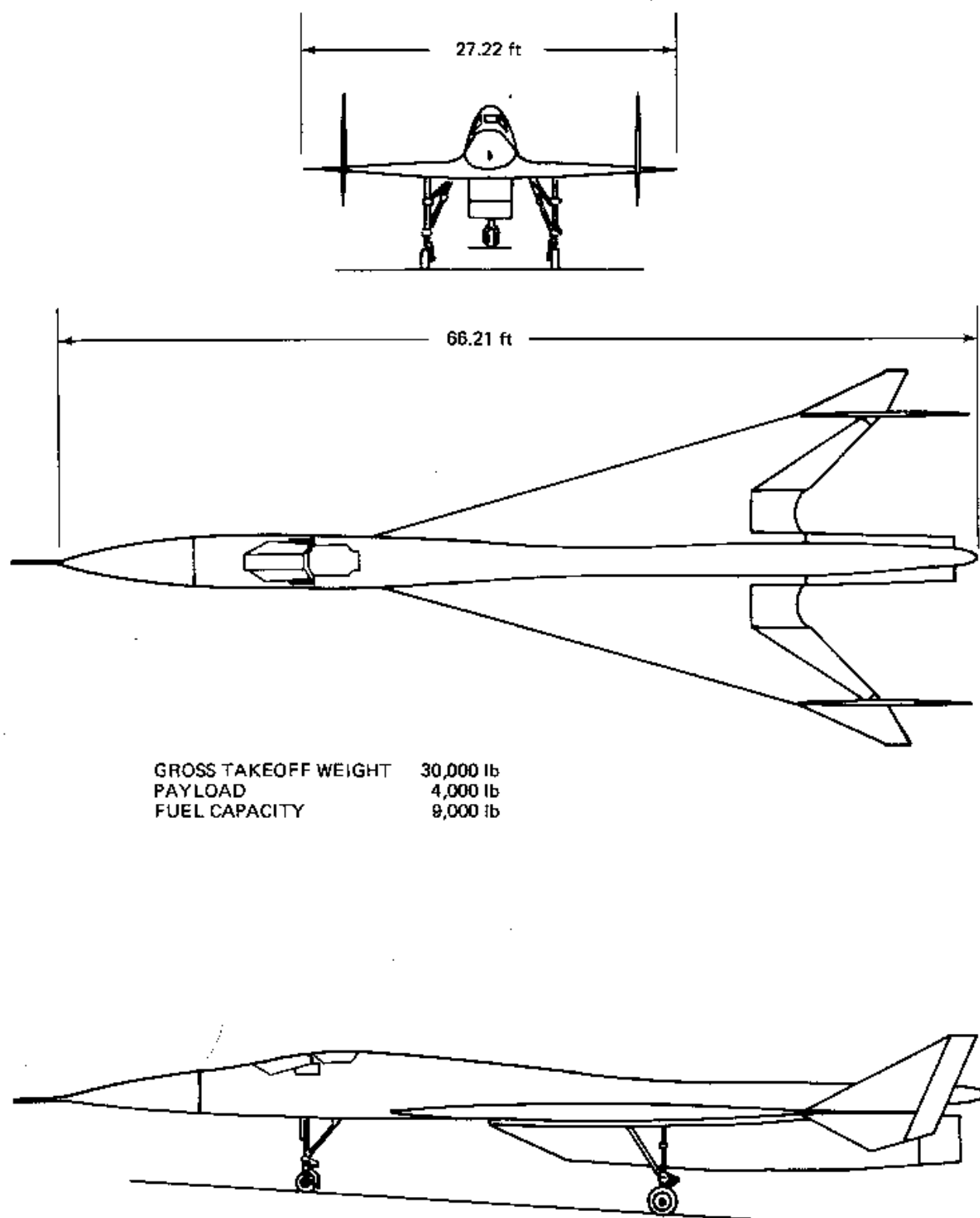


Figure 34 Study Reference Airplane, Model 3056-1

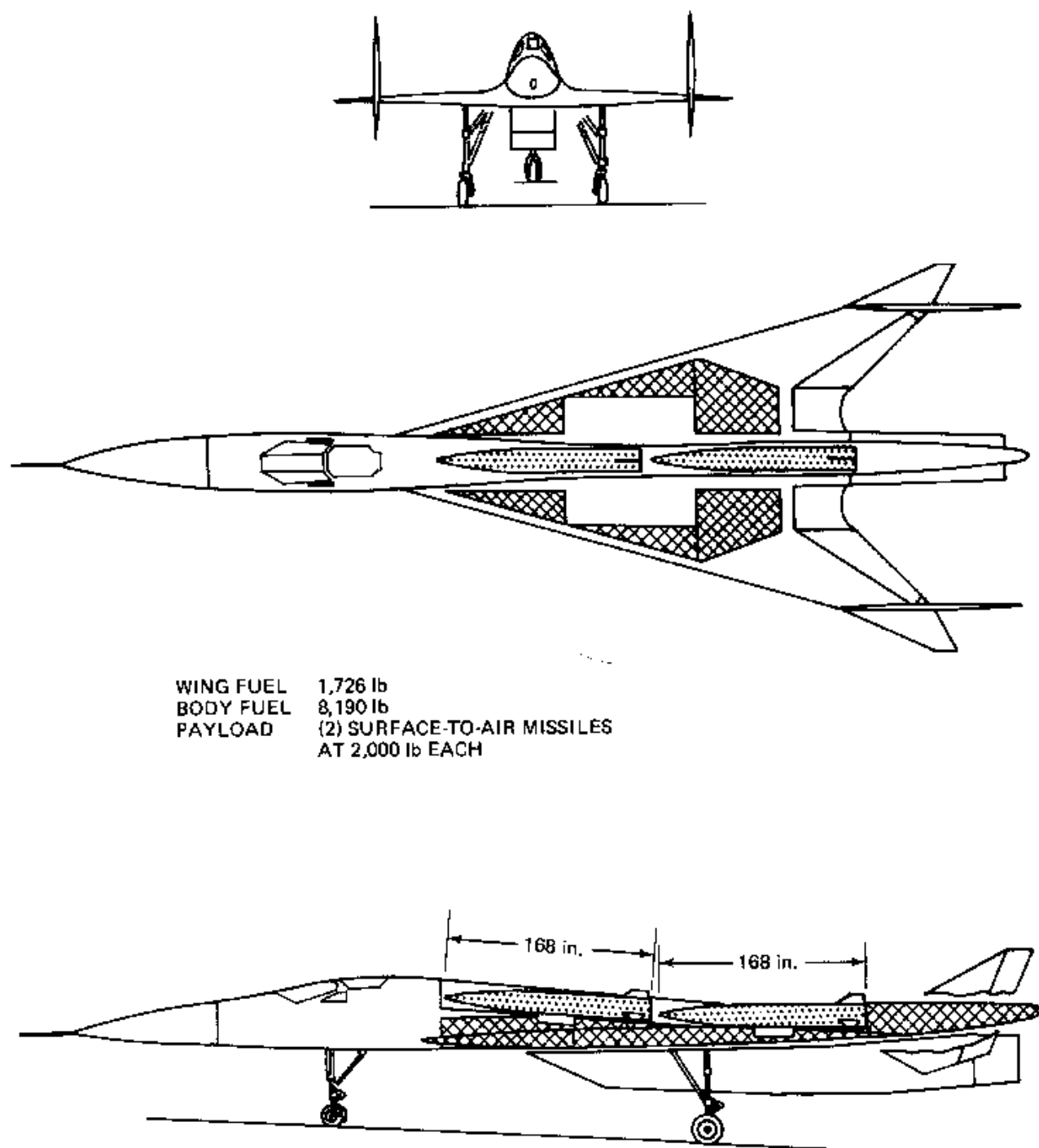


Figure 35 Fuel Tanks and Weapons Installation, Model 3056-1

NOTES

- THIS IS AN AERODYNAMIC REFERENCE AIRPLANE ONLY, A M30 VERSION OF NON-FAVOURABLE INTERFERENCE DESIGN, BASED ON N.T. MODEL PER DUG. US-AIR FORCE NR 7586-03-412P AND ON.
- THIS A/P IS DESIGNED TO MEET REQUIREMENT SPECIF. IN QST 7220-1-60

1 MAINLAND GEAR GEOMETRY PER BOEING DUG LOD-STR-129

2 BASED $\frac{1}{2}C - \frac{1}{2}C$ VERT. STAB

3 THICKNESS, AIRFOIL & CAMBER PER DUG NR 7586-03-3940 (WING) & 7586-03-3950, AIR FORCE IDENT. NO. 14530 (VERT. STAB)

4 .175 FOR UPPER AREA 0 FOR LOWER AREA

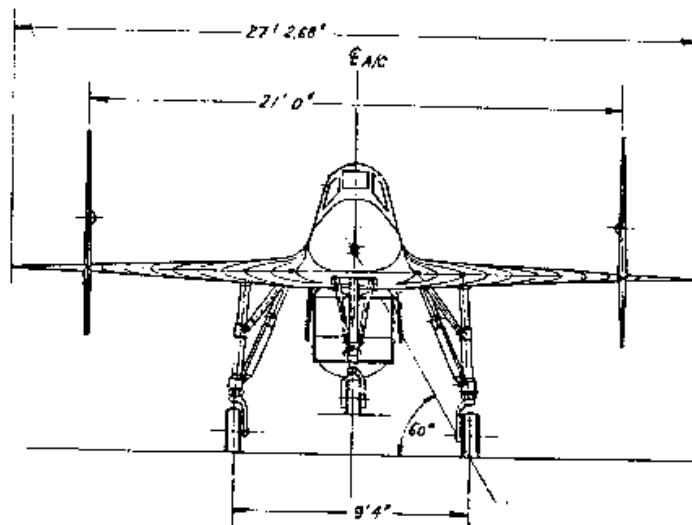
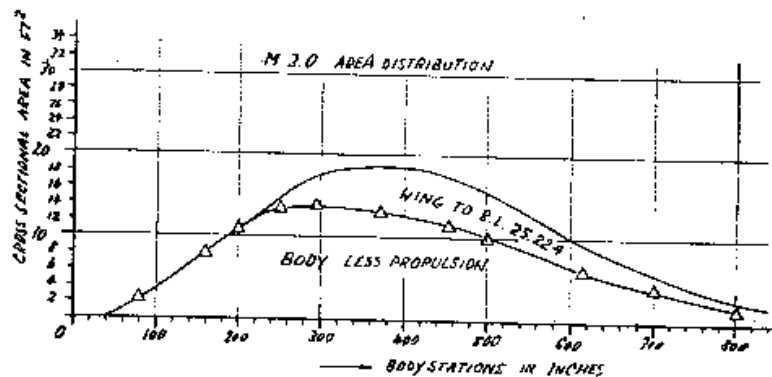
5 $\frac{C_D}{A_F} = C_D/A_F$

6 WING AREA BASED ON FHBCDEJHG. REF MAC (E) BASED ON ORIG. SCATISF PLATFORM: ABCDEK. FOR COMPARISON AND AVAILABLE REF. DATA. GEOMETRY PER 7

7 DESIGN EMPTY WEIGHT, PILOT INCLUDED

8 SIZE & VOLUME PER SRAM, WEIGHT ADJUSTED TO 2000 LBS. EACH

DESIGN CRUISE			
M 3.0	1	2	
REFERENCE A/P	HTCMT	MYLBD	F. V.
	30000	4000	16500
SURFACES			
AREA	WING	VERT. ST.	ELEVON
ASP. RATIO	1.68	1.37	26.2 TOP
TAPER RATIO	.04		
THICKN. RATIO			
INCIDENCE	0°	0°	
DIHEDRAL	0°	0°	
L.E. SWEEP	74°, 65°	62.95°, 62.5°	
SPAN	326.682"	100.414"	
MAC	258.28"	86.631"	36.197"
TAIL ARM	-	251.238"	196.308"
VOL. COEFFICIENT	-	.18	.05
BODY			
LENGTH	MAX AREA	MYLBD	
66' 1.5"	13.72 FT²		1
PROPULSION			
INTAKE	AIRFLOW	TYPE	
140-DH7	185 lbs/s	ADJ/CYC 18	
LAND. GEAR			
NOSE	MAIN	LOCAT.	
0/18+6.5	0/24+8	62.3% C	
FUEL CAPACITY			
BODY	WING	TOTAL	
8190	1726	9916	
C-G LOCATION			
T.O.	CRUISE		
41% C	45% C	46.1% C	
SCALE 1/80			



3056-1

Go Friebe

Oct 31-77

Figure 36 Reference Zero Interference Airplane General Arrangement, Model 3056-1

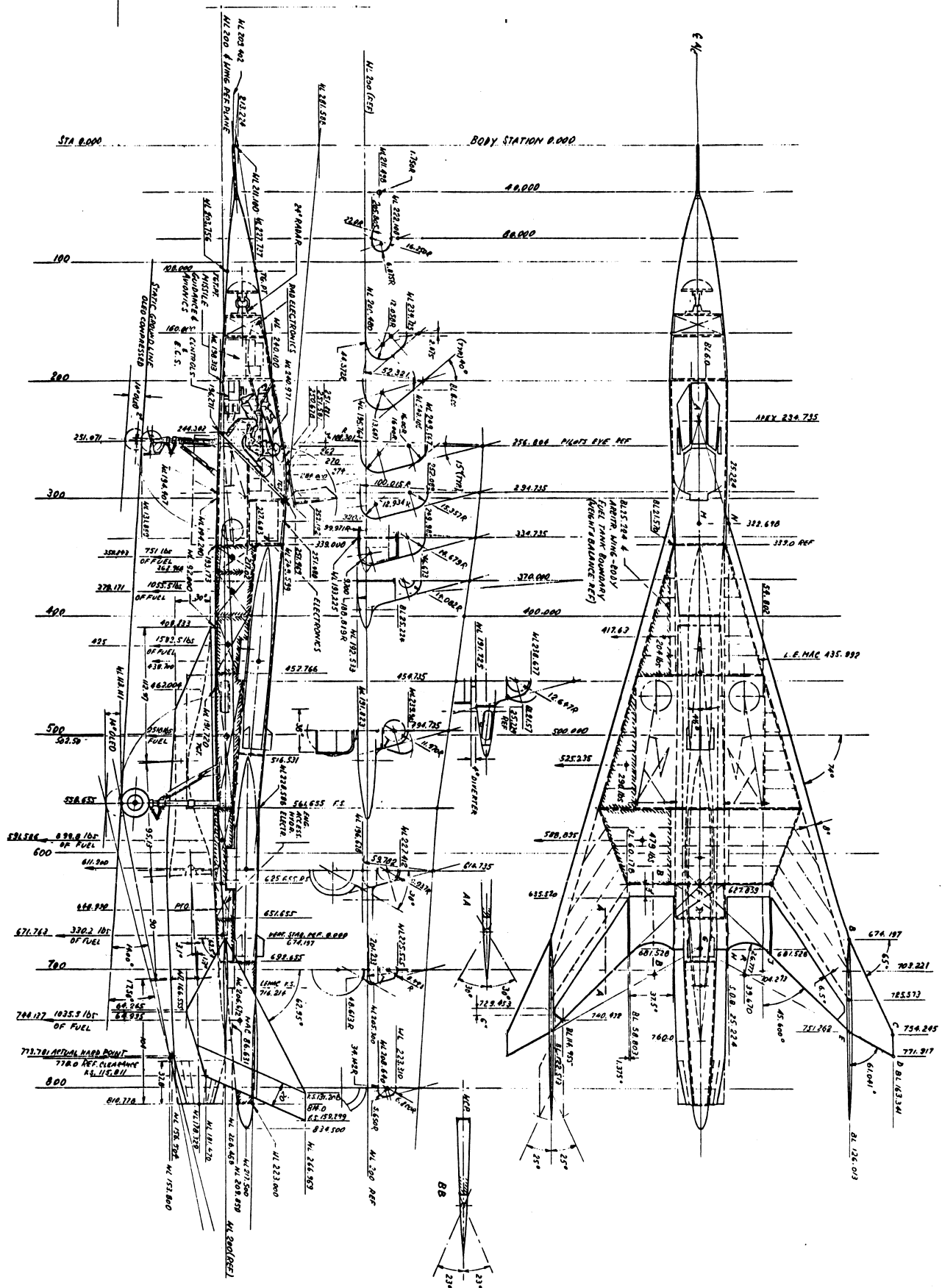


Figure 35b Reference Zero Interference Airplane General Arrangement, Model 3056-

relative to a comparable axisymmetric inlet. The integrated engine arrangement, indicated by the reference wind tunnel model definition, could not be used because of the increased fuel volume requirements for Mach 3.0 operations and because of the location of the aft fuel tanks necessary to balance the airplane. The inlet is designed for Mach 3.0 cruise operation and is separated from the wing-body lower surface by a 9 degree, 4 inch boundary layer diverter.

2. Favorable Supersonic Interference Configuration, Model 3056-2

The supersonic favorable interference configuration that has been developed is designated Model 3056-2. The aerodynamic features of this configuration include:

- Twin parasol wing planform that was designed to capture the nacelle interference pressures. The hyperbolic wing planform projected shape is designed to capture the maximum amount of nacelle lift per unit wing area.
- The planform curvature in the front view was designed to enhance the interference lift generation. The planform has a parabolic curvature between the nacelle and the body and an additional parabolic section near the wing tip. The nacelle is at the focus of each

parabolic section. The flat midwing section provides additional wing span and greater lift capture area.

- The wing camber and twist have been designed to minimize the unfavorable nacelle/wing interference drag.
- The body has been area ruled to optimize the body/nacelle and body/wing interference effects.

Model 3056-2 has been designed for a maximum takeoff gross weight of 26,000 pounds with an overload condition of 30,000 pounds. The overload condition includes a dispensable payload of 4,000 pounds. The basic fuel volume is based on the 26,000 lb gross weight. The design provides for an all-fuel overload configuration through utilization of available wing volume with the use of special tanks designed to fill the payload cavities. The geometrical features of the favorable interference airplane are shown in Figure 37. The fuel tanks locations and weapons installations are shown in Figure 38. The general arrangement of this configuration is shown in Figure 39.

The wing area is 440 ft². The empennage consists of an all-moving horizontal stabilizer, a fixed vertical stabilizer with rudder and a double, low aspect ratio, "W"-ventral. The ventrals and chines were added to provide lateral stability at high angles

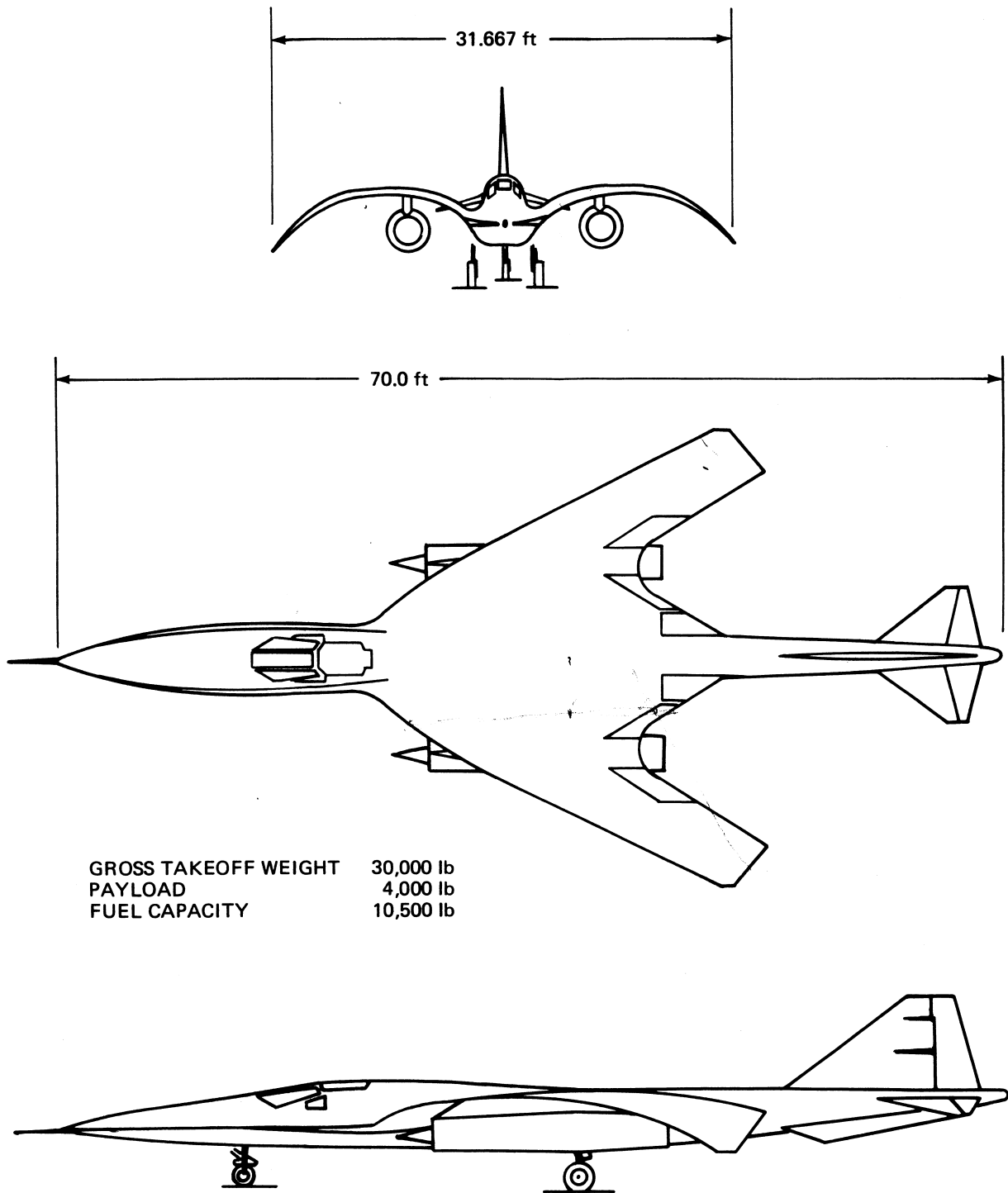


Figure 37 *Favorable Interference Double Parasol Airplane, Model 3056-2*

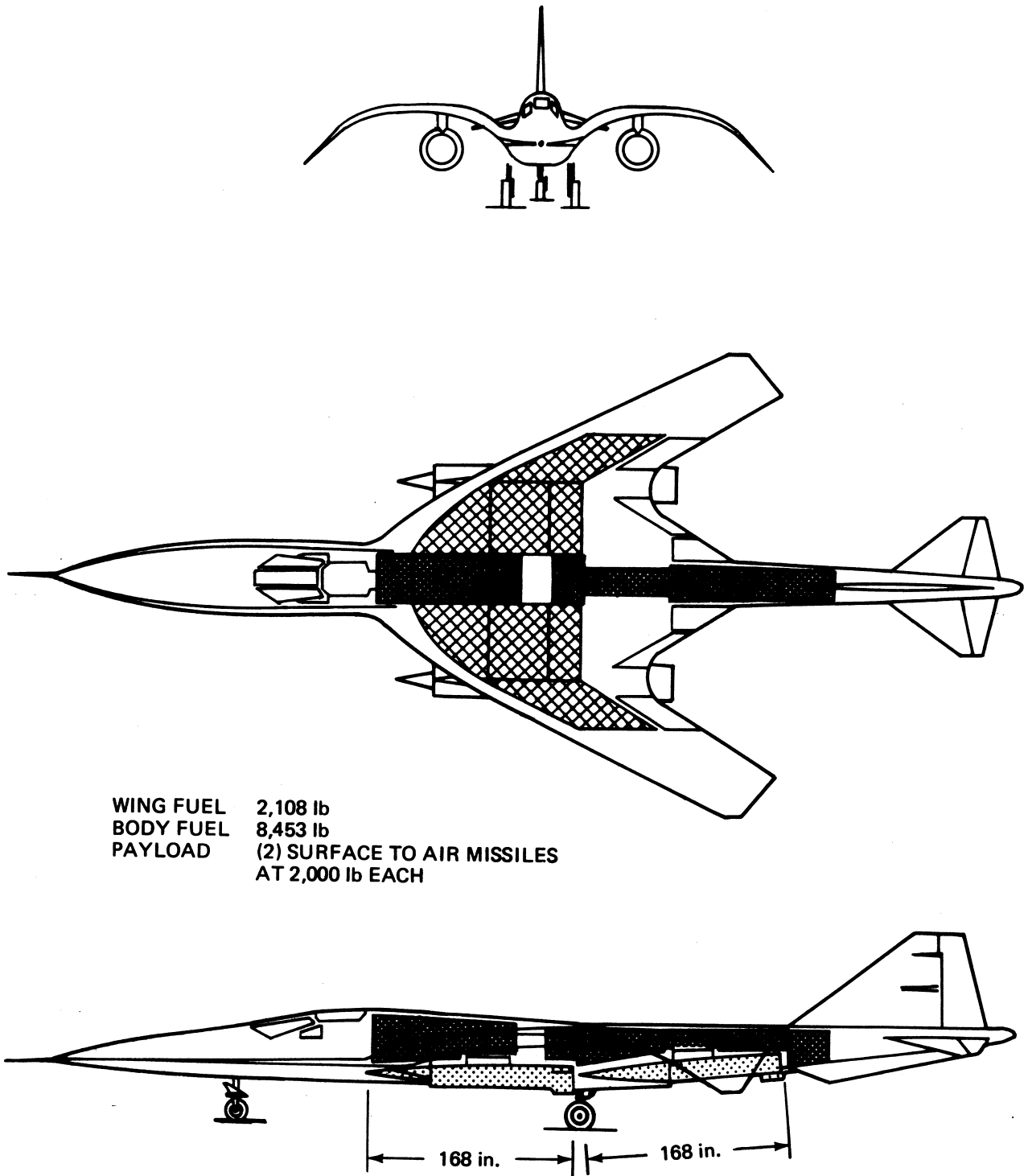
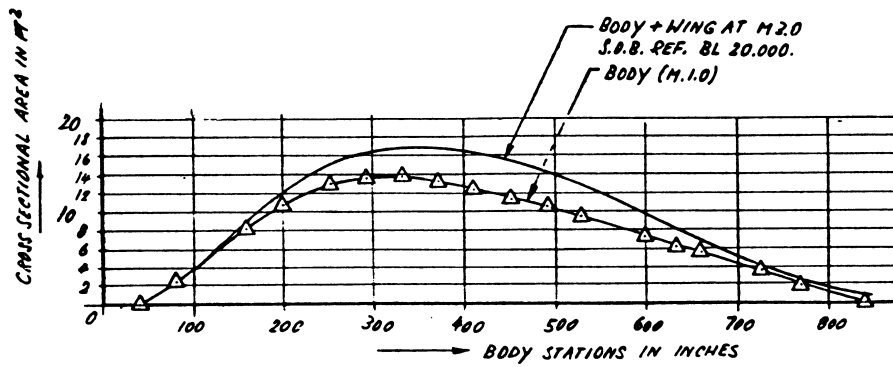


Figure 38 Fuel Tanks and Weapons Installation Model 3056-2



9
WING DIEDRAL AT 1G-MIDCRUISE CONDITION

	Y	Z
0	0	-30.990
1	5	-23.602
2	10	-16.760
3	20	-4.625
4	30	5.475
5	40	13.602
6	50	19.818
7	59.563	22.025
8	60	24.182
9	70	26.756
10	80	27.600

	Y	Z
H	120.000	27.600
N	125.000	27.600
P	130.000	27.260
Q	140.000	24.652
R	160.000	12.771
S	180.000	-6.609
T	190.000	-17.640
U	195.000	-23.185

10
WING PLANFORM DEFINITION.
ALL DATA AT 1G-MID CRUISE CONDITION

	B.L.	WING ST.
0	0.000	0.000
1	5.800	.395
2	10.000	1.561
3	20.000	6.089
4	30.000	13.347
5	40.000	23.101
6	50.000	35.114
7	59.563	41.282
8	60.000	49.151
9	70.000	64.977
10	80.000	82.357
B	97.243	115.235
11	157.397	235.394
12	195.000	310.000

	B. L.	WING ST.
13	157.397	244.642
14	97.243	247.627
15	90.000	240.087
16	80.000	236.122
17	70.000	236.531
18	60.000	241.591
19	59.563	247.936
20	20.000	305.542
21	0.000	338.875

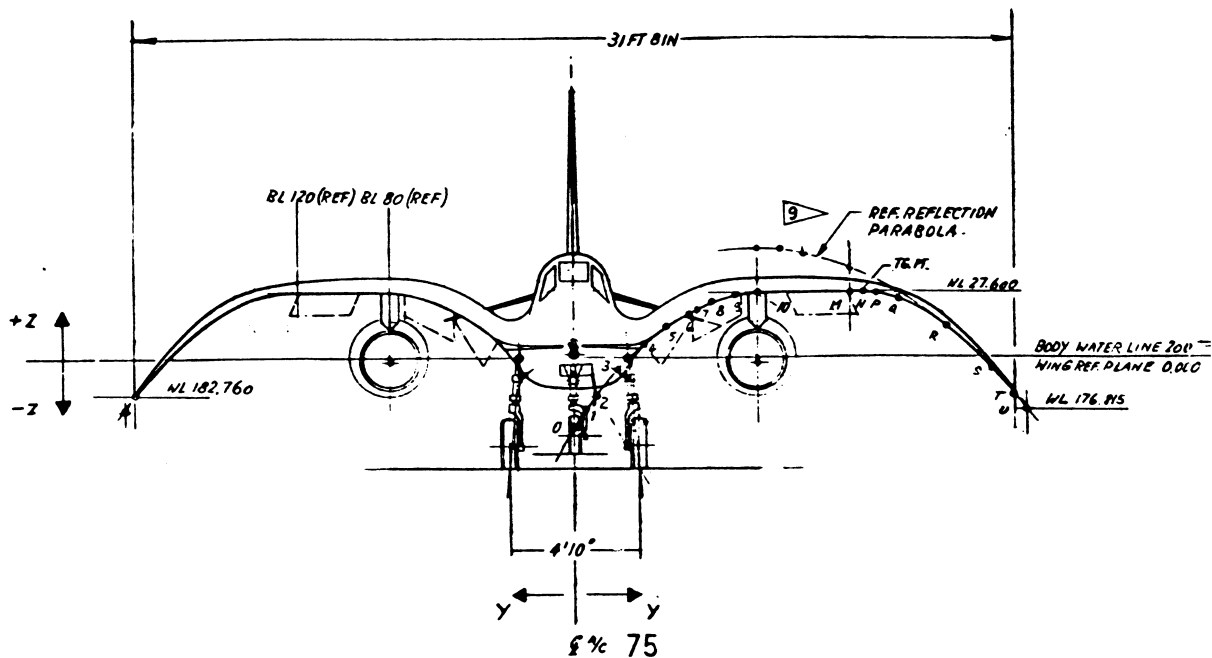


Figure 39a Double Parasol Wing Configuration General Arrangement, Model 3056-2

27. THE PROPULSION SYST. CONSISTS OF AN ADVANCED CYCLE ENGINE THE FREE STREAM INLET MAY REQUIRE AN AS YET TO BE DETERMINED DRYKE WHICH REDUCES DISTORTION & SHOCK EXPULSION AT HIGH α
26. FULL TIME STABILITY AUGMENTATION TRIPLE REDUNDANCY.
25. ACTUATION SYST: HYDRAULICS-ELECTR. "FLIGHT BY WIRE".
24. VERT. STAB. STRUCTURE: FULL DEPTH TIT. HONEYCOMB WITH SPAR REINFORCEMENT. VENTR. + HOR. ST. FULL DEPTH HONEYCOMB.
23. BODY STRUCTURE: IN AREAS OF FUEL TANKS: SINE WAVE TIT. HONEYCOMB SANDWICH. FWD OF STA 300 SKIN-STRINGER. COMPOSITE NOSE & TAIL CONES.
22. WING STRUCTURE: MULTISPAR, TITANIUM HONEYCOMB-ADVANCED COMPOSITE CONSTRUCTION. OUTBOARD BL. 120 FULL DEPTH TITANIUM HONEYCOMB SANDWICH.
21. CONTROLS: SIDE ARM CONTROL WITH ARM REST
20. ECS: MAX 80°F ON A COOL DAY MIN 60°F ON A HOT DAY 5 LBS/INCH² COCKPIT PRESSURIZATION
19. ESCAPE PROVISIONS FOR SUBSONIC ESCAPE ONLY
18. PILOT IN SPACE SUIT
17. THE LAND. GEAR IS DESIGNED FOR 14 FT/SEC SINK SPEED AND 220 KN TAKE-OFF SPEED.

28 BODY, TOP & BOTTOM CONTOURS, CROWN RADII, BOTTOM RADII, WING FILLET RADII, CHINE ANGLES

STATION	W L U°	W L L°	R	R	W	α°	P	FT²
1	80.000	216.362	198.812	-	-	-	7.334	2.22
2	180.000	229.637	194.260	-	-	-	22.152	8.22
3	200.000	235.744	192.260	-	-	-	29.536	10.30
4	256.800	244.853	190.682	14.362	-	-	40.023	12.90
5	299.735	246.625	188.590	14.362	-	-	47.024	12.33
6	334.735	245.507	187.494	14.362	25.000	1.775 (48.000)	2.615	13.89
7	370.000	243.276	186.921	14.362	25.000	1.259	5.127	12.90
8	410.000	240.466	186.780	14.362	25.000	1.044	8.024	12.22
9	432.740	238.926	186.833	13.829	25.000	1.180	9.637	-
10	450.000	237.666	187.109	12.387	25.000	1.429	10.614	11.33
11	473.806	236.100	187.723	12.501	25.000	1.390	8.813	-
12	490.000	236.000	188.315	12.332	25.000	2.515	7.765	10.56
13	570.000	236.000	190.283	11.913	25.000	2.286	4.124	10.89
14	600.000	236.000	195.063	11.180	14.917	-	4.250	6.45
15	676.000	236.000	198.916	10.804	13.281	-	-	5.78
16	660.000	236.000	201.542	10.550	13.297	-	-	5.23
17	720.000	236.000	209.581	9.812	11.259	-	-	3.78
18	776.000	236.000	217.151	4.903	5.382	-	-	1.90

* REF. RADII ONLY

29 PLANIMETERED, CROSS-SECTIONAL AREA. TOLERANCE ± 0.15 FT²
SIDE OF BODY REF. LINE (S.O.B.) B.L. ± 20.000

30 BODY FUEL IN LBS AND C.G. LOCATIONS (IN)

NO	QUANTITY	C.G. STA
1	1401	318
2	2210	364
3	714	408
4	931	459
5	1374	505
6	314	556
7	857	605
8	652	664
TOTAL	8453	448

31 AVAILABLE WING TANKAGE IN LBS. & C.G.

	QUANTITY	STA.	B.L.
A	226	373	38
B	270	412	45
C	368	455	46
D	190	470	99
TOTAL	2108	429	54

- 16 T.O. C.G. BASED ON 26000 LBS + 4000 PAYLOAD. LAND. C.G. BASED ON OPER. EMPTY WEIGHT + ANY AMOUNT OF FUEL. CRUISE C.G. OBTAINED BY MEANS OF SCHEDULED BURN-OFF.
- 15 THERE IS VOLUME FOR 2001 LBS OF FUEL, AT 68°F, IN THE WING. THE MAX THICKN. IS < 10° AND CONSIDERED TO SHALLOW FOR MAINTENANCE AND INSPECTION.
- 14 PAYLOAD: FULLY SUBMERGED ATTACK MISSILE OF SRAM DENSITY, WITH RETRACTABLE FINS.
13. TAIL ARM REPRESENTS DIST.: 25° WING - .40° TAIL AREA
12. MAC FOR HOR. STAB. & VENTRAL BASED ON EXR AREA
- 11 THE SPAN QUOTED FOR HOR. STAB. & VENTRAL REPRESENTS THE PLANVIEW PROJECTION
10. WING L.E. SWEEP PER TABULATION MARKED ON DWG
9. WING DIHEDRAL AS PER DEFINITION IN FRONT VIEW
- 8 ASP. RATIO WING TO B.L. 190. ASP. RATIO AND AREA OF HORIZ. STAB REPRESENTS EXPOSED AREA.
7. AREAS ARE TRUE AREAS EXCEPT FOR THE WING WING AREA QUOTED IS THE PROJECTED PLANVIEW AREA
6. DES. EMPTY WEIGHT IS THE ASSUMED EMPTY WEIGHT AT THE BEGINNING OF THE DESIGN
5. DESIGN GROSS-WEIGHT = 26000 LBS

4. (OMITTED)
3. ALL MASTER DIMS AT 16 CRUISE CONDITION
2. 3-DEC-PLACE DIMENSIONS ARE MASTER DIMS.
1. MODEL 3056-2 IS A FAVOURABLE INTERFERENCE, AERODYNAMIC REFERENCE, A/P ONLY.

DES. CRUISE SPEED		MACH 3.0		5		6	
AERO. REF. A/P		MTGWT	PAYLOAD	DES. E.W.			
F33615-76-C-3056		30000 LBS	4000 LBS	18300 LBS			
SURFACES	WING	HOR. ST.	VERT. ST.	VENTRAL			
AREA	FT²	437.6	38.5	57.4	20.0 EA		
ASP. RATIO		2.29	1.60	.76	.13		
TAPER RATIO		-	.20	.25	.75		
THICKN. RATIO		4%	3%	3%	3%		
INCIDENCE		0°	VARIABLE	-	- 3½°		
DIHEDRAL		9	-15°	-	-45°		
L.E. SWEEP		10	53°	53°	60°		
SPAN (IN)		380.000	109.165	79.260	46.332		
MAC		206.740	65.917	116.017	151.198		
TAIL ARM		-	353.091	214.770	298.762		
VOL. COEFFNT.		-	.15	.109	.050		

BODY	LENGTH	MAX. AREA	PAYLOAD
	66 FT 6 IN	13.89 FT²	14
PROPULSION	INTAKE	AIRFLOW	TYPE
	AXI-SYM	85 LBS/S. EA	ADV. U.A.B.
LAND. GEAR	N.D.S.	MAIN	M. L.C.
	(1) 18" x 6.5	(2) 25" x 6.5	50.7% E
FUEL CAPACITY	BODY	WING	TOTAL
	8453 LBS	18	8543 LBS
C.G. LOCATION	T.O.	CRUISE	E.W.
	40.3% E	44% E	37% E
SCALE	1/40		

3056-2

G.O. Libal

DEC 11-77

Figure 39b Double Parasol Wing Configuration General Arrangement, Model 3056-2

of attack. Ailerons and flaperons are provided for roll control. More effective roll control devices would require redesign of the wing trailing edge.

The wing structure is of multispar design covered with titanium honeycomb sandwich. The leading edge, the trailing edge and the wing outboard of B.L. 120 is of titanium, solid honeycomb sandwich. Structural members carrying highly concentrated loads are made of composites.

The fuselage is of multispar design in the area of the wing box. Fuselage frames connect to wing spars. In the area of the wing tanks the cover material is titanium sine-wave honeycomb sandwich, which also serves as fuel tank insulation. Forward of station 300, the structure is of the skin stringer design, with heat insulation for the pilots compartment. The nose cone and the tail cone are made of composites.

The vertical stabilizer is 3% thick and has hexagonal airfoil. The structure is titanium, solid honeycomb sandwich, spar-reinforced, to take actuation loads and hinge moments. The horizontal stabilizer and the two ventrals are of titanium, solid honeycomb sandwich.

The 4,000 pounds payload was assumed to be in the form of two short-range attack missiles. Volume, ejection systems, and guidance, reflect SRAM design and technology.

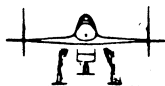
A 5% stability margin was assumed. The wing is located relative to the fuselage such, that the O.E.W. c.g. acts at 37% of the mean aerodynamic chord. The maximum takeoff gross weight c.g. is also at 37% M.A.C. The overload, 30,000 pounds gross weight c.g., is at 40.3% M.A.C. Inflight c.g. shifts, required for minimum trim drag operation are accomplished through simple fuel management.

3. Configuration Weight Comparisons

The weight and balance analyses for the two study configurations were estimated using Boeing parametric-statistical weight methods. Stiffness requirements were not accounted for in these analyses.

Design data used in the weight analyses are summarized in Table 3. Both aircraft use 1985 technology titanium for most primary structure with graphite/polymide composite for other structure. The structural weight of both aircraft was decreased by approximately 10 percent due to incorporating advanced technology materials. The results of the weight analyses are summarized in Table 4 and Figure 40. The structural weights of

Table 3 Design Data



Parameter	Reference Airplane, Model 3056-1	Favorable Interference Double-Parasol Airplane, Model 3056-2
General		
Flight design weight, lb	26,000	26,000
Ultimate vertical load factor	9.75	9.75
Landing weight, lb	22,500	22,500
Maximum cruise altitude, ft	70,000	70,000
Design cruise Mach number	3.0	3.0
Maximum sea level Mach number	1.2	1.2
C_L (landing)	0.6	0.6
Wing		
Reference area, ft ²	440	438
Aspect ratio	1.68	2.29
Thickness ratio	0.04	0.04
Leading-edge sweep, deg	74	Varies across span
Dihedral, deg	0	Variable (parabolic)
Horizontal tail		
Reference area, ft ²	None	38.5
Aspect ratio	—	1.68
Thickness ratio	—	0.03
Leading-edge sweep, deg	—	53
Tail arm, ft	—	29.4
Pitch acceleration, radians/sec ²	—	6
Type	—	Fully moveable
Vertical tail		
Type	(2) On wing tip, with rudder	With rudder
Reference area, ft ²	51 ea.	51.4
Aspect ratio	1.37	0.76
Thickness ratio	0.04	0.03
Leading-edge sweep, deg	63	53
Tail arm, ft	20.9	26.2
Reference ventral area, ft ²	None	(2) 20.0 each
Body		
Surface area, ft ²	636	610
Length, ft	69.5	70.0
Maximum cross sectional area, ft ²	13.7	15.8
Chine area, ft ²	None	11
Landing gear		
Main gear type	Wing-mounted, 2 wheels	Wing-mounted, 2 wheels
Main gear extended length, ft	7.3	6.2
Nose gear extended length, ft	4.4	3.8

Table 3 Design Data (continued)



Parameter	Reference airplane, Model 3056-1	Favorable interference double-parasol airplane, Model 3056-2
<u>Propulsion</u>		
Engine type and number	Variable gas turbine with afterburner (1)	Variable gas turbine with afterburner (2)
Thrust at sea level	21,530	10,765 each
SFC at sea level and maximum thrust	2.0	2.0
Nozzle type	Convergent/divergent	Convergent/divergent
Inlet type	Two-dimensional, mixed compression	Axisymmetric, mixed compression
Nacelle surface area, ft ²	285	169 each
<u>Systems</u>		
Flight control type	Fly-by-wire	Fly-by-wire
Air conditioning	Short-range cruise	Short-range cruise
Crew number	1	1
<u>Payload</u>		
Type	(2) x 2,000-lb missiles	(2) x 2,000-lb missiles
Carriage	Internal	Internal

Table 4 Group Weight Statement—Pounds



Item	Reference Airplane, Model 3056-1	Favorable Interference Double-parasol Airplane, Model 3056-2
Wing	2,735	3,374
Horizontal tail		263
Vertical tail	659	303
Body + chine	3,536	3,403
Main gear	824	717
Nose gear	220	184
Nacelle + inlet	1,742	1,527
Structure	9,716	9,771
Engine	2,543	2,614
Engine accessories	50	100
Fuel system	498	535
Engine control	80	160
Starting system	100	200
Propulsion	3,271	3,609
Flight control	397	459
Auxiliary power plant	286	309
Instruments	130	160
Hydraulic + pneumatic	354	354
Electrical	486	554
Avionics	1,170	1,170
Armament	60	60
Furnishings + equipment	235	235
Air conditioning + anti-icing	547	565
Load and handling	20	20
Fixed equipment	3,685	3,886
Weight empty	16,672	17,266
Crew	215	215
Unusable fuel	99	84
Oil + trapped oil	85	105
Weapon installation	240	240
Crew equipment	20	20
Nonexpended useful load	659	664
Operating weight	17,331	17,930
[Payload—overload condition]	[4,000]	[4,000]
Fuel	8,669 ¹	8,070 ²
Takeoff gross weight	26,000	26,000

Notes: ¹ Fuel capacity = 8,190 lb in body and 1,726 lb in wing

² Fuel capacity = 8,453 lb in body (2,108 lb in wing was not included in the design)

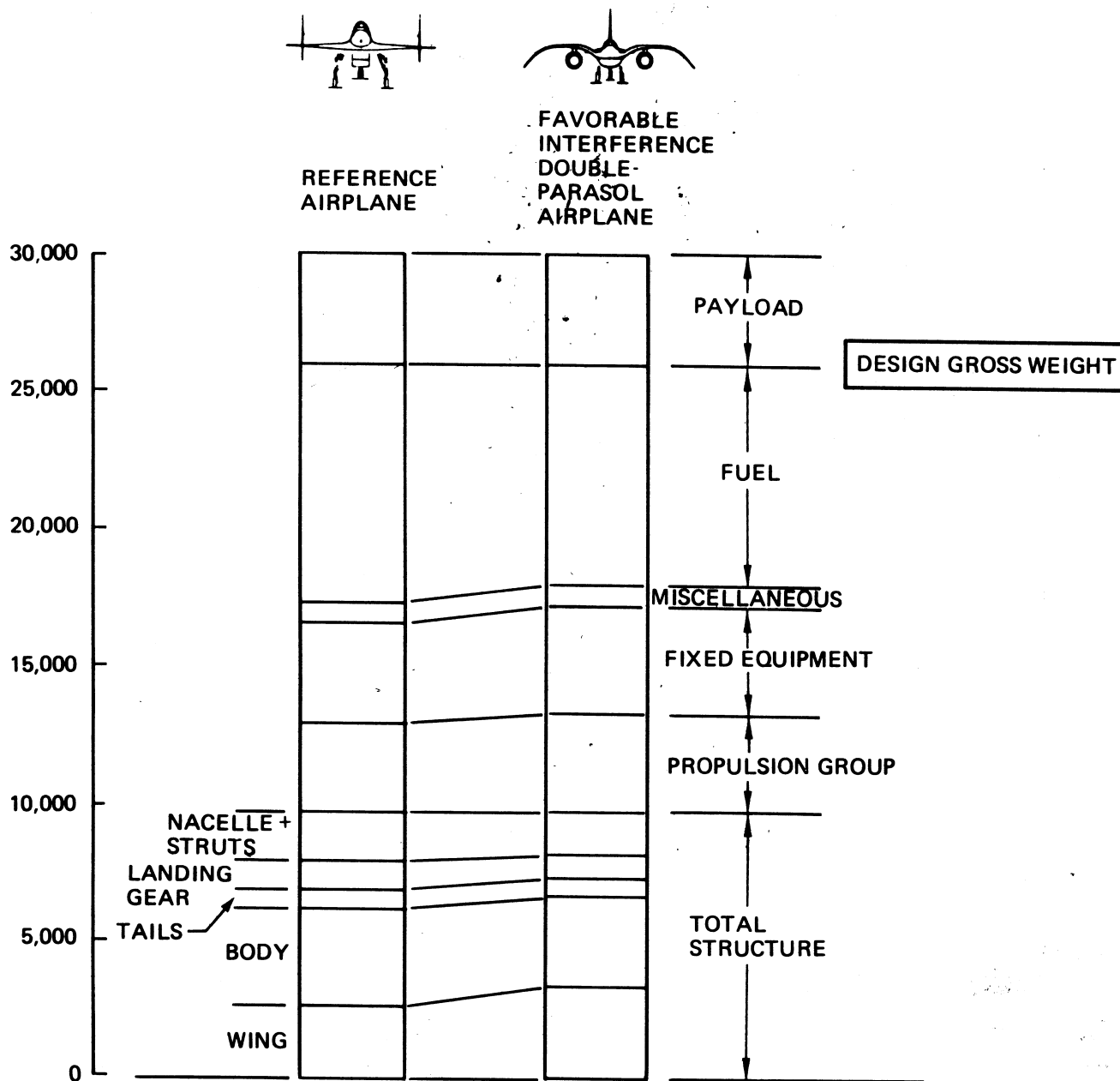


Figure 40 Weight Comparison

both configurations are nearly equal. However, the operating weight of the favorable interference concept is approximately 600 lbs heavier because of increased propulsion and fixed equipment weights. The balance data for both configurations are shown in Table 5.

The aerodynamic and performance comparisons of these two configurations are presented in Section VIII.

Table 5 Weight and Balance Summary



Condition	Reference Airplane, Model 3056-1		Favorable Interference Double-Parasol Airplane, Model 3056-2	
	Weight, lb	Longitudinal cg ¹ Station, in. (% MAC)	Weight, lb	Longitudinal cg ² Station, in. (% MAC)
Weight empty (gear down) ⁴	16,672	518 (31.7)	17,226	424 (25.6)
Nonexpended useful load	659	445	664	392
Operating weight (gear down)	17,331	515 (30.6)	17,930	423 (25.1)
Operating weight (gear up)	17,331	513 (29.8)	17,930	424 (25.6)
Payload	4,000	525	4,000	482
Fuel capacity, body	8,190	505	8,453	448
Fuel capacity, wing	1,726	535	2,108 ³	429
Maximum gross weight (gear up)	31,247	514 (30.2)	32,491	438 (32.4)
Design takeoff gross weight (gear up)	26,000	514 (30.2)	26,000	437 (31.9)

- Notes:
- ¹ Nose pitot tube = Sta. 0. Wing MAC = 258.3 in. and leading edge MAC = Sta. 436.0.
 - ² Nose pitot tube = Sta. 0. Wing MAC = 206.7 in. and leading edge MAC = Sta. 371.5.
 - ³ Wing fuel was not used in the weight analysis for Model 3056-2
 - ⁴ Main landing gear (down) Sta. = 558.7 in. (47.5% MAC) for Model 3056-1 and 476.3 in. (50.7% MAC) for Model 3056-2.

SECTION VIII

CONFIGURATION AERODYNAMIC AND PERFORMANCE COMPARISONS

This section contains the aerodynamic comparisons of the study reference conventional type airplane and the final favorable interference concept incorporating the double parasol concept. The methods of analysis are summarized. The parametric variations that were made to optimize the double parasol wing concept are discussed.

1. Aerodynamic Analysis Approach

The aerodynamic design and analyses methods that were used for the study configurations are discussed in Appendix A.

The reference conventional type aircraft, Model 3056-1, was analyzed by a "straightforward" application of the ADASSA methods and empirical leading edge suction data as discussed in Appendix A. The computer representation of this configuration is shown in Figure 41. Note that the computer modeling requires the representation of the nacelle as a body of revolution.

The double parasol wing configuration Model 3056-2 was analyzed using ADASSA, FLEXSTAB and empirical data for leading edge suction corrections and also for multiple reflection effects on interference lift (as discussed in Section VI). ADASSA was used for the volume wave drag, drag due to lift, trim and

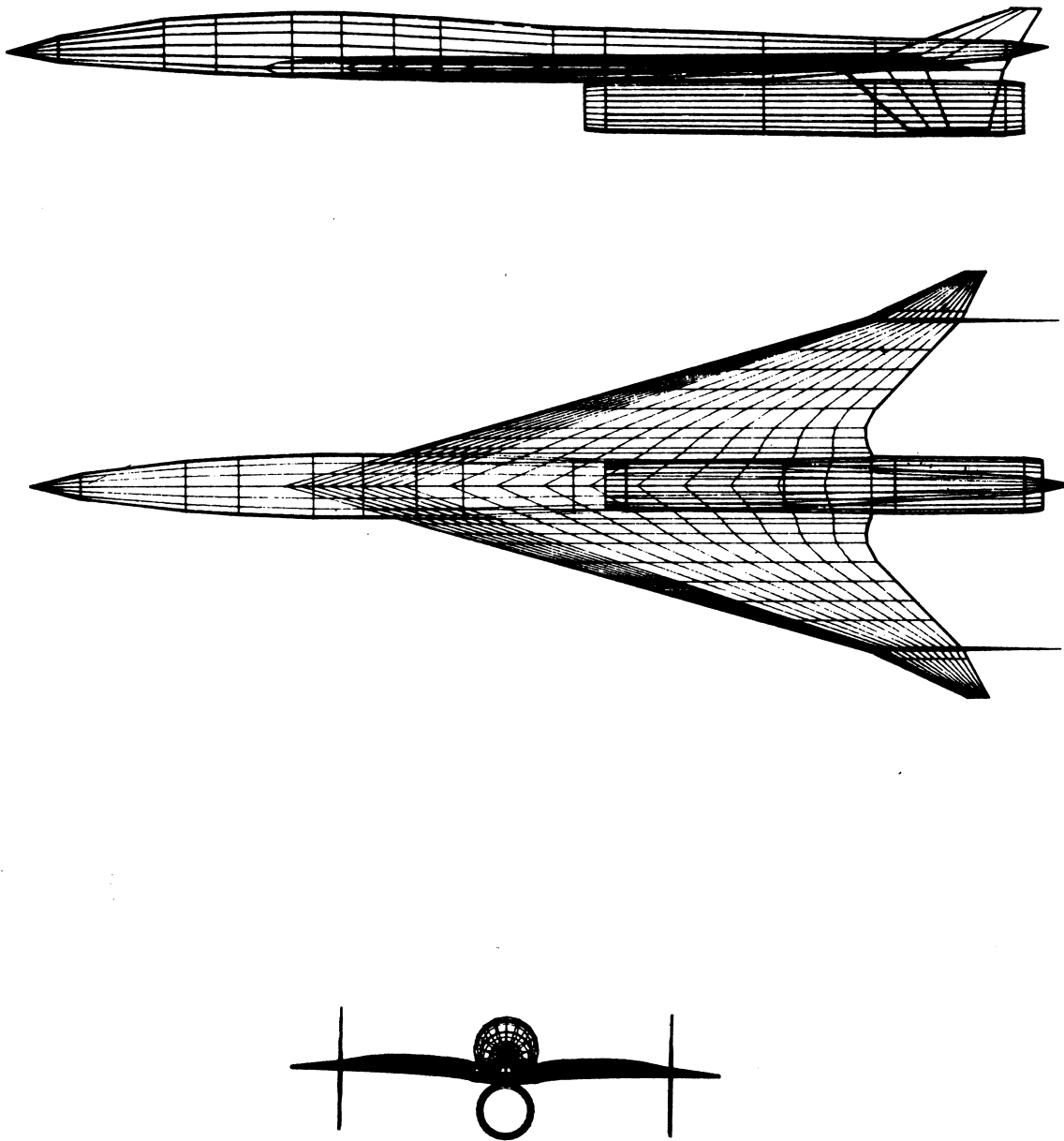


Figure 41 Computer Representation of Model 3056-1

friction drag. FLEXSTAB was used to calculate planform lateral curvature effects on interference lift, ΔC_L , and on lift curve slope $C_{L\alpha}$. The computer representation of this configuration used for the aerodynamic analyses is shown in Figure 42.

2. Parasol Wing A/P Optimization Studies

Parametric studies were made to determine the optimum nacelle area growth for the parasol wing with and without lateral curvature. The figure of merit was selected as the $M = 3.0$ cruise maximum lift/drag ratio. The results are shown in Figure 43.

Increasing the nacelle forecowl angle increased the $(L/D)_{MAX}$ of the double parasol wing configuration from 6.5 to 7.0. It is also seen that lateral curvature provided only a slight improvement of the parasol wing configuration without lateral curvature. This is because the favorable effect of interference lift enhancement by the lateral curvature is nearly canceled by the degradation of lift curve slope.

Most of the interference lift benefits come from the inboard wing and also most favorable effects on $C_{L\alpha}$ occur in the outboard portion of the wing. It is, therefore, possible that the lift/drag ratio could be further increased by reducing the lateral curvature near the wing tip.

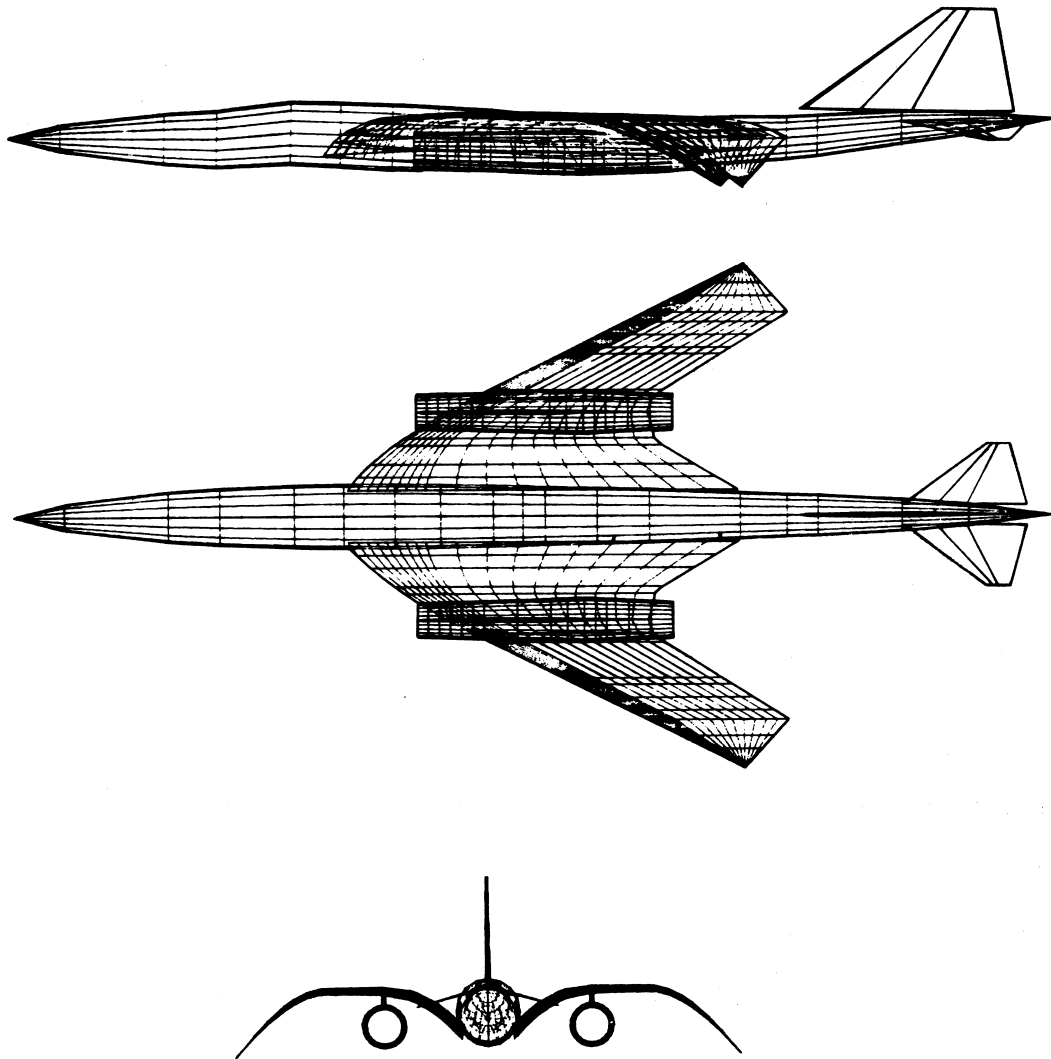
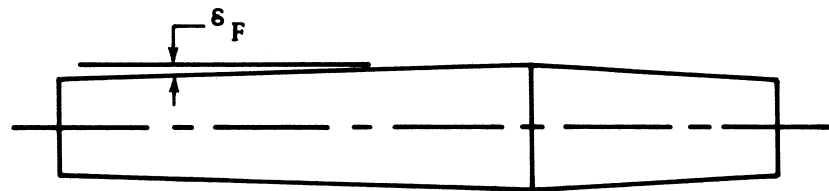


Figure 42 Computer Representation of Model 3056-2



BASIC NACELLE

MACH = 3.0

OPTIMIZED CAMBER SCALING

— WING WITH LATERAL CURVATURE
 --- WING WITHOUT LATERAL CURVATURE

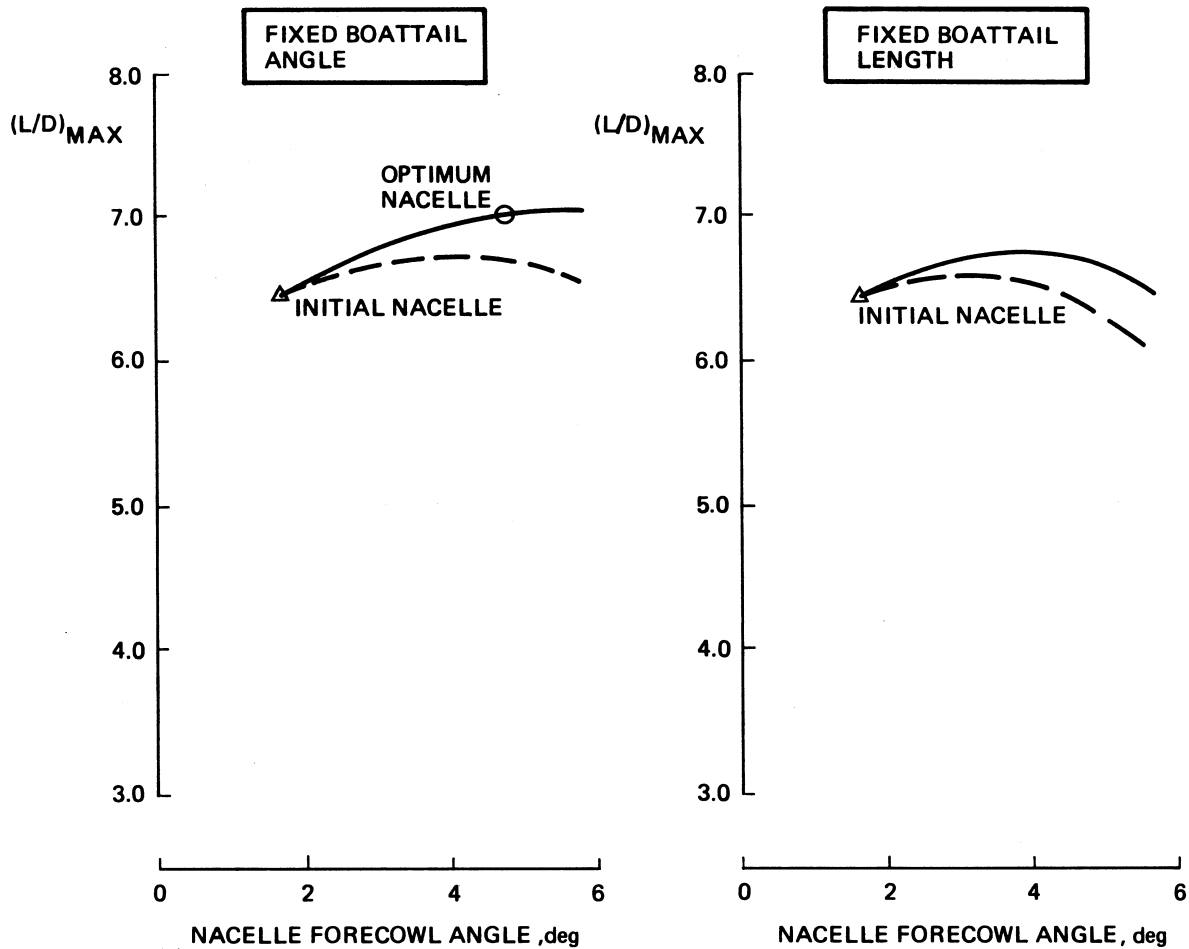


Figure 43 Double-Parasol Wing-Nacelle Optimization

The wing camber design for Model 3056-2 was developed with the basic nacelle. The design camber was reoptimized by a linear scaling factor for the optimum area growth nacelle. The results are shown in Figure 44.

The results obtained with the original nacelle and wing camber, and also with the optimized wing camber and nacelle area growth are compared with the aerodynamic characteristics of the reference airplane in the next section.

3. Aerodynamic Comparisons

The subsonic and supersonic drag polars for the reference conventional airplane Model 3056-1 are shown in Figure 45. The favorable interference double parasol wing configuration drag polars are shown in Figures 46 and 47 respectively.

The calculated lift curve slopes are shown in Figure 48. The lift curve slope, $C_{L\alpha}$ of the parasol wing concept exceeds the $C_{L\alpha}$ of the reference airplane because of its higher aspect ratio and lower sweep.

The maximum lift drag ratios of the favorable interference parasol wing concept and the reference airplane are shown in Figures 49 and 50.

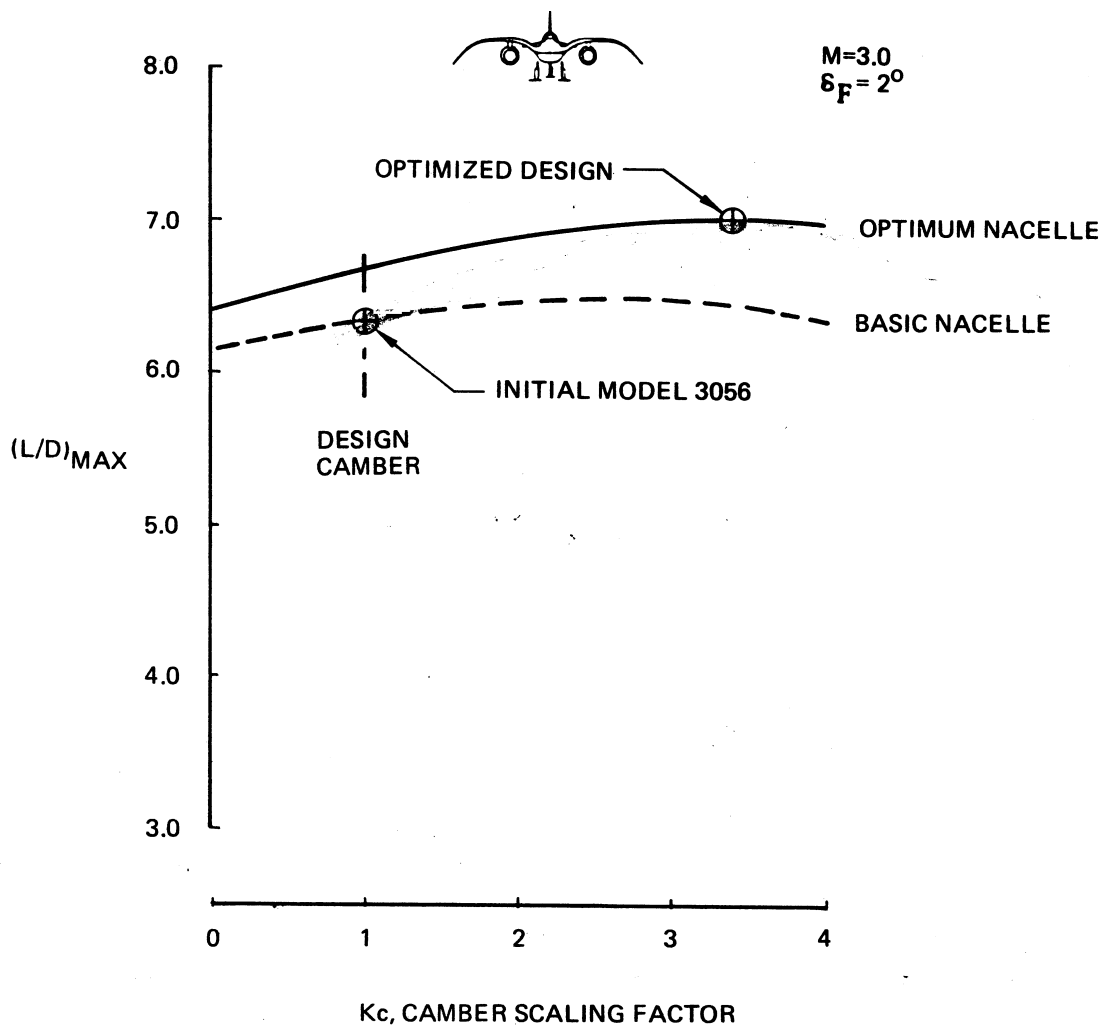


Figure 44 Double-Parasol Wing Camber Optimization

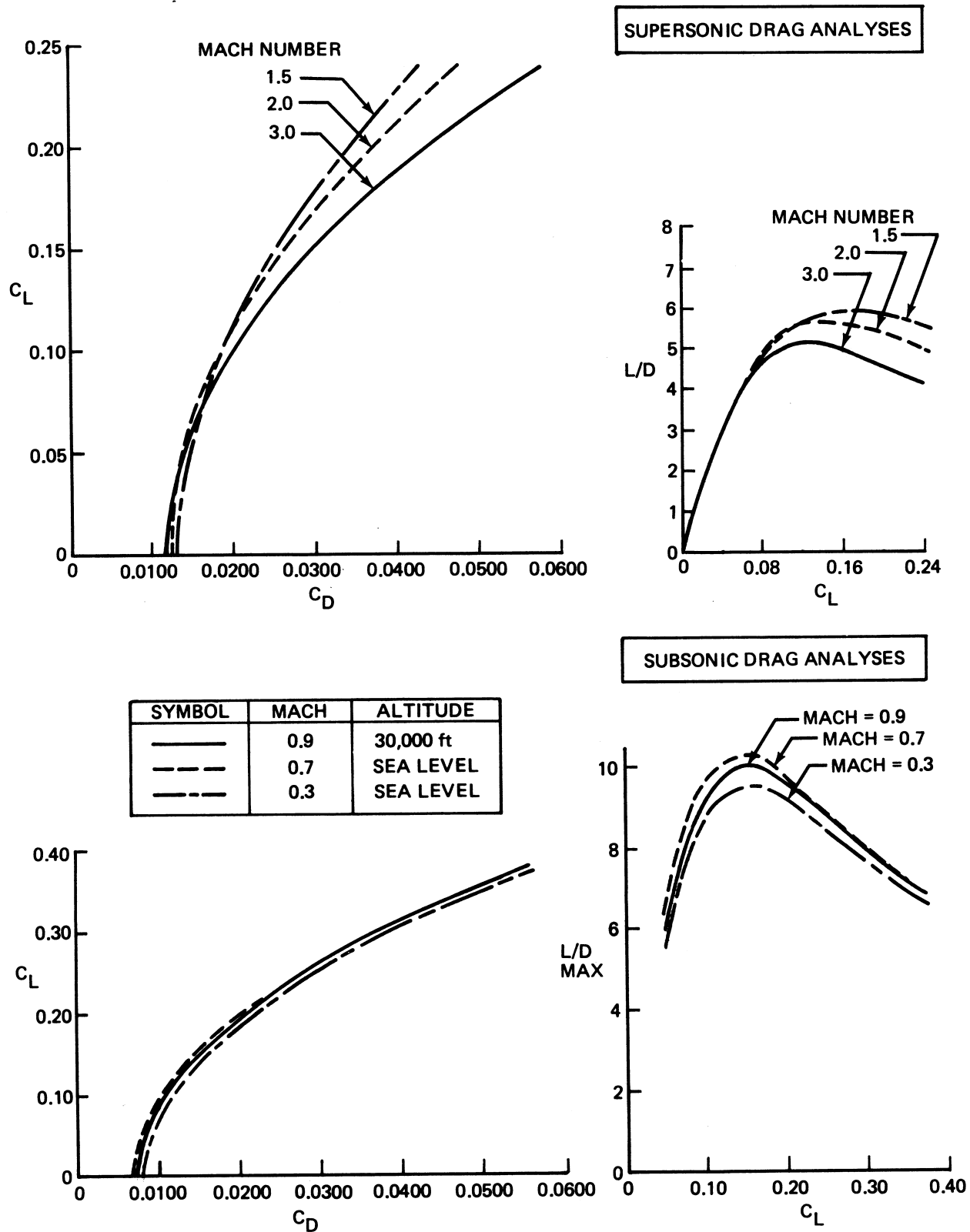
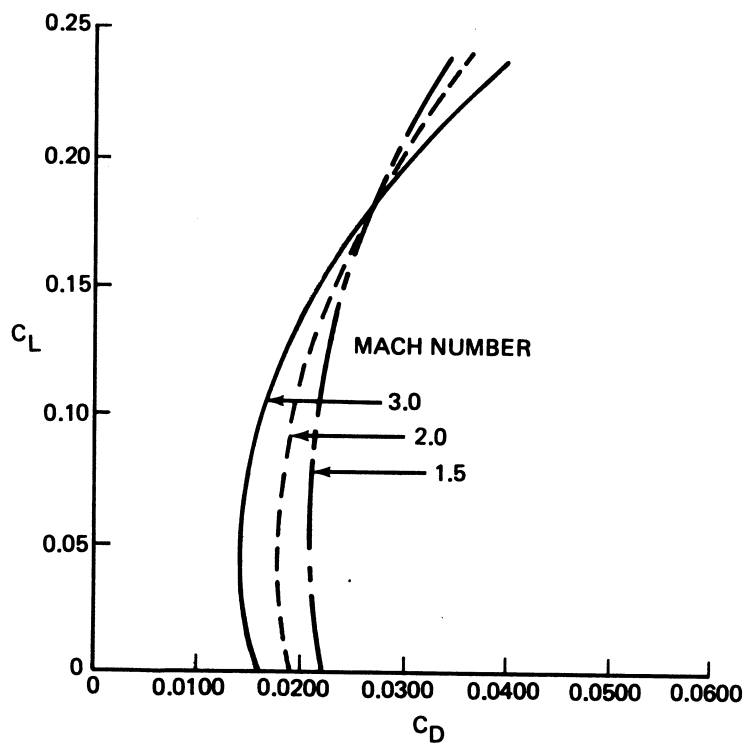
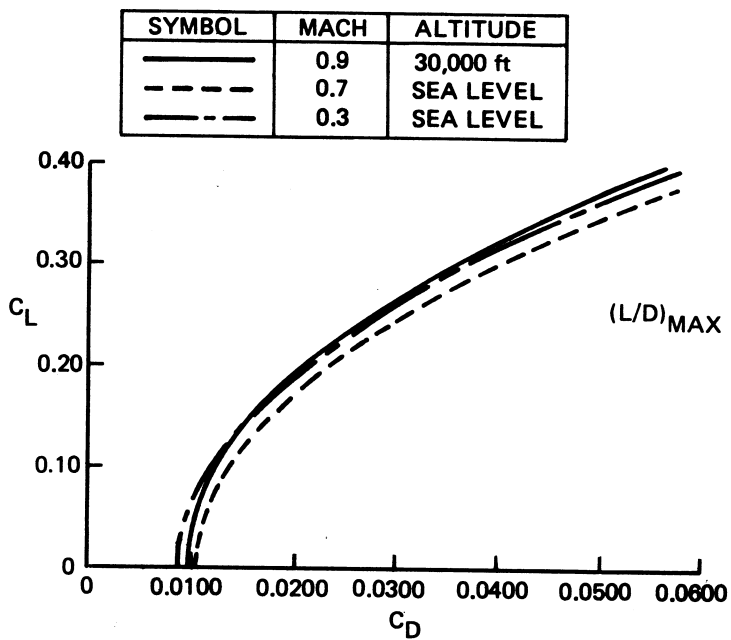
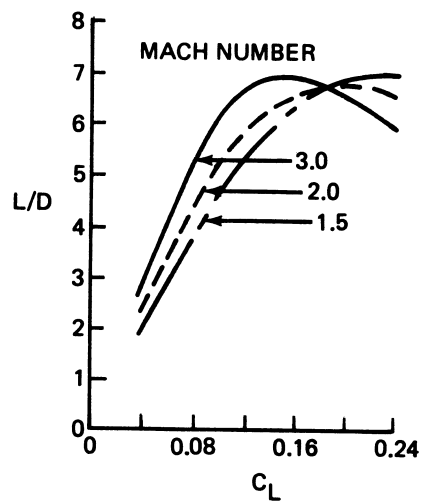


Figure 45 Reference Configuration, Model 3056-1, Drag Analysis



SUPERSONIC DRAG ANALYSES



SUBSONIC DRAG ANALYSES

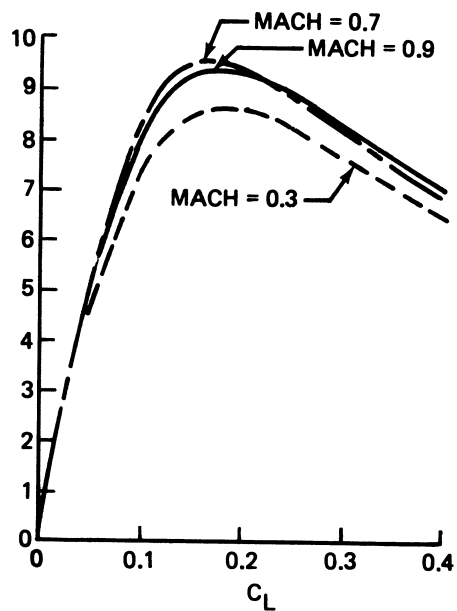


Figure 46 Double-Parasol Wing Configuration, Model 3056-2, Drag Analyses

DOUBLE-PARASOL WING L/D IMPROVEMENTS

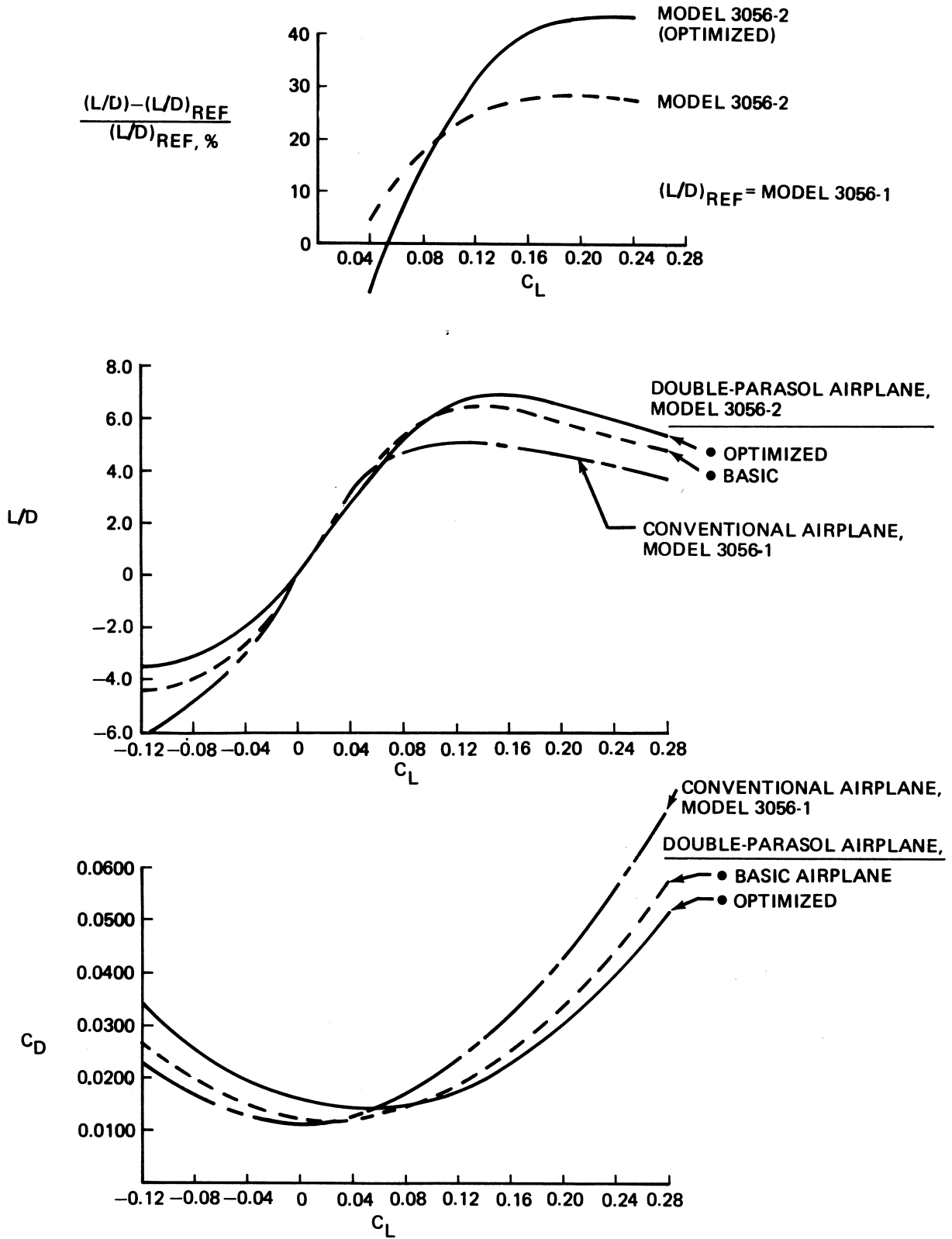


Figure 47 Double-Parasol Wing Configuration, Model 3056-2, Mach = 3.0 Cruise Drag Analysis

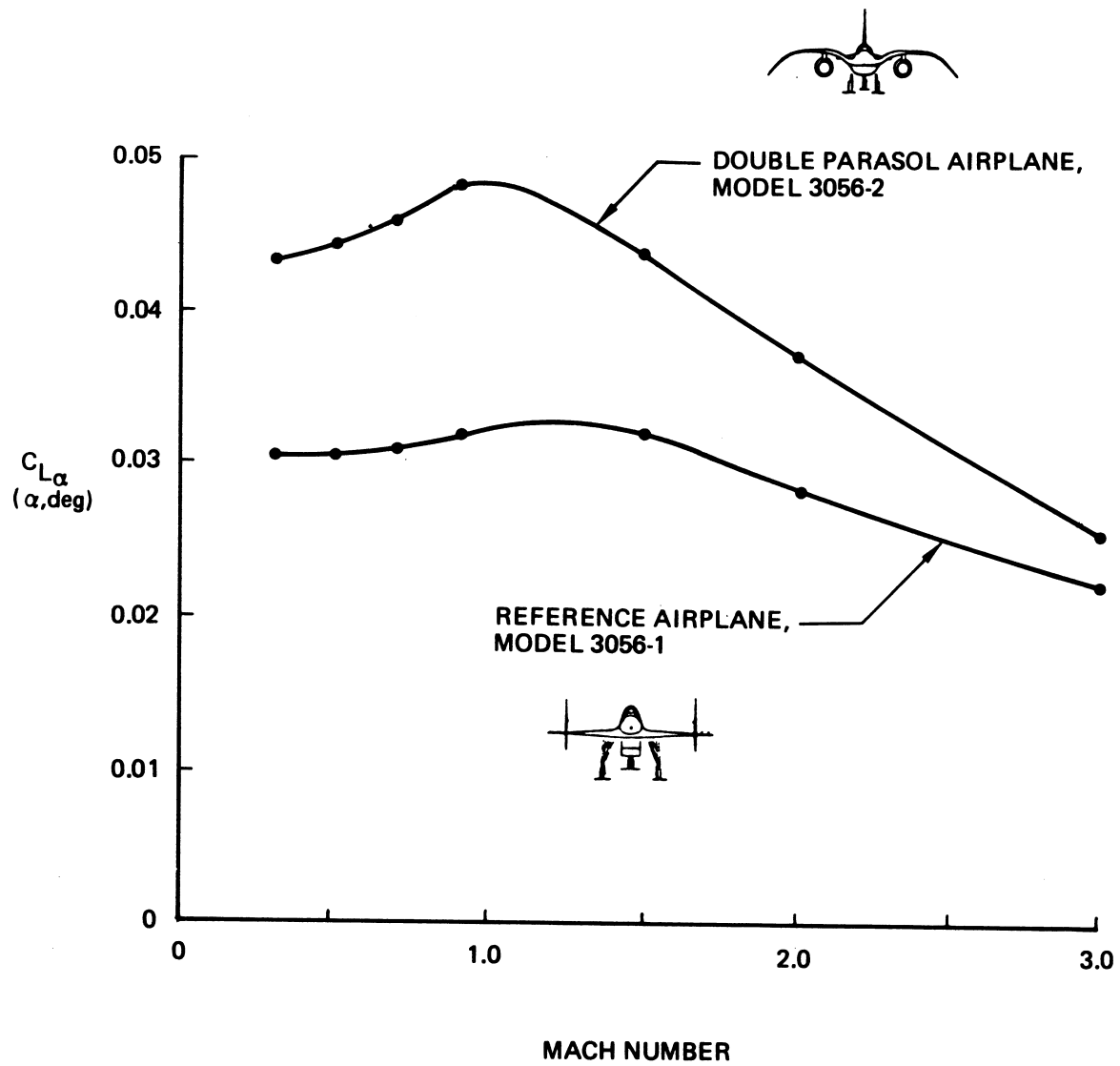


Figure 48 Lift Curve Slope Comparison

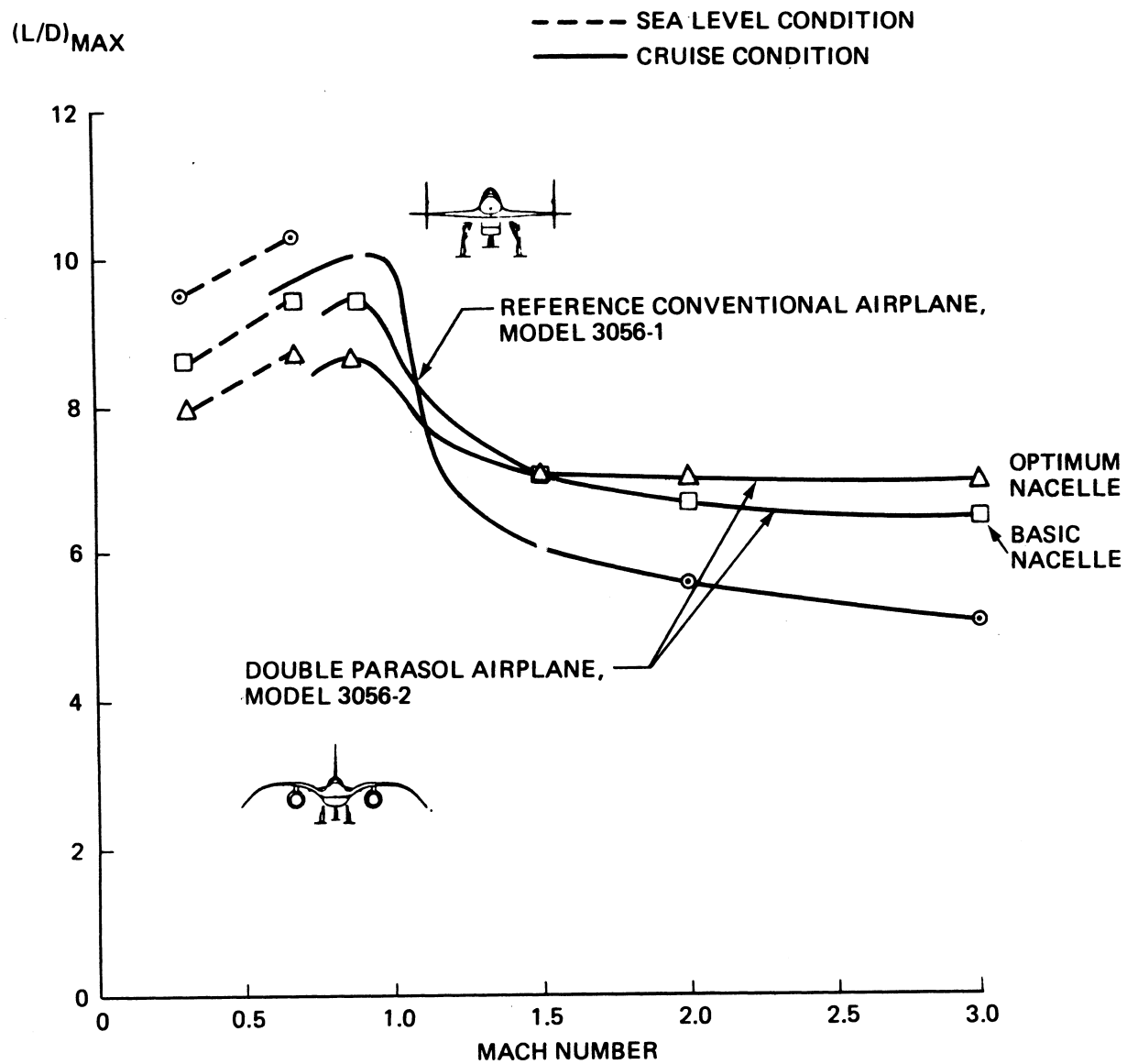


Figure 49 Maximum Lift/Drag Ratio Comparison

MACH = 3.0

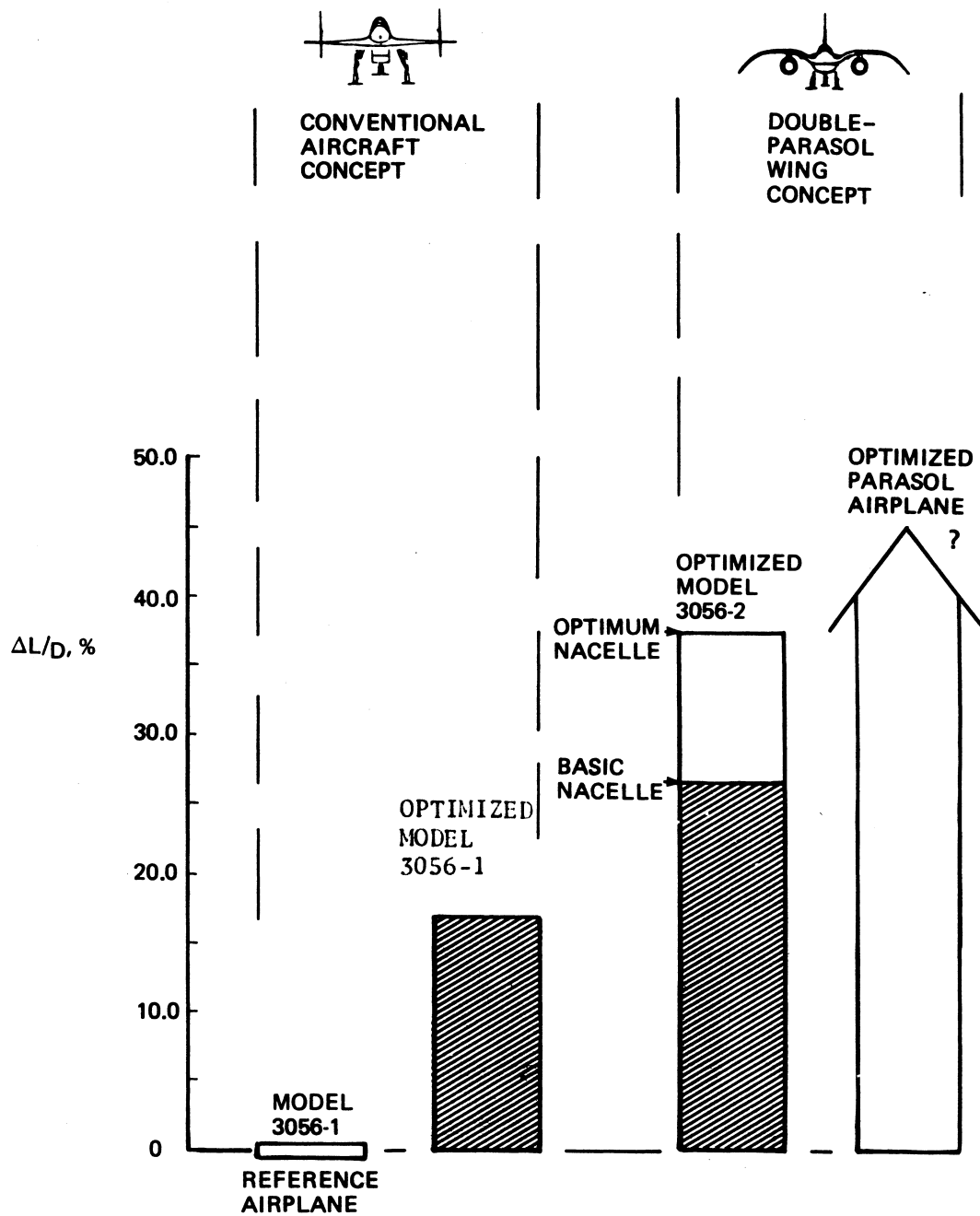


Figure 50 Double-Parasol Wing Aerodynamic L/D Improvement

The double parasol wing configuration at the Mach 3.0 design condition offers a potential improvement in the lift drag ratio of approximately 37%. Additional theoretical and coordinated experimental studies will be necessary to fully identify the potential benefits of this configuration concept.

4. Performance Comparisons

A performance evaluation was made on the two final configurations, the "zero interference" baseline aircraft (3056-1) and the favorable interference aircraft (3056-2). These comparisons were made for the mission as presented in Figure 33 of Section VII using the mission guidelines used for the Boeing ATS supercruiser studies. In brief, the mission rules optimize the combined stages of the flight path for maximum radius.

In the preliminary performance analysis for the baseline aircraft, the engine thrust to weight ratio and the vehicle wing loading were found to be dictated by the 3 1/2g maneuver requirement at Mach 0.9 and 30,000 ft altitude. This engine-airplane sizing was then prescribed for the favorable interference double parasol aircraft. These considerations and the cruise altitude dictated by the mission optimization required both aircraft to cruise at a C_L below that corresponding to $(L/D)_{MAX}$. Figure 51a shows the cruise C_L and C_L at $(L/D)_{MAX}$ for both aircraft. Mission optimization of the favorable

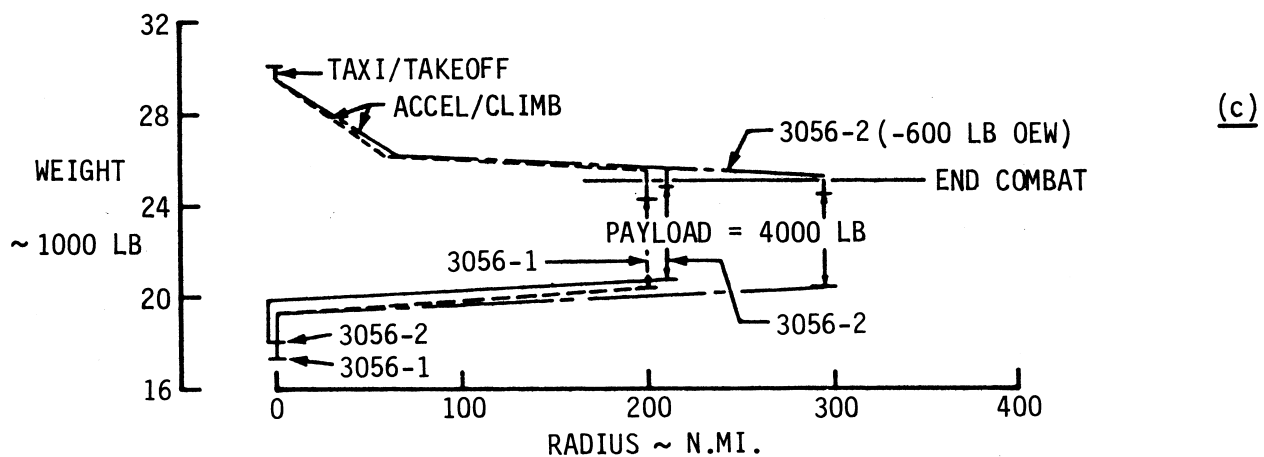
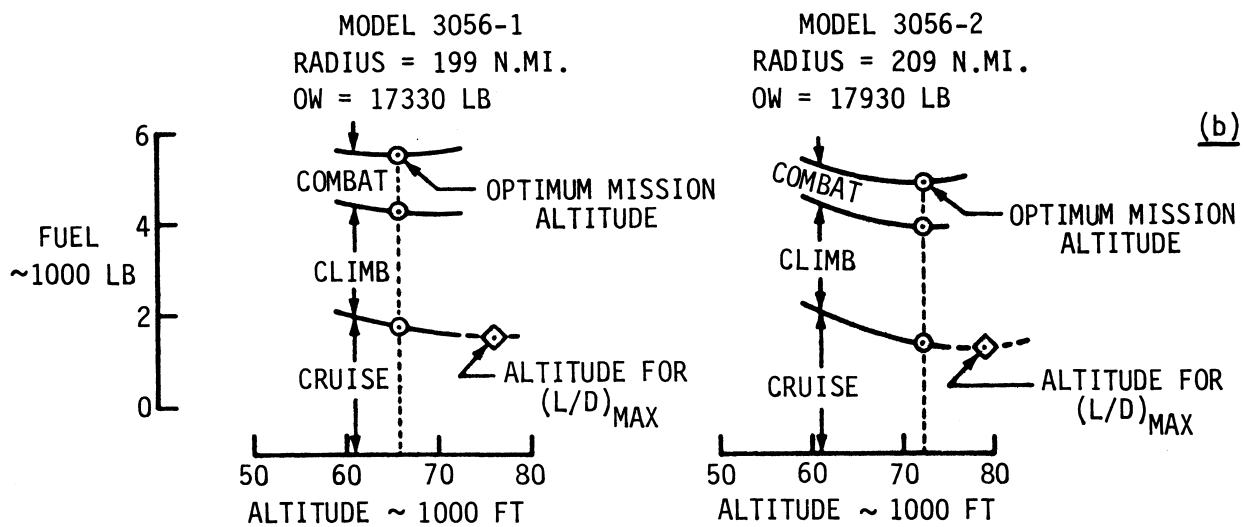
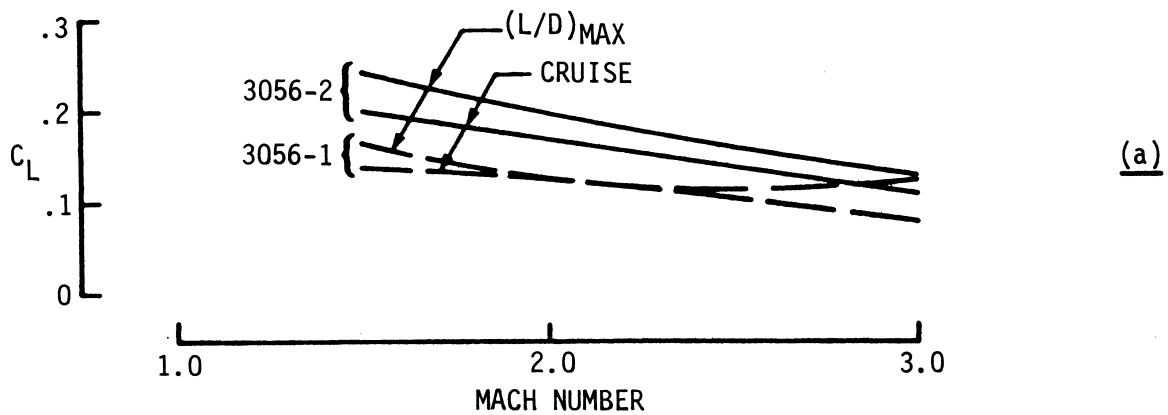


FIGURE 51 CRUISE PERFORMANCE

interference configuration with a higher C_L at $(L/D)_{MAX}$ than for the zero interference supercruiser, specified a higher cruise altitude. The fuel burned at altitude is presented in Figure 51b for the various mission legs. Due to a higher structural weight, the double-parasol aircraft has 600 lb less fuel to burn. Figure 51c shows the aircraft weight history during the mission for the two comparison aircraft. Here also is shown the mission radius penalty due to the 600 lb greater OEW for the double parasol configuration. If the OEW of the latter were no higher than the baseline configuration, Figure 51c indicates a 41% improvement in range for the double parasol configuration.

The total percent fuel used by the favorable and zero interference configurations for the different stages of the Mach 3.0 cruise mission is presented in Figure 51d. At the lower cruise Mach numbers, the double-parasol aircraft requires a higher percentage of its total fuel for climb to altitude than the baseline, degrading its range capability.

Optimum mission radius for cruise for $1.5 \leq M \leq 3.0$ is presented in Figure 51e, for the two configurations. At Mach 3.0, the favorable interference aircraft has a 5% improvement in range over the baseline aircraft carrying the same 4,000 lb store payload. Reducing the payload to 2,000 lb and increasing the fuel weight by 2,000 lb show the double-parasol supercruiser to

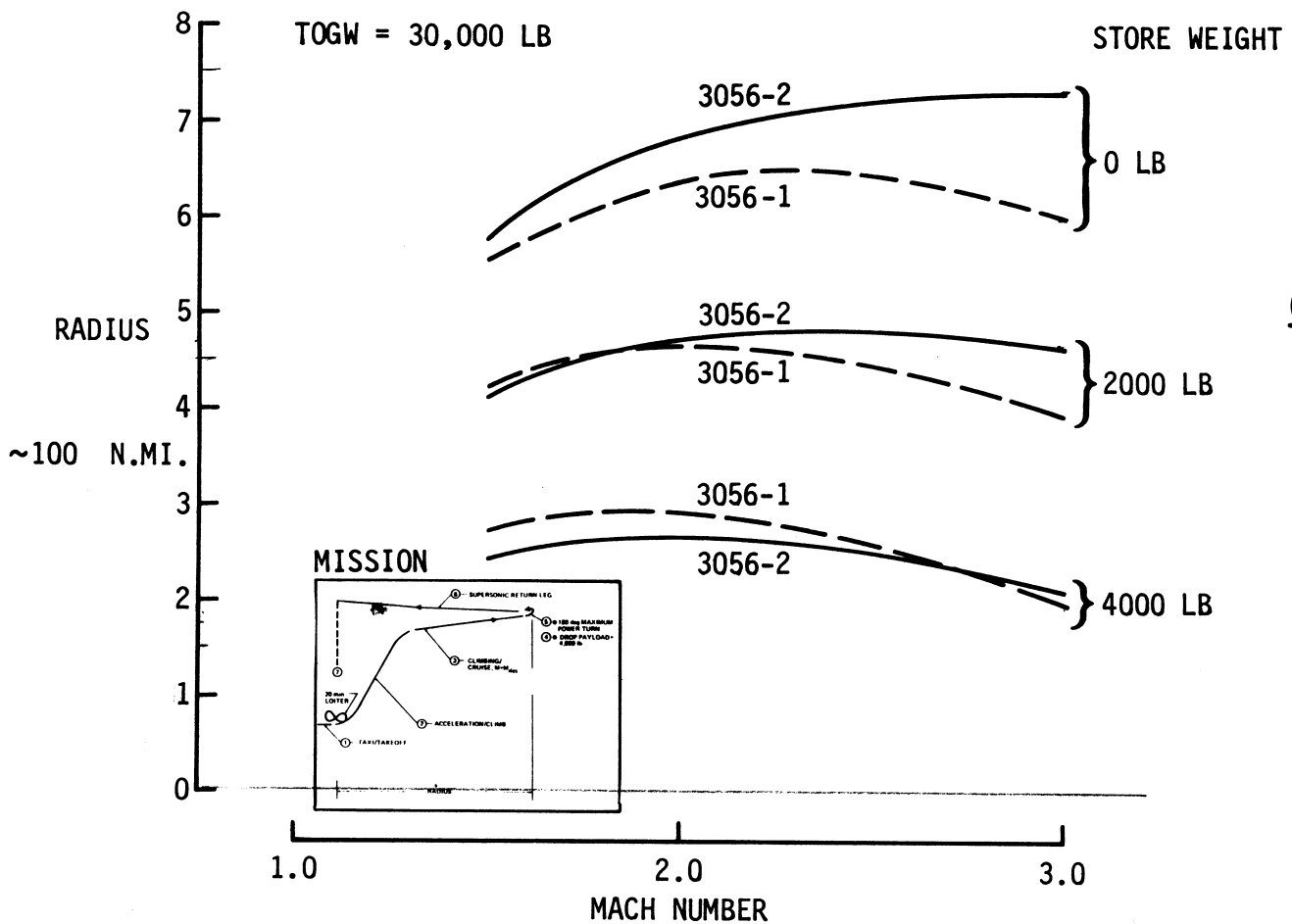
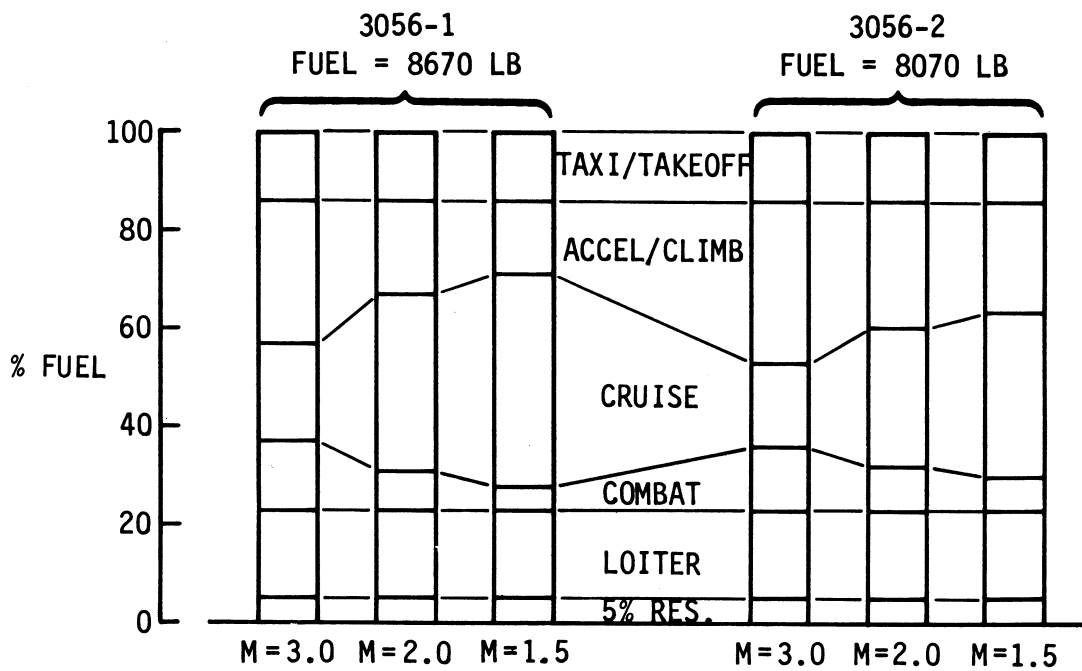


FIGURE 51 CRUISE PERFORMANCE (CONT.)

have a 17.5% improvement in range over the baseline carrying the same payload. Further relative improvement in radius is shown when all the payload is replaced by fuel.

These latter considerations show the severe performance penalties for both comparison aircraft by constraining the overall vehicle weight to 30,000 lb for the Mach 3 cruise. Increasing the prescribed vehicle gross weight to higher values would permit proportionately greater fuel weight leading to increased mission radii. With increased radii the improved L/D of the double parasol configuration would then lead to more significant improvements of the radius relative to the baseline configuration.

SECTION IX

CONCLUSIONS

The purpose of the study was to identify various ways that favorable interference can increase the aerodynamic efficiency of supersonic aircraft. Comparisons were made between the aerodynamic and weight characteristics of a reference conventional type configuration and a favorable interference concept incorporating a double parasol wing concept.

Major conclusions of the study that apply specifically to a small supersonic aircraft include.

- The parasol wing concept was identified as offering the greatest potential aerodynamic benefits relative to the other concepts considered ("wave riders", supersonic biplanes, flat top wing/bodies).
- The best aerodynamic concept is very dependent upon the design Mach number. The interference concepts considered in this study become more difficult to integrate to a viable aircraft configuration as the design Mach number is reduced.
- The maximum lift/drag ratio of the double parasol-wing configuration exceeds that of the reference airplane from approximately 18% at $M = 1.5$ to 37% at $M = 3.0$.

- The parabolic lateral curvature of the double parasol wing configuration offered a slight improvement over an equivalent double parasol configuration without lateral curvature when the nacelle area growth was optimized.
- Removal of the lateral curvature on the outboard portion of the wing may further increase the aerodynamic efficiency of the double parasol wing concept.
- Existing aerodynamic and design tools, ADASSA and FLEXSTAB, can predict the force and moment characteristics of flat type configuration applications. Neither method can predict multiple reflection effects on interference lift for bodies very close to a parasol wing surface.
- FLEXSTAB can predict lateral curvature effects on interference lift in agreement with slender body theory predictions. However, ADASSA which uses Witham's theory to predict body shocks is more accurate than FLEXSTAB for predicting the interference pressure patterns. This is particularly true as the body fineness ratio is reduced (i.e., body becomes thicker).

- The significant improvement in the cruise L/D obtained for the favorable interference double parasol aircraft did not lead to comparable improvement in the mission radius due to the gross weight constraint of 30,000 lb. Increasing the latter would permit greater fuel weight ratios, and hence more significant radius improvements for the double parasol configuration.
- More aerodynamic design and detailed design studies are necessary to determine the potential of the double parasol A/P concept.
- An alternate body parasol configuration should be developed and compared with the double parasol concept for both design and off design conditions.

- The significant improvement in the cruise L/D obtained for the favorable interference double parasol aircraft did not lead to comparable improvement in the mission radius due to the gross weight constraint of 30,000 lb. Increasing the latter would permit greater fuel weight ratios, and hence more significant radius improvements for the double parasol configuration.
- More aerodynamic design and detailed design studies are necessary to determine the potential of the double parasol A/P concept.
- An alternate body parasol configuration should be developed and compared with the double parasol concept for both design and off design conditions.

APPENDIX

AERODYNAMIC METHODS SUBSTANTIATION

The aerodynamic design and analyses methods that have been used in the study are described in this section. Test versus theory comparisons that were made to validate the use of these methods for the study configurations are also included in this section.

1. Aerodynamic Design and Analysis Methods

The methods used for the aerodynamic design of the study configurations are summarized in Table 6. The aerodynamic evaluation procedures are shown in Table 7. The aerodynamic analytical methods used for a particular aerodynamic concept application depended on the nature of the configuration, the Mach number, and the desire to use the most efficient applicable analytical tool.

The "Aerodynamic Design and Analysis System for Supersonic Aircraft," (33) ADASSA (Boeing Computer Code A389), represents currently one of the best supersonic aerodynamic design and analysis tools. This is an integrated system of computer programs that compute:

- 1) Turbulent skin friction

Table 6 Drag Estimation Procedures

Drag component	Method	Mach		Interference capability				Boeing computer program	
		Subsonic	Supersonic	Isolated	Volume—volume	Volume—lift	Lift—lift		Lift—sideforce
C_{D_F} . . . Friction drag	<ul style="list-style-type: none">• Sommer and short T^* method• Local “q” and 3-D corrections	X	X	X					A389
C_{D_W} . . . Volume wave drag	<ul style="list-style-type: none">• Supersonic area rule• Middleton—ADASSA• Woodward—AIC• FLEXSTAB• Exact shock expansion		X	X	X				A80, A389
			X	X	X				A389
		X	X	X	X	X			A217
		X	X	X	X	X			A260
			X	X	X	X			—
C_{D_L} . . . Drag due to lift	<ul style="list-style-type: none">• Middleton—ADASSA• Woodward—AIC• FLEXSTAB• Feifel vortex lattice• Exact shock expansion		X	X		X			A389
and		X	X	X		X	X	X	A217
$C_{D_{TRIM}}$. . . Trim drag		X		X		X	X	X	A260
(attached flow)			X	X		X	X	X	A372
			X	X		X	X	X	—

Table 7 Aerodynamic Design Methods

Aero-design item	Method	Mach		Component capability								Boeing computer program	
		Subsonic	Supersonic	Wing + body	Multibodies	Planar	Nonplanar	Multiwings	Fins	Tails	Canards		Flaps
●Camber and twist ●Component alignment	● Middleton—ADASSA		X	X		X				X	X	X	A389
	● Woodward—AIC	X	X	X		X	X	X	X	X	X	X	A217
	● FLEXSTAB	X	X	X		X	X	X	X	X	X	X	A260
	● Feifel vortex lattice	X				X	X	X	X	X	X	X	A372
Body contouring	● Supersonic area rule		X	X	X	X			X	X	X		A80, A389
	● Middleton—ADASSA		X	X	X	X			X	X	X		A389
Stores and nacelles Design and location	● Middleton—ADASSA		X	X	X	X							A389
	● FLEXSTAB	X	X	X	X	X	X	X					A260

- 2) Near-field theory wave drag
- 3) Far-field theory wave drag and also provides wing-body area rule optimization
- 4) Lift, pitching moment, and drag due to lift calculation
- 5) Optimum wing camber and twist designs for specified design constraints including lift, pitching moment, and pressure limits. Effects of the fuselage, canards, and nacelles are included.

The code is restricted to planar wings, i.e., lifting surfaces which lie in a single plane. The code does include non-linear methods that provide realistic determination of shock waves produced by general bodies and also the intersection of the shock waves and pressure fields with adjacent bodies and wings.

The aerodynamic influence coefficient, AIC, method used in FLEXSTAB (34) provides the capability of the design and analysis of supersonic as well as subsonic planar or non-planar aerodynamic configurations. The FLEXSTAB program can account for the mutual interference of lifting and thickness effects of the various airplane components.

The drag due to lift calculated by either FLEXSTAB or by ADASSA programs is obtained by integration of the lifting

pressures times the local mean line slope at the appropriate angle of attack. Theoretical drag due to lift for wings with subsonic leading edges should include a thrust component associated with the very large leading edge expansion pressures acting on the front portion of the wing airfoils. (35) The drag evaluations in the studies reported herein include an empirical fraction of leading edge suction force correction to the theoretical drag due to lift calculations. This correction was not significant at the cruise Mach number = 3.0 for the study configurations but was important only at the lower Mach numbers.

The three-dimensional vortex lattice program (program A372) developed by Winfred Feifel of Boeing can be used for the subsonic design evaluations. The vortex lattice program (A372) is a rather efficient subsonic design analysis and optimization program capable of handling the most general planar or non-planar configurations.

Exact shock-expansion techniques have been used to evaluate supersonic aerodynamic characteristics of the non-planar caret wing and Nonweiler wing concepts.

The skin friction calculations assumed fully turbulent flow on all the component surfaces. Estimates of miscellaneous drag items such as forebody canopy drag, boundary layer diverter drag,

and roughness drag, are based on Boeing experimental data correlations.

2. Conventional Aircraft Configurations Test Versus Theory Comparisons

These aerodynamic design and analysis methods have been used by Boeing in government funded, in addition to company funded, supersonic aircraft systems studies. These methods have been well substantiated for conventional wing/body and wing/body/nacelle configurations. Figure 52 contains the results of recent test-theory comparisons for the Lightweight Experimental Supercruise Model LES 216.

These and other similar test versus theory comparisons indicate these linear theory methods provide a good evaluation of the aerodynamic characteristics of conventional type supercruise aircraft configurations such as the study reference configuration.

3. Parasol Wing-Body Test Versus Theory Comparisons

Results of other test-theory comparisons have indicated these methods are capable of predicting interference lift, mutual body interference, and body wave drag cancellation effects inherent in the parasol wing concept.

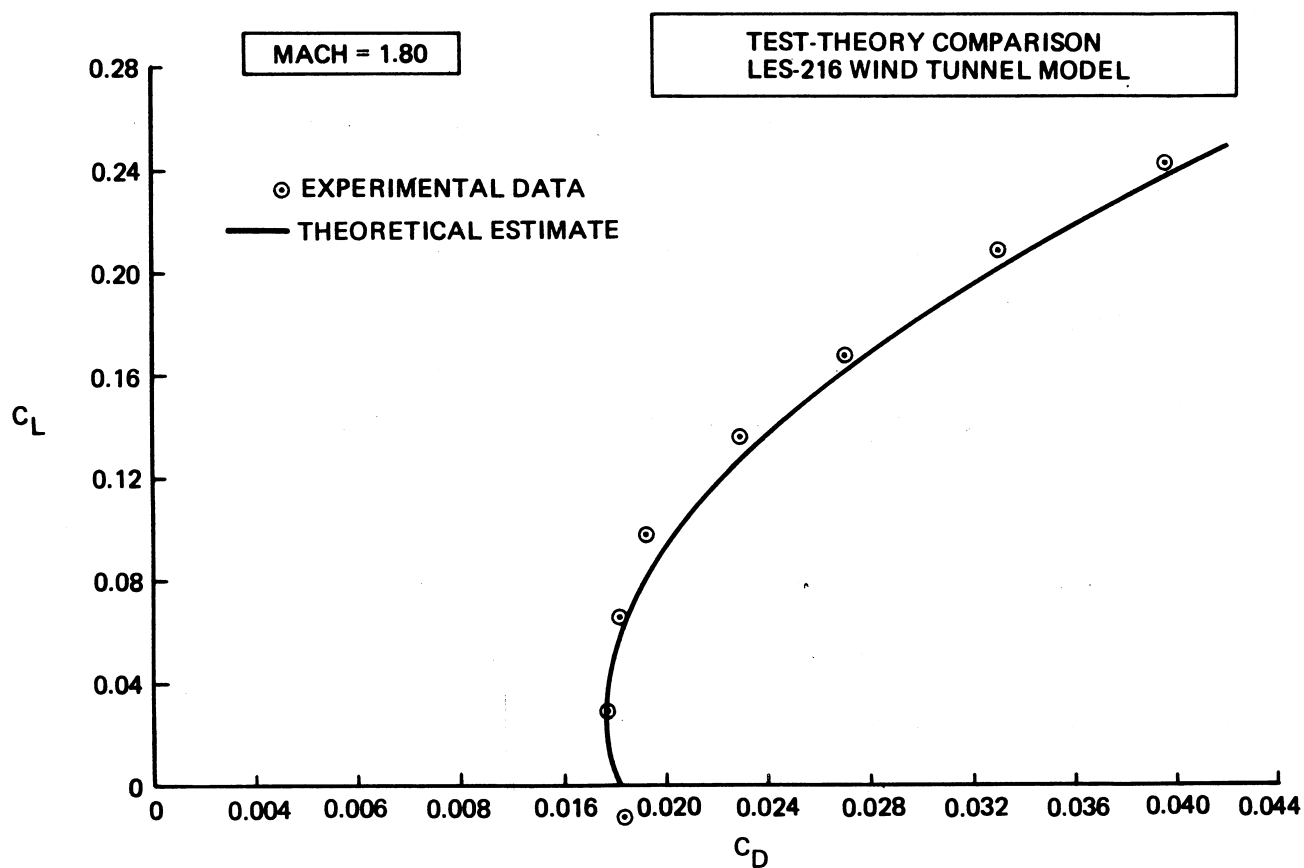
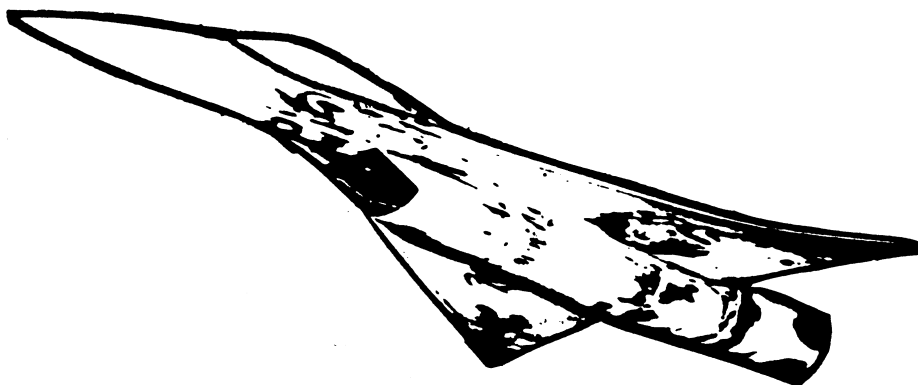


Figure 52 Supercruiser Type Configuration—Test Theory Comparison

In order to further substantiate these methods theoretical predictions were made of the NASA parasol wing wind tunnel model (28) shown in Figure 53. The computer representations of the parasol wing wind tunnel model is shown in Figure 54.

The test-theory comparisons are shown in Figure 55. The lift, drag and lift/drag ratio predictions are quite good. The differences between the experimental and theoretical pitching moment data indicate that the predicted aerodynamic center is further aft than indicated by the test data.

Figure 56 contains a summary test-theory comparison of maximum lift/drag ratio and interference lift coefficient, ΔC_L .

A major difference between the theoretical calculations obtained with FLEXSTAB and the results obtained with ADASSA is illustrated in Figure 57. ADASSA predicts the body bow shock wave which forms forward of the Mach wave cone from the body nose. The linear theory results of FLEXSTAB restrict the body influence to the area behind the Mach cone.

The Mach cone at Mach 3.0 from the body nose intersects the parasol wing behind the leading edge. However, the predicted shock wave actually falls in front of the wing leading edge as shown in Figure 57. The ADASSA results which predict slightly

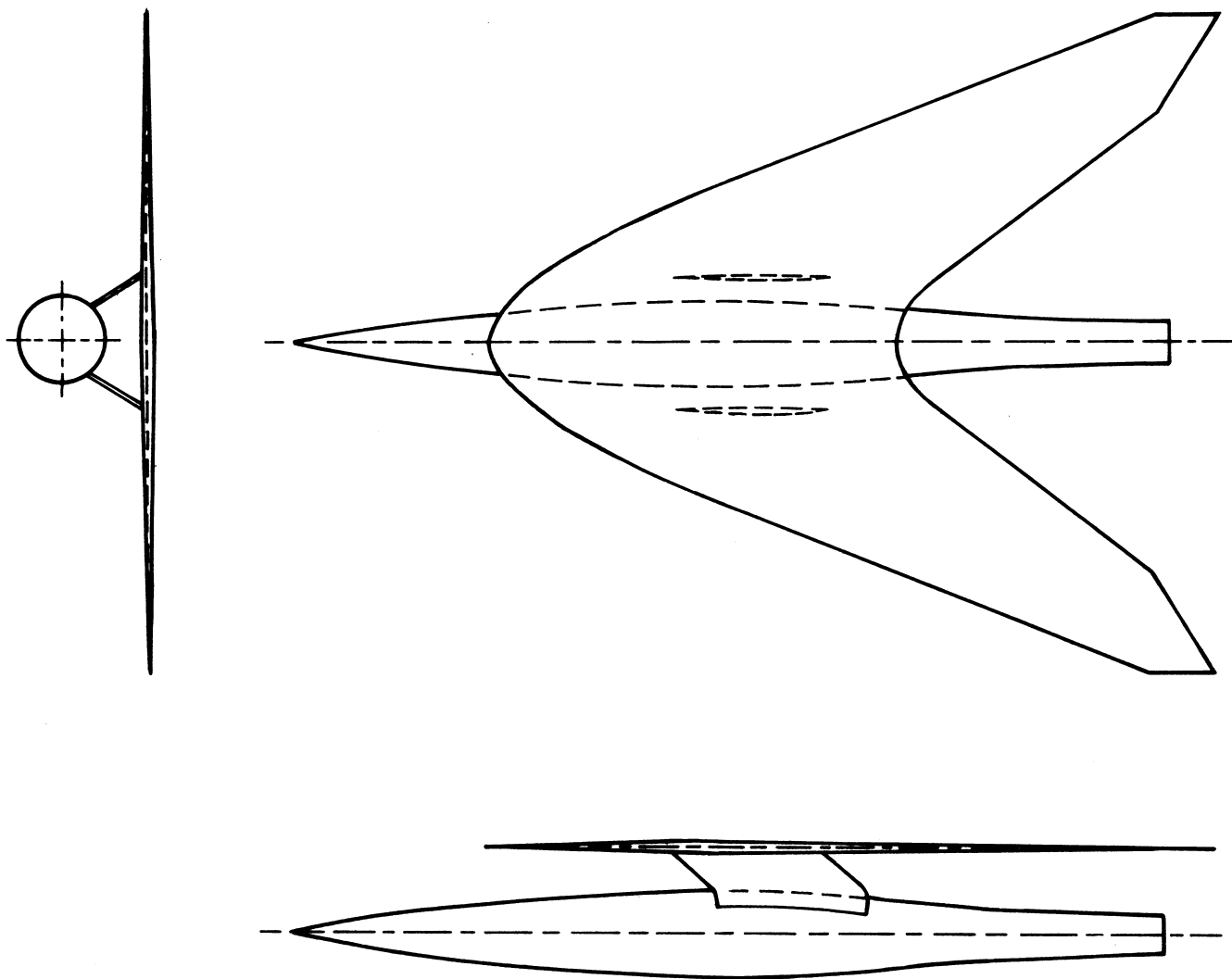


Figure 53 NASA Parasol Wing-Body Wind Tunnel Model

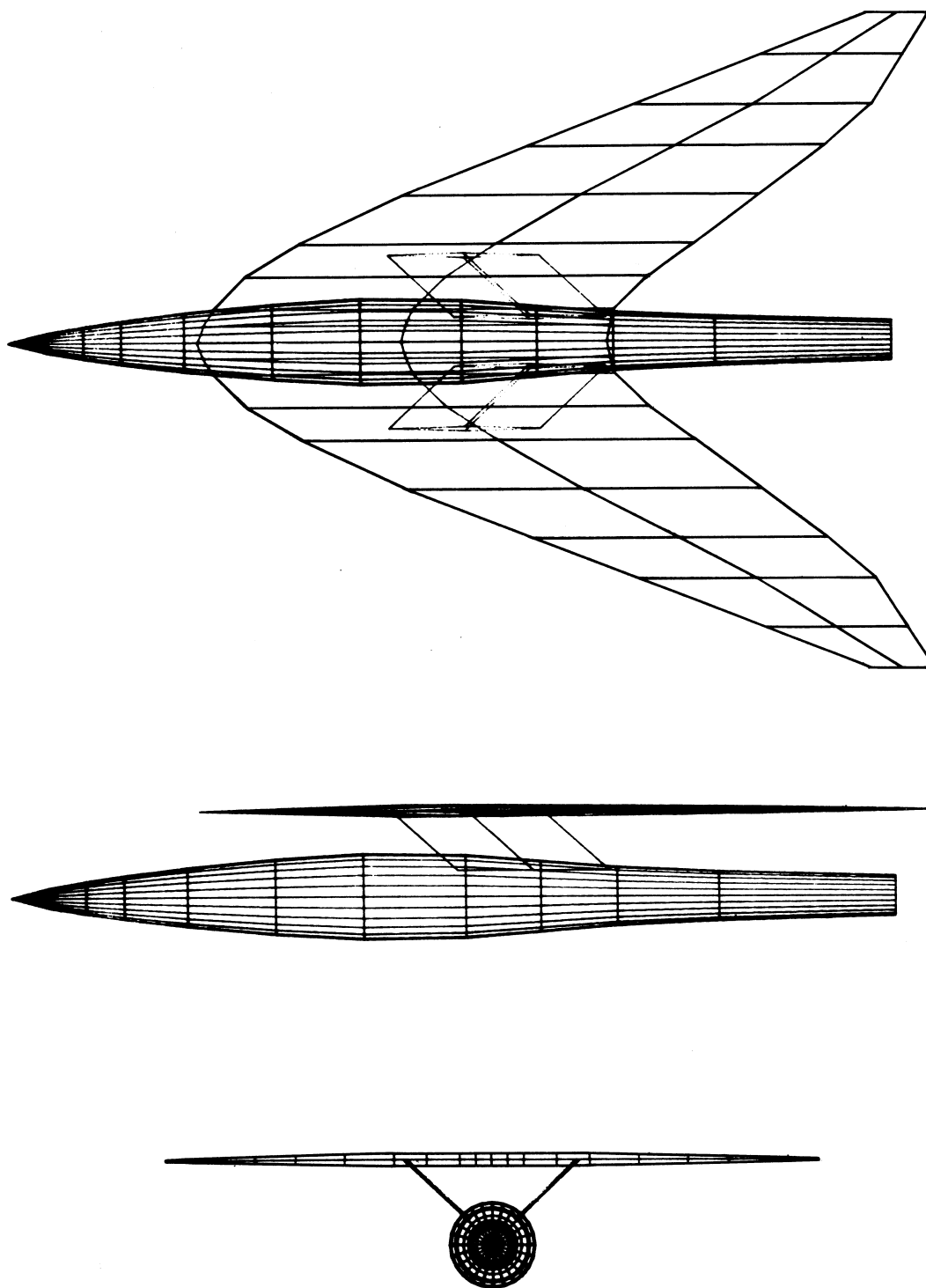


Figure 54 *Analytic Model of the NASA Parawing Wind Tunnel Model*

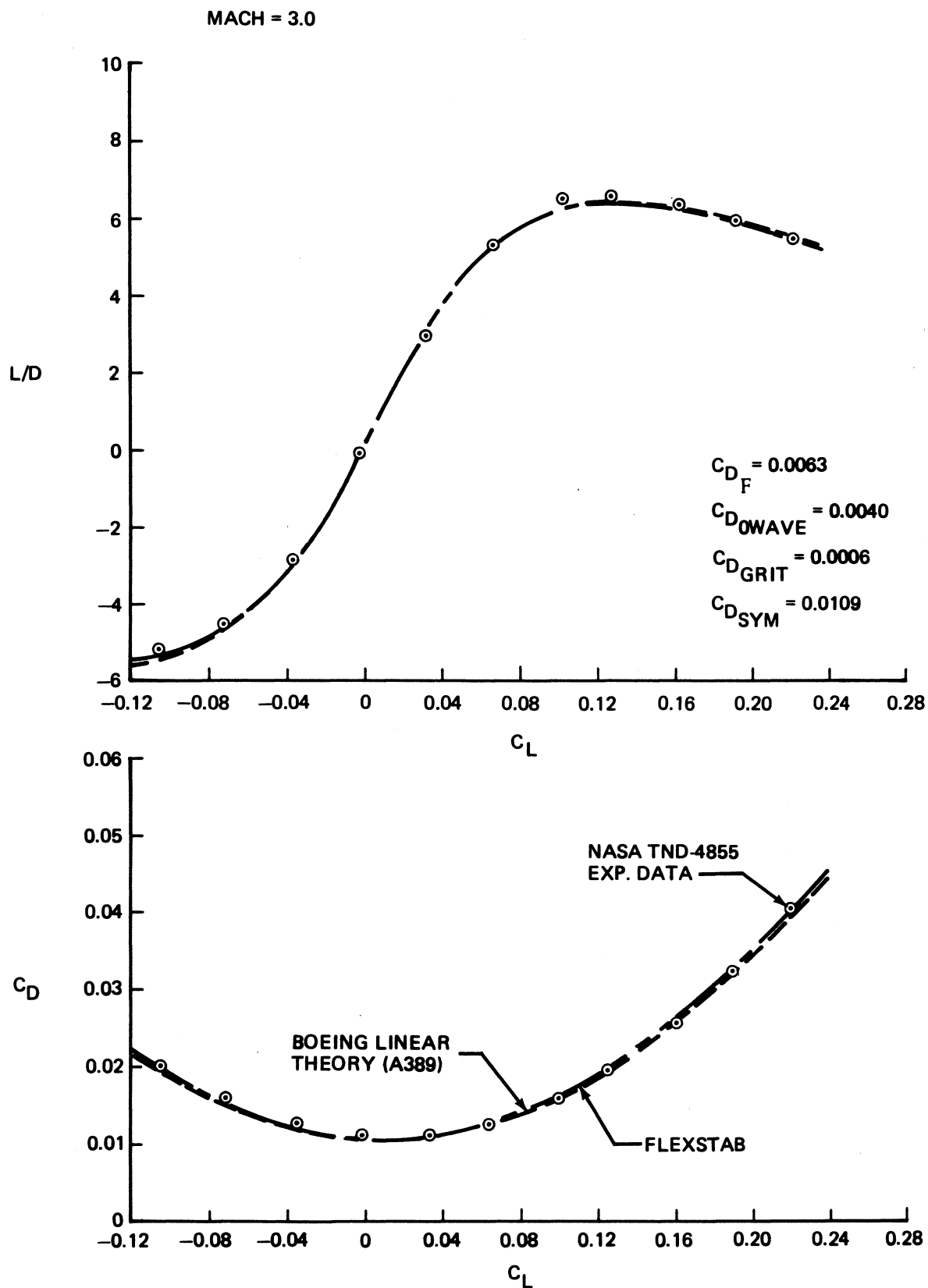


Figure 55a Comparison of Parasol Wing Theoretical Predictions

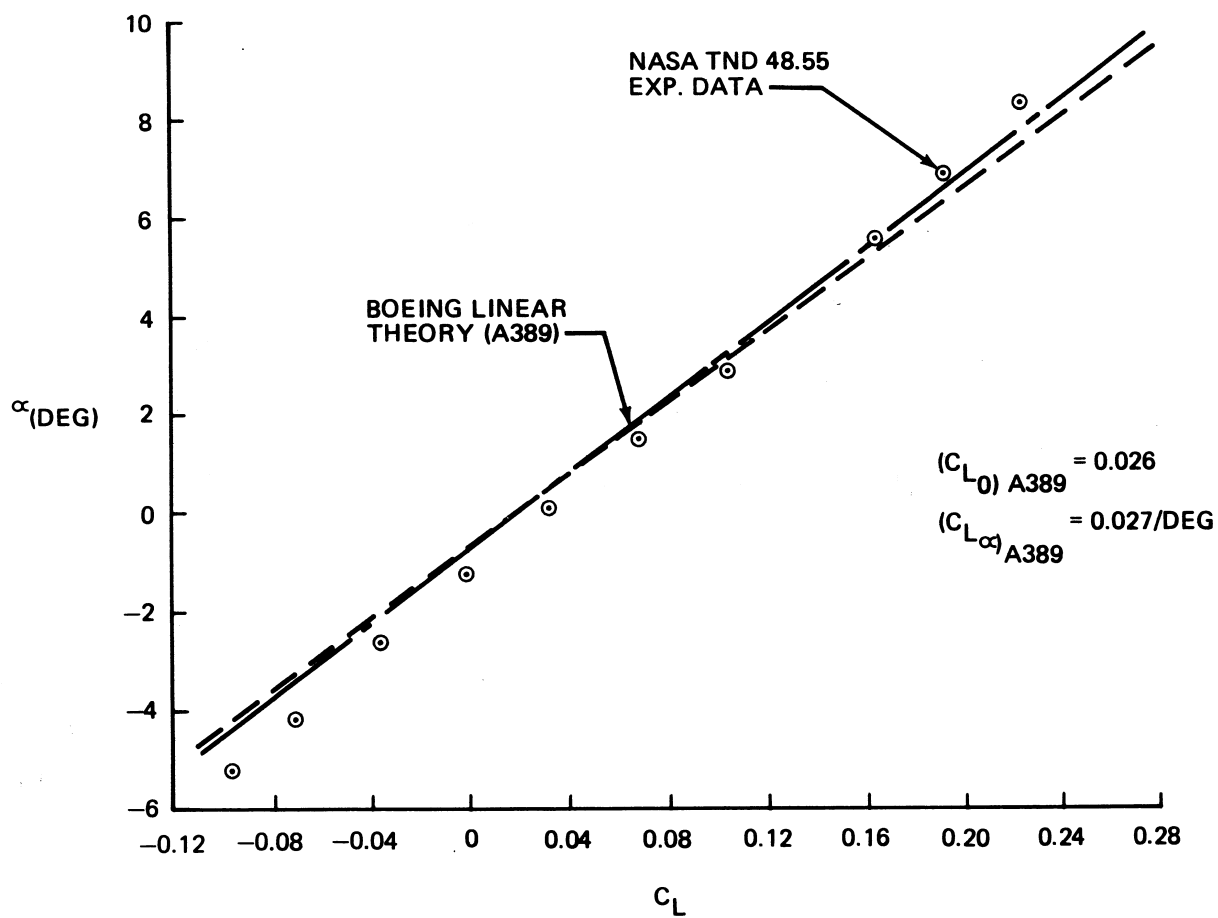
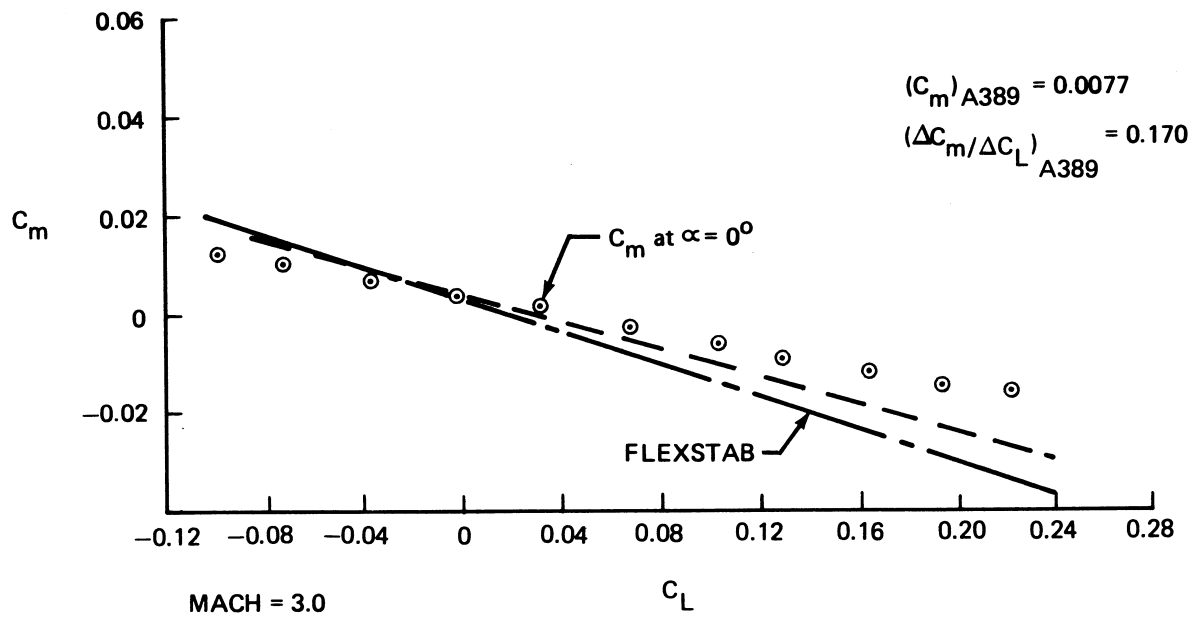
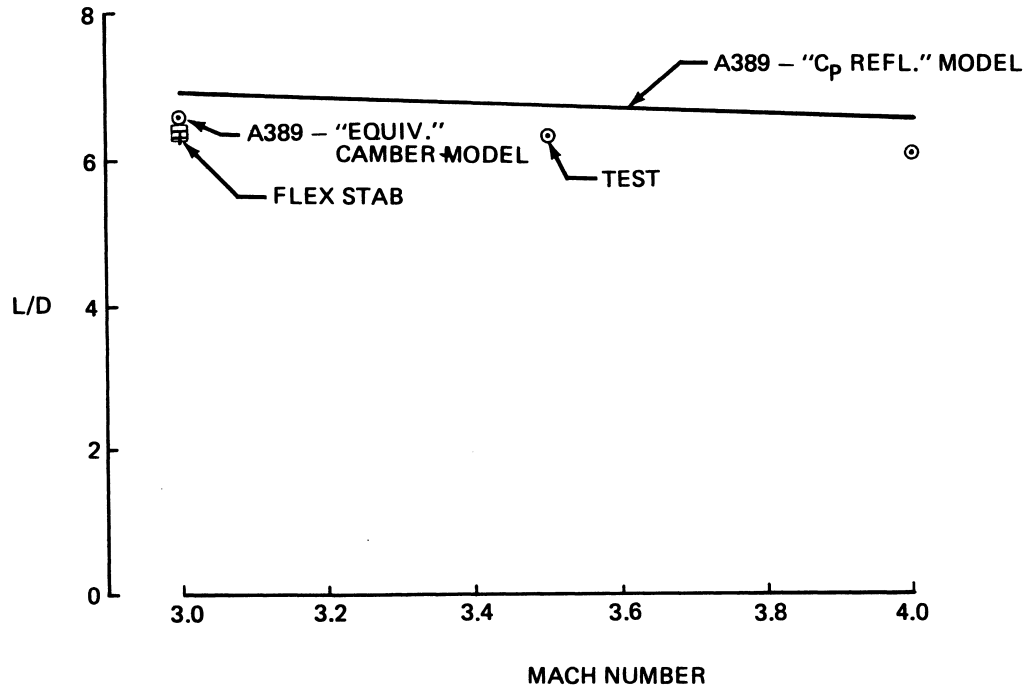


Figure 55b Comparison of Parasol Wing Theoretical Predictions

MAXIMUM LIFT/DRAG RATIO



BODY-INDUCED INTERFERENCE LIFT

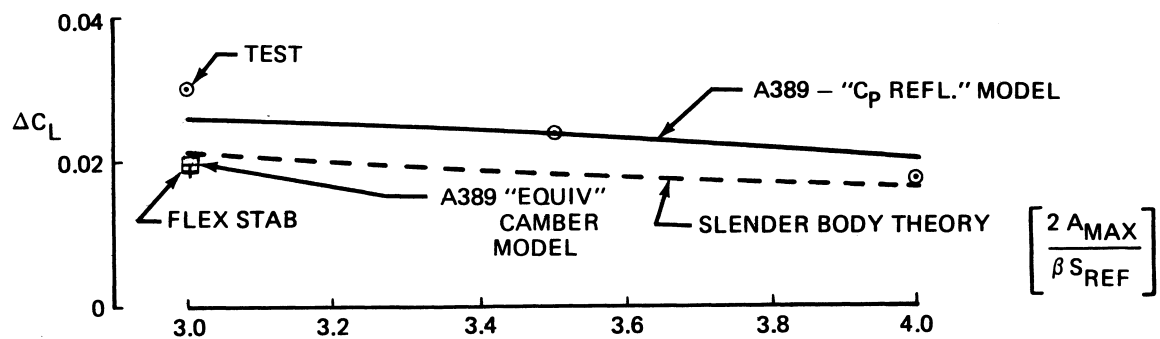


Figure 56. Lift/Drag Ratio and Interference Lift Test/Theory Comparisons

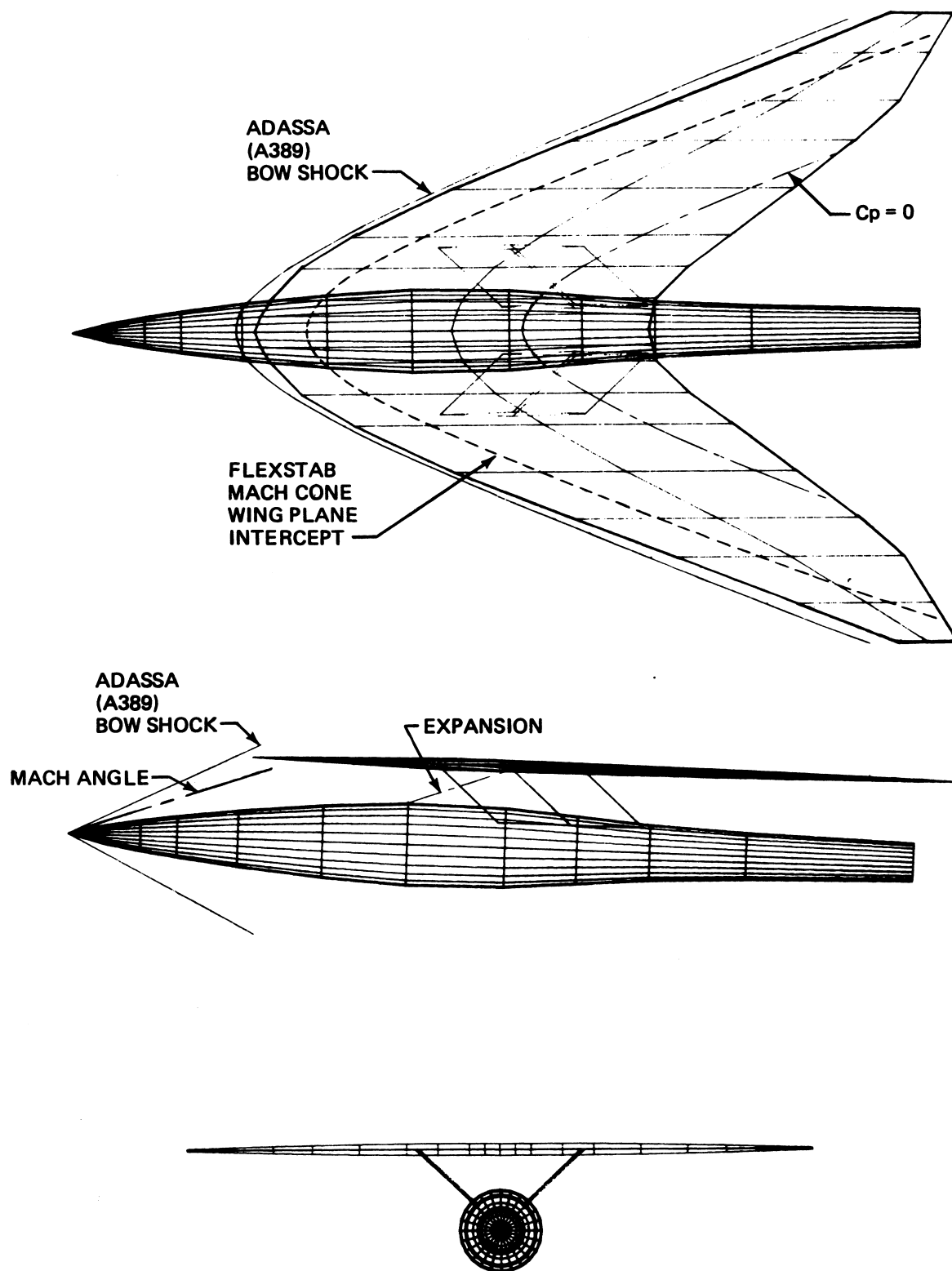


Figure 57 Comparison of Predicted Shock Locations

more lift and "nose up" pitching moment at zero incidence angle than FLEXSTAB, agree slightly better with the test data.

These test-theory comparisons indicate that both the FLEXSTAB and ADASSA linear theory programs can predict the aerodynamic characteristics of a wing-body parasol wing configuration provided multiple reflections do not occur between the wing and body. The drag predictions are correct for the case of multiple reflections; however, theory will underestimate the interference lift as discussed in Section VI. The shock wave locations calculated by ADASSA should be used in the design of a parasol wing planform instead of the FLEXSTAB calculated interference areas.

REFERENCES

1. Beane, B. J., "Notes on the Variation of Drag with Mach Number of a Busemann Biplane", Douglas Aircraft Rep. S.M. 18737.
2. Graham, E. W., et al., (1957), "A Theoretical Investigation of the Drag of Generalized Aircraft Configurations in Supersonic Flow", NASA TM-1421, January 1957 (22 References).
3. Graham, M. E. (1955), "Application of Drag-Reduction Methods to Supersonic Biplanes", Douglas Aircraft Company Report No. SM-19258, September 1955, (14 References).
4. Licher, R. M., "Optimum Two-Dimensional Multiplanes in Supersonic Flow", Douglas Aircraft Ref. S.M. 18688, (1955).
5. Lomax, H., and Heaslet, M. A., (1956), "Recent Developments in the Theory of Wing-Body Wave Drag", J.A.S. Vol. 23, No. 12.
6. Flower, J. W., (1963), "Configurations for High Supersonic Speeds Derived from Simple Shock-Waves and Expansions", R.A.S. Journal, May 1963.
7. Küchemann, D., (1965), "Hypersonic Aircraft and Their Aerodynamic Problems", Progress in Aeronautical Sciences,

Vol. 6, 1965. Editors Kuchemann, D., and Steinle, L.H.G., pp 271-352, (83 References).

8. Norweiler, T., (1963), "Delta Wings of Shapes Amenable to Exact Shock Wave Theory, Journal of R.A.S., Vol. 67, pp 39, 40, January 1963.
9. Peckham, D. H., "On Three-Dimensional Bodies of Delta Planform which can Support Plane Attached Shock Waves", A.R.C. C.P. No. 640, March 1962.
10. Squire, W. C., (1963), "Pressure Distributions and Flow Patterns at $M = 4.0$ on Some Delta Wings", ARC R&M No. 3373, 1964.
11. Squire, L. C. (1967), "Calculated Pressure Distributions and Shock Shapes on Thick Conical Wings at High Supersonic Speeds", May 1976, Aeronautical Quarterly, Vol. XVIII, Part 2, pp 185-206.
12. Goldsmith, E. L., and Cook, P. H., (1964), "Some Mutual Interference Effects Between a 5.7° Cone and a Sonic L.E. Delta Wing at $M_\infty = 2.49$ ", R.A.E. Tech. Note No. Aero 2936, 1964.

13. Eggers, A. J., Jr. and Syvertson, C. A., (1956), "Aircraft Configurations Developing High Lift-Drag Ratios at High Supersonic Speeds", NACA RM A 55L05, 1956.
14. Eggers, A. J., Jr., (1960), "Some Considerations of Aircraft Configurations Suitable for Long-Range Hypersonic Flight". In Hypersonic Flow (ed. A. R. Collar and J. Tinkler). Butterworth London.
15. Goldsmith, E. L., and Cook, P. H., (1965), "Half-Body and Wing Combinations in Supersonic Flow: A Review of Some Principles and Possibilities", R.A.E., Tech. Report 65040, 1965.
16. Boyd, J. A. (1965), "Optimal Utilization of Supersonic Favorable Interference to Obtain High Lift-Drag Ratios", AIAA Paper No. 65-752, November 1965, (12 References).
17. Brown, C. E. and McLean, F. E., (1959), "The Problem of Obtaining High Lift-Drag Ratios at Supersonic Speeds", J.A.S. May 1959, pp 298-302, (17 References).
18. Sigalla, A., (1959), "The Optimization for Minimum Wave Drag of a Fuselage Located under a Wing", Boeing Airplane Company Report D65189, December 1959, (7 References).

19. Chen, C. F., and Clarke, J. H. (1960), "A Study of Configurations Composed of a Body Under a Lifting Wing in Supersonic Flow", Division of Engineering, Brown University, Air Force Office of Scientific Research TN 59-1276, 1960.
20. Chen, C. F., and Clarke, J. H. (1961), "Body Under Lifting Wing", J.A.S., Vol. 28, No. 7, July 1961, pp 547-562, (8 References).
21. Clarke, J. H. (1959), "The Forces on Wing-Fuselage Combinations in Supersonic Flow", Boeing Document D1-82-0018, August 1959, (17 References).
22. Cook, P. H., (1966), "Further Experimental Results on the Mutual Interference Between Separated Wings and Bodies at $M = 2.49$ ", R.A.E. Tech. Report No. 66228, July 1966.
23. Gapcynski, J. P., and Carlson, H. (1954), "A Pressure-Distribution Investigation of the Aerodynamic Characteristics of a Body of Revolution in the Vicinity of a Reflection Plane at Mach Numbers of 1.41 and 2.01", NACA RM-L54J29, October 1954, (4 References).
24. Graham, E. W., and Licher, R. M. (1959), "The Calculation of Interference Drag Between Wing Lift and Fuselage Thickness at Supersonic Speeds", Douglas Aircraft Report No. SM-23446, February 1959, (22 References).

25. Jones, R. T., (1957), "Minimum Wave Drag for Arbitrary Arrangements of Wings and Bodies", NACA TN 1335, 1957, (14 References).
26. Ferri, A., Clarke, J. H., and Ting, L., (1957), "Favorable Interference in Lifting Systems in Supersonic Flow", J.A.S. Vol. 24, No. 11, pp 791-804, November 1957, (19 References).
27. Morris, O. A., Lamb, M., "Aerodynamic Characteristics in Pitch of a Modified Half-Ring-Wing-Body Combination and a Swept Wing-Body Combination at Mach 2.16 to 3.70", NASA TM X-1551, April 1968.
28. Morris, O. A., Mack, R. J., "Aerodynamic Characteristics of a Parasol-Wing-Body Combination Utilizing Favorable Lift Interference at Mach Numbers from 3.00 to 4.63", NASA TN D-4855, October 1968.
29. Mysliwetz, F., (1960), "Supersonic Interference of a Body Under a Wing", Boeing Document D6-5207, July 1960, (7 References).
30. Mysliwetz, F., "Supersonic Interference Lift of a Body-Wing Combination", AIAA Journal, Vol. 1, June 1963, pp 1432-1434.

31. Woodward, F. A., (1962), "Pressures and Forces on Wings and Bodies in Close Proximity at Supersonic Speeds", Boeing Document D6-8927, April 1962, (14 References).
32. Moore, K. C., Jones, J. G., "Some Aspects of the Design of Half-Ring Wing-Body Combinations with Prescribed Wing Loadings", Royal Aircraft Establishment, February 1965.
33. Middleton, W. D., and Lundry, J. L., "A Computational System for Aerodynamic Design and Analysis of Supersonic Aircraft", NASA Contract NAS1-13732, NASA CR-2715, July 1976, (Boeing Program A389).
34. Dusto, A. R. et al., "A Method for Predicting the Stability Characteristics of an Elastic Airplane, Volume I FLEXSTAB Theoretical Manual", NASA CR 114712, 1974.
35. Kulfan, R. M., and Sigalla, A., "Real Flow Limitations in Supersonic Airplane Design", AIAA Paper 78-147, January 1978.